ISSN 1028-8546

Azərbaycan Milli Elmlər Akademiyası
Fizika-Riyaziyyat və Texnika Elmləri Bölməsi
Fizika İnstitutu

4

Fizika

Cild
XI
2005

Bakı ✵ Elm

REACTIVE CHARACTERISTICS OF BARRIER STRUCTURE ON BASE OF SILICON UNDER ILLUMINATION

E.A. JAFAROVA
Institute of Physics of National Academy of Sciences of Azerbaijan
Baku AZ-1143, H. Javid ave., 33

There have investigated reactive properties of diffusion Si photocells in which high level of injection is made by both external voltage and lighting by intensity light. It is shown that sample lighting by focused light increases full capacity for photocarrier accumulation in corresponding regions of p-n structure at low frequencies of alternating signal. At bigger lighting accumulated charge of mobile carriers results in conductivity modulation of basic region due to inductive effect and capacity decrease.

There are been also investigated influence of electric field and lighting of photosensitivity of Si based MISIM structures. It is shown that spectral sensitivity of In_2O_3 – SiO_2 – Si - SiO_2 – M structures is controlled by applied voltage.

1. Introduction

Non-stationary electron process investigations in different semiconductive materials of p-n and MIS structures allow electrophysical properties to be varied, in particular reaction properties of these structures. In is important in creation of sensitive elements with controllable parameters under the effect of electric field, temperature and etc.

Earlier [1,2] we showed that at high levels of injection when $\omega\tau \geq 1$ (where ω – frequency of the test signal, τ – lifetime of minority carriers) and concentration of injected majority carriers (the forward bias p-n junction) is to be equal to concentration of majority carriers, reaction resistance of capacity behavior passes into inductive one. It is of interest the creation high injection levels when capacity passes into inductance without applying forward bias (photoinjection). Such approach is of practical interest with big scientific meaning, as there has been possibility of non-conduct control of reactive properties of p-n structure [3]. The influence of spurious capacity of conducting wires has been also exuded. It is also known that in metering circuits there have been used semiconductive lightsensitive varicaps, which allow transformation of light energy into electric one and parametric amplification of the given signal to be overlapped.

2. Experimental

There have been investigated reactive properties of Si diffusion p-n structures (photocells, Si with ρ=400 Ohm·cm) which is made by both external voltage (dark characteristics) and its illuminating by light. For sample light there have been used focused light of electric lamp by 170 wt with λ=1mkm water filter cutting off infrared part of spectrum. Measurements of reactive properties of p-n structures are made on installation with the use of bridge of full conductivity MPP 300.

MISIM structures have been prepared on p-Si-based with $\rho=10^3$ Ohm·cm. SiO_2 is obtained by thermal oxidation in wet and dry oxygen (d_{ox}≈0,3÷0,5 mcm). Field electrode of In_2O_3 light modulated with the frequency 300Hz from monochromator DMR-4. Alongside MISIM-structure there has been mainted silicon photodiode FD-27 K graduared in power of incident light.

3. Results and discussion

It is known that by photocell light the accumulated photoelectrons in n-region and photoholes in p-region are due to the additional capacity.

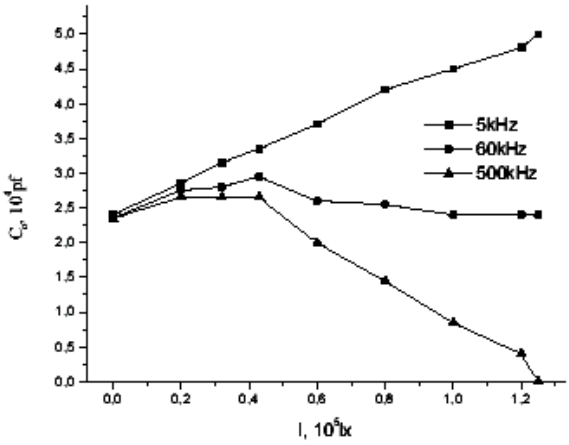

Fig.1. Dependence of Si photocell capacity on lighting at T=300K and different frequencies of alternative test signal.

Therefore by sample light we need to increase its complete capacity observed in the experiment (Fig.1). With the increase of light intensity at rather low frequencies p-n junction capacity rises linearly, at medium frequencies (f<60 kHz) it does not change. In 100÷600 kHz the capacity from $A=4\cdot10^4 Lx$ reduces linearly with the light. At low intensity of light sample capacity (C^{ph}) at all frequencies is a little more than initial capacity in the darkness (Co^d) and does not almost depend on the frequency, as the capacity Co^d. And with the increase of light intensity the pattern changes sharply up to frequency f≤60 kHz the capacity being more Co^d rises with the increase of light intensity and decreases with the growth of changing signal frequency: at f=60-70 kHz $C=Co^d$, i.e. reactance of the light elements does not change, but at f>70 kHz capacity of photocell decreases as with the increase of frequency as with the increase of light, i.e. $C^{ph}<Co^d$. At maximum light intensity and f=250-300 kHz, Co^{ph}, i.e. light photocell has reactance equal to 0 and purely effective resistance to be remained. At f≈300 kHz sample capacity by light goes into the inductance without applying external voltage. Such character of C^{ph} with the photocell light level is similar to the change of diode capacity with direct shift [1,2]: at low levels of injection (low intensities of light or small forward voltage) capacity increase is related to the rise of number of nonequilibrium carriers and is due to the accumulation of mobile change carriers. At high levels of

injection charge accumulation goes on, however this sufficiently big accumulated charge causes the decrease of basic region conductivity that is due to the inductive effect. Inductive effect exists simultaneously with the capacitive one causing first capacity decrease and then with the injection level increase shows more sharply giving rise to the capacity decrease below to 0 and its transition into the inductance (Fig.2).

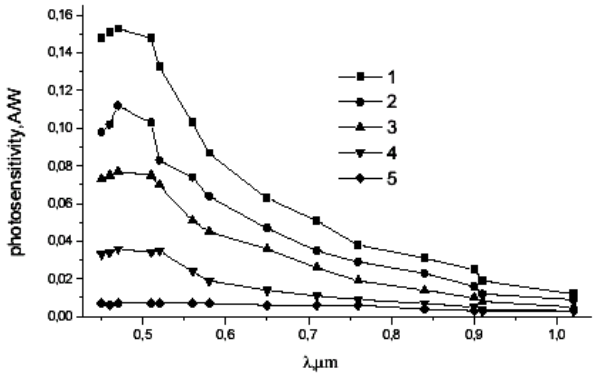

Fig.2. Frequency dependence of Si photocell capacity at different lighting.

Capacity transition into inductance in photocells causes about at $f \geq 70$ kHz. It appears to be connected with the fact that at photocell light the lifetime of nonequilibrium carriers increases a little, so $\omega\tau \approx 1$ (when capacity goes into the inductance) corresponds to a less frequency. Besides under the light inversion voltage at all frequencies where reactances sign inversion is observed shifts to the low value of forward voltage. Decrease of U_{inv} value at light can be explained as by the influence of decrease of series resistance of photocell as the carrier photoinjection appears to be carried out easier than the injection caused by external voltage. By photoinjection the sauce number of carriers overcauces the barrier at rather less value of voltage.

It is noted that capacity inversion voltage U_{inv} into inductance of Si p-n structures under investigation almost decreases linearly with the increase of light intensity, and light sensitivity of inversion voltage increases with the frequency growth ω of bigger $\omega_{cr} \approx 1/\tau$. Both in darkness and at lighting inversion voltage decrease linearly with the coefficient $æ \approx 2{,}2 \div 2{,}7$ mv/deg.

It is known that effects of carrier canilibrium distribution breakages in semiconductors are with background of the most semiconductive devices and they arise both during current passage through the structure and its illumination by light. Transition processes in semiconductor – insulator structures are accompanied by sharp capacity change and general resistance of the structure, in this case the structure has the possibility of transformation and memory of images [3-5]. We present investigation results of electric field influence and illumination on In_2O_3-SiO_2-Si-SiO_2-M structure photosensitivity.

VAC of the structures under investigation are linear and currents through the structure at U_p in some volts are nanoampers. It is shown at applying constant voltage to MISIM-structure photocurrent decreases significantly and falls up to the noise level at U_c=12V and at further increase of voltage it changes the sign, increases in absolute value and tends to the saturation.

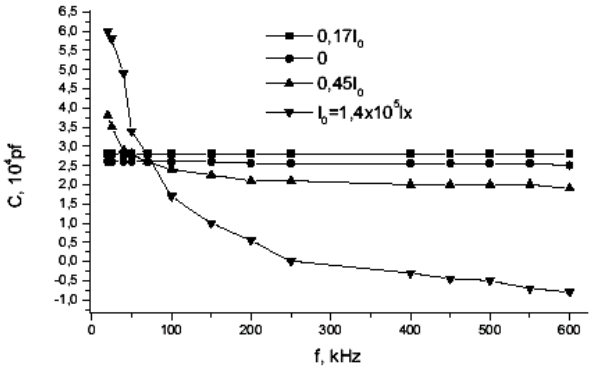

Fig.3. Spectral characteristic of Si MISIM-structure at different voltages: 1-U_f=2V; 2-U_f=0V; 3-U_f=-5V; 4-U_f=-10V; 5- U_f=-20V

Spectral dependence of MISIM-structure taken at different values of voltage is given in Fig.3. It is seen that in spectral characteristics in photovoltaic regime (curve 2) and at applying voltage (curves 1,3,4,5) sensitivity maximum at λ=0,5mkm is observed and photo response value changes significantly with applied voltage. Thus it is shown that spectral sensitivity of MISIM-structure is controlled by applied voltage.

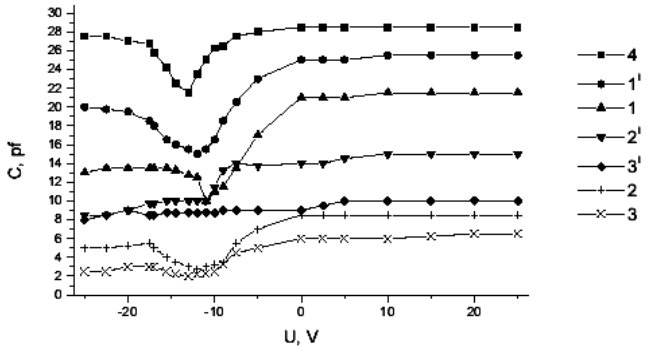

Fig.4. Dependence capacity for In_2O_3-SiO_2-Si-SiO_2-Al structures on voltage at different frequencies: 1-465kHz, 2- 1MHz, 3- 5MHz, 4- kHz (in dark); 1´, 2´, 3´ -at white lighting.

By investigation of structure photocapacity dependence on the voltage at different frequencies of test signal (f=0,001÷5 MHz) and illumination power 0,4 mV it is shown that unlike MIS-structure capacity of In_2O_3-SiO_2-Si-SiO_2-M structures in the interval of external voltage is sensitive to the light. At positive and small negative voltages photocapacity is constant. Pronounced dependence of photocapacity on the voltage is observed in the neighborhood of minimum at voltages from 0,5÷5V up to 15V. (This dependence has a complex behavior). It is possible that at lighting the capacity of quasineutral volume mainly increases.

4. Summary

Investigations under the study show that at light of diffusion Si photoelements focused by light there have been observed the increase of its complete capacity. Capacity dependence on the light sample has a complex character: it changes linearly at low frequencies (f<5kHz), it does not

almost change at medium ones (f<60kHz) and decreases at high frequencies (f≥500kHz). Such change of capacity is due to the accumulation of mobile nonequilibrium carriers at low levels of injection. At big light there have been taken place modulation of base conductivity that leads to the capacity decrease and its transition into the inductance (negative capacity).

It is also shown that the capacity of investigated In_2O_3-SiO_2-Si-SiO_2-Al structures within the range of applied voltage U_f=(-20÷+2)V is sensitive to the light and this dependence has a complex character. One can suggest that light of above-mentioned structures by the white light brings about the increase of the capacity of quasi-neutral volume.

[1] *G.B. Abdullayev, S.A. Iskender-sade, E.A. Jafarova.* 1968 Solid State Electronics 11, 233-239.

[2] *G.B. Abdullayev, S.A. Iskender-sade, E.A. Jafarova.* 1971 Reports of Academy of Sciences of USSR 200, 314-315.

[3] *A.Z. Badalov, S.A. Iskender-sade, E.A. Jafarova.* 1984 Journal of Technical Physics 54, 645-646.

[4] *V.V. Vasilyev, A.F. Kravchenko.* 2002, Fizika i Tekhnika Poluprovodnikov (Semiconductors) 36, 1068-1070.

[5] *Kh.T. Igamberdiyev, A.G. Mamadalimov*. 2003, Fizika i Tekhnika Poluprovodnikov (Semiconductors) 37, 29-31.

E.Ə. Cəfərova

İŞIĞIN TƏSİRİ ALTINDA Si ƏSASINDA ÇƏPƏR QURULUŞLARININ REAKTİV XASSƏLƏRİ

Xarici elektrik və yüksək işıq intensivliyi altında əmələ gələn injeksiyanın diffuziya yölu ilə alınmış silisium fotoceviricilərin reaktiv xassələrinə təsiri öyrənilmişdir. Nümunələrin fokuslanmış işıq vasitəsiilə işıqlandırılması p-n strukturunun müəyyən oblastında dəyişən siqnalın kiçik tezliklərində yükdaşıyıcıların artması hesabına faydalı tutumun çoxalmasına gətirib çıxarır. Yüksək işıqlanmada yığılmış mütəhərlik yüksək baza oblastının keçiriciliyini modulyasiya edir ki, bunun nəticəsində induktivlik effekti baş verir, bu da tutumun azalmasına gətirir.

Həmçinin elektrik sahəsinin və əlavə işıqlanmanın silisium MDYDM-strukturunun həssaslığına təsiri öyrənilmişdir. Göstərilmişdir ki, In_2O_3-SiO_2-Si-SiO_2-M strukturunun spektral həssaslığı verilən gərginliklə idarə olunur.

Э.А. Джафарова

РЕАКТИВНЫЕ ХАРАКТЕРИСТИКИ БАРЬЕРНЫХ СТРУКТУР НА ОСНОВЕ КРЕМНИЯ ПОД ДЕЙСТВИЕМ ОСВЕЩЕНИЯ

Исследованы реактивные свойства диффузионных Si фотоэлементов, в которых высокий уровень инжекции создавался как внешним напряжением, так и освещением его интенсивным светом. Показано, что освещение образцов сфокусированным светом увеличивает полную емкость из-за накопления фотоносителей в соответствующих областях p-n структуры при низких частотах переменного сигнала. При больших освещенностях накопленный заряд подвижных носителей вызывает модуляцию проводимости базовой области, обуславливающую индуктивный эффект и уменьшение емкости.

Также исследовано влияние электрического поля и подсветки на фоточувствительность МДПДМ структур на основе кремния. Показано, что спектральная чувствительность In_2O_3-SiO_2-Si-SiO_2-M структур управляется приложенным напряжением.

Received: 15.12.05

THE PLASMA OSCILLATOR FOR ION DEPOSITION OF DIAMOND-LIKE FILMS

I.S. GASANOV, V.A. ORUDJEV
Institute of Physics of NAS of Azerbaijan
H. Javid av.,33, AZ1143, Baku. E-mail: ilhamg@hotmail.com

The calculation of the parameters of the oscillator of carbonic plasma for the synthesis of amorphic diamond-like coverings in the vacuum conditions has been carried out. The construction of the source with electron-ray heating of the graphite cathode and water cooling of anode camera has been constructed, produced and tested on the base of the carried out estimations. The suggested method allows us to treat the optimal modes of ion deposition of the films.

The synthesis of amorphic diamond-like coverings in the vacuum conditions is widely used in scientific and industrial aims. The magnetron dispersion carbonic targets allow us to obtain the films of high quality and on the big square [1]. The method of vacuum arc discharge on the constant or impulse current at which the coverings with microhardness which close to the microhardness of nature diamond has the biggest velocity of film deposition [2]. However, the given method has the significant disadvantage: the carbonic erosion carries out in the cathode spot and creating microparticles of different sizes, getting to the substrate, make worth the quality of the grown films [3]. Such films become useless for the optical and other analogical applications. The biggest hopes from the known different methods of the liquidation of the fine-dispersated phase are put on the plasmooptical separation of plasma fluid, at which the ion multiplier along magnetic field directs to the substrate, and hard microparticles set down on the walls of plasma entrance [3,4]. The given method shows is difficult and don't allow to obtain the homogeneous fluids on the big square.

In the present paper the possibility of the deposition of zero-defects diamond-like films by the means of discharge plasma with electron-ray heating of the carbonic cathode. The prevention of the oscillation of microparticles on the cathode surface is predicted because of the control of the power of cathode ray [5,6]. In the vacuum arc with cathode spot such mode is impossible, i.e. the mode of high-current vacuum discharge is established by the self-coordinated method.

The calculation of all nodes of the device, the characteristics of which are mutually connected in definite way, is needed for the evaluation of the parameters of the ion deposition. The oscillator of the carbonic plasma, the scheme of which is given on the fig.1, has been treated and produced in the result of the carried out evaluations and test experiments.

The discharge is burned between carbonic cathode and cooled anode camera of cylinder form. The carbonic evaporates in the result of heating of the block of the cathode by the in-focus cathode ray. The discharge plasma through the holes in the camera cover penetrates in the region of ion deposition before the substrate, the temperature of which is controlled by the thermocouple. The negative potential by the value till 100 V for the extension of the positive carbon ions from the plasma is given on the substrate. The internal diameter of the discharge camera is equal to 50 mm that allows us to precipitate the films by the square till 20 sm^2. The device is installed inside the industrial vacuum installation by the type ВУ-1 with diffusion spooling and limited vacuum in useful capacity $3 \cdot 10^{-6}$ mm of mercury.

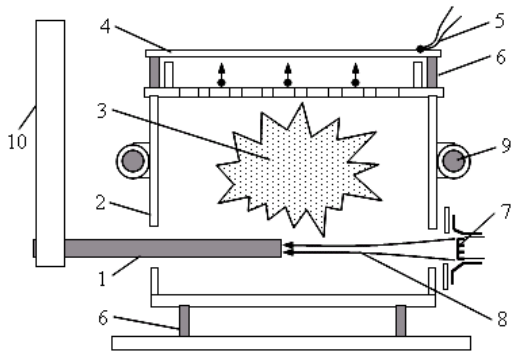

Fig.1. The scheme of the oscillator of the carbonic plasma: 1 – carbonic cathode; 2 – anode chamber; 3 – discharge plasma; 4 – substrate; 5 – thermocouple; 6 – isolator; 7 – filament; 8 – cathode ray; 9 – cooling; 10 – cathode holder.

The high enough specific power of cathode beam is needed for the carbonic evaporation. The standard electron-ray evaporator of ВУ-1 installation with magnetic turn of the ray on 180^0 doesn't allow us to realize the high enough beam pressure in the transversal direction. That's why the longitudinal acceleration of the electrons by the means of the quazipier system of the electrodes had been used [7]. In this system the conical form of the limiting electrode causes the creation of the radial electric field, which leads to the focusing of the accelerated of the electrode beam. The limiting electrode has the potential of filament. The electron energy is equal to 6 keV, the current of the beam can be increased till 0,5 A, regulating the filament current of the tungsten filament by diameter 0,5 mm. The cathode presents itself the rod by the length 120 mm and diameter 6 mm from the carbonic of optical frequency. As experiments show, the quazipirs system of the acceleration and focusing allows us totally to localize the cathode ray on the block of the heated cathode.

As it is known, the pressure of the carbonic steams 10^{-2} mm of mercury is achieved at its temperature 2600-2700°C. At such pressure the discharge is easily burned on the constant current. Such high temperature of the cathode causes the significant energy loss on the radiation, and also on the heating of the cathode holder.

On the formula Stefan-Bolzman we can calculate the value of radiation power:

$$W_1 = \varepsilon_T \sigma T^4 S \ , \qquad (1)$$

where ε_T=0,52 is coefficient of the carbonic gray colour. The radiation power is equal to 180Vt at the cathode temperature 2800K and effective heating square 100 mm^2.

The construction of the cathode holder consists on two joint parts: cooled brazen cylinder and steel uncooled collet. Allowing the heating of the brazen cylinder till 50°C, the steel collet till 350°C, we obtain, that the square of the collet cross-section by 1,5 cm^2 is needed for the heating of the cathode block till work temperature. At that the heat fluid from the heated end of the carbonic till brazen holder is defined by the equation of the heat conductivity:

$$W_2 = \lambda \frac{\Delta T}{l}, \qquad (2)$$

where λ is averaged heat conductivity, l is rod length. In the given paper the heat fluid has the value 20 Vt.

Thus, the common power, locally introducing into cathode, shouldn't be less:

$$W = W_1 + W_2 \approx 200\,Vt\,.$$

The carried out experiments have been proved, that the significant evaporation of the carbonic, which is enough for the burning of the discharge in the work chamber carries out at the power of the cathode ray 250 Vt.

It is need to note, that cathode heating till the needed temperature and the stabilization of the discharge mode are needed the definite time. If all this time the substrate will be under output window of the discharge chamber, then the carbonic film will be marking on its surface continuously. That's why the special turn mechanism had been worked, by the means of which the substrate was established under the output window only after achieving of the working parameters of the discharge plasma.

The best structure of the marked films obtains at the substrate temperature near 200°C. The substrate is heated with the help of the regulated plane heater, which doesn't show on the fig.1.

In the source construction the substrate is separated from the discharge by the cavity, in which the plasma comes through the holes. This is made in order to the substrate potential doesn't influence on the discharge conditions.

The enough high degree of the ionization of the carbonic plasma is needed for the synthesis of diamond-like coverings. Otherwise the neutral component will cause mainly to the creation of the carbonic film. The following calculative method has been treated for the evaluation of the ionization degree of the carbonic film.

The ion concentration in the plasma is defined from Bom formula for the ion saturation current [8]:

$$j_i = 0{,}4en_i\sqrt{\frac{2kT_e}{M_i}}, \qquad (3)$$

where T_e is temperature of plasma electrons, M_i is ion mass. The ion saturation current is measured by the voltage-current characteristics of the interval of the anode plasma-substrate at the discharge constant current and power of the electron beam. The electron temperature in the discharges of such type doesn't exceed 10 eV.

The atom fluid of the evaporating substance is the function of the evaporator temperature:

$$q = n_s \vartheta \exp(-Q/kT), \qquad (4)$$

where n_s~2·10^{15} cm^{-2} is surface atom density, η~5·10^{12} s^{-1} is typical frequency of atom oscillations, Q is energy of the carbonic evaporation. Knowing the volume of the discharge chamber, on the formula (4) we can evaluate the average concentration of the carbonic steams at the fixed value of the cathode temperature (power of electron beam).

In the given case the degree of plasma ionization is defined as the ratio of the ion concentration to the concentration of the neutral particles at the discharge absence.

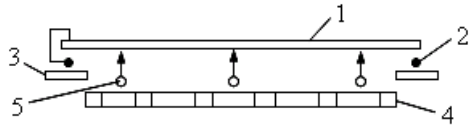

Fig.2. The system of the neutralization of the surface charge: 1 – substrate; 2 – ring filament; 3 – screen; 4 – output window of the discharge chamber; 5 – carbonic ions.

As the diamond-like dielectric film is evaporating, its surface will be charged by the ions, and ions, drawing the field will be decreased. In these conditions the potential fixation of the surface of the dielectric film is needed. With the aim of the neutralization of the surface charge the system of the automatic fixation of the potential by the means of the filament (fig.2). The ring filament from the tungsten incandesces till the temperature of thermionic emission; it electrically is connected with substrate. The screen impedes to the departure of the electrons into discharge plasma. At the charging of the dielectric the electrons will be precipitated on its surface, and decrease its potential till substrate potential.

Following to the above mentioned procedure, the dependence of the ionization degree of the plasma on the discharge parameters is established: current, voltage, cathode temperature. After the film deposition the connection between their physic-mechanical characteristics and degree of the ionization of discharge plasma will be defined. This will allow us to treat the optimal modes of the synthesis of amorphic diamond-like coverings in the given experimental conditions.

The work has been carried out at the support of the fond CRDF-AMEF (grant №3101).

[1] *B.F.Coll*. Thin Films. Ed. by G.Hecht, F.Richter, J.Hahn. Proc. of the joint TATF'94 and HVITF'94, Dresden, March 7-11, (1994), p. 3-17.

[2] *I.I. Aksenov, V.E. Strelnitskyi*. "The synthesis hydrogen-free films of diamond-like carbon", Proceeding of 12-th International Symposium "Thin films in electronics", 23-27 April, 2001, Kharkov, Ukraine, p. 96-105.

[3] *I.I. Aksenov*. "Vakuumno-dugovie istochniki filtrovannoy plazmi: istoriya, teoriya, praktika, perspektivi". Sb. dokl. 6 Mejd. conf. "Vakuumniye

tekhnologii i oborudovanie", 21-26 aprelya 2003, Kharkov, Ukraina, c.238-258.
[4] *A.Anders.* Surf. and Coat. Techn. 1999,v.120-121, p.319.
[5] *I.S. Gasanov, I.I. Gurbanov*. Прикладная физика, 2004, №3, c.28-29.
[6] *I.S. Gasanov, V.A. Orudjev.* Vakuumnoe osajdenie almazopodobnikh plyonok. Fizikanın aktual problemləri. III resp. elmi konfr. mat. Bakı, 2004, s.100-101.
[7] *M. Siladi*. Elektronnaya I ionnaya optika. Moskva. Mir, 1990, 639 c.
[8] *M.D. Gabovich, N.V. Pleshivtsev, N.N. Semashko.* Puchki ionov I atomov dlya upravlyaemogo termoyadernogo sinteza I tekhnologicheskix tseley. Moskva, Energoatomizdat, 1986, 263 p.

İ.S. Həsənov, V.Ə. Orucov

ALMAZABƏNZƏR TƏBƏQƏLƏRİN İON ÇÖKDÜRÜLMƏSİ ÜÇÜN PLAZMANIN GENERATORU

Vakuum şəraitində amorf almazabənzər örtüklərin sintezi üçün carbon plazma generatoru parametrlərinin hesablanması aparılıb. Yerinə yetirilmiş hesablamaların əsasında qrafit katodun elektron-şüa qızdırılması və anod kamerasının su soyudulması ilə mənbənin konstruksiyası işlənib, hazırlanıb və sınanılmışdır. Təklif edilən metodika təbəqələrin ion çökdürülməsinin optimal rejimlərinin işlənməsinə imkan verir.

И.С. Гасанов, В.А. Оруджев

ГЕНЕРАТОР ПЛАЗМЫ ДЛЯ ИОННОГО ОСАЖДЕНИЯ АЛМАЗОПОДОБНЫХ ПЛЕНОК

Проведен расчет параметров генератора углеродной плазмы для синтеза аморфных алмазоподобных покрытий в вакуумных условиях. На основе выполненных оценок разработана, изготовлена и испытана конструкция источника с электронно-лучевым нагревом графитового катода и водяным охлаждением анодной камеры. Предлагаемая методика позволяет отработать оптимальные режимы ионного осаждения пленок.

Received: 06.12.05

ELECTROPHYSICAL RESEARCHES OF MECHANIZM OF CORROSION CARBONACROUS STEEL IN DEMINERALIZATIONAL WATER

A.F. ALIYEV

Azerbaijan Power Research and Design Institute, Baku, Azerbaijan

Investigation results of carbon steel corrosion mechanisms in atomic desalting plant (water-freshener) distillate are given. An effective method of corrosion protection by means of adding bicomponent polyphosphate composition and anionic surfactant info water has been developed.

Many atomic electric power stations produce considerable quantity of demineralized water due to using of nuclear reactor heat removal energy. This water obtained in technological cycle on thermal desalters represents a valuable product – distillate that can be used as refrigerant in circulating systems of water-supply. Using of distillate for heat exchange apparatus is safe from the point of view of scale formation because its composition is free of salt-forming ions of calcium , magnesium, sulphates, etc. and, as well, of bioovergrowth because lack of microorganisms and corresponding flora. However as experience of plastic plant operation of Shevcenco (now Actau, Kazakhstan) showed at using in technical water-supply carbon steel equipment contacting with distillate it necessary to take measures for metal corrosion protection. Investigations were carried out under the leader-ship of this paper author directly at above-mentioned plant as well at Baku branch of VNII VODGEO (now NIPI "SUCANAL") and in NI Ph ChI (Scientific-Research Physical and Chemical Institute after L.Ya. Karpov, Moscow).

Experiments have been carried out with distillate of the largest in the Former USSR atomic water-freshener (Shevchenko, Kazarh SSR). Distillate replenishment salt composition and circulating water data are given in Table 1 (in comparison with portable water standards).

Table 1.

Distillate and circulating water salt composition.

Refrigerant (cooling agent)	Ca^{2+}, mg-eqv/l	Mg^{2+}, mg- eqv/l	SO_4^{2-}, mg/l	Cl^-, mg/l	General mineralization, mg/l
Replenishment distillate	0,025-0,1	0,04-0,15	0,8-1,0	0,1-0,2	0,1-0,15
Circulating water	0,03-0,12	0,048-0,18	0,9-1,2	0,2-0,3	0,2-0,25
Portable water [1]	$\sum(Ca^2+Mg^{2+})$, no more than 7,0		$\leq$ 500,0	$\leq$ 350,0	$\leq$ 1000,0

It is known that water corrosivity, firstly, depends on its salt composition. As it is seen from Table 1 analyzed water hardness is very small (tens fold lower of maximum permissible concentration standard of portable water). Such water cannot form protective carbonate film on metal surface and, hence, according to this factor has high corrosivity. Secondly, according to small content of pitting forming chloride ions (hundreds fold lower of maximum permissible concentration standard of portable water and using of this water is not dangerous from the point of view of formation more dangerous pointed and pitting corrosion on metal surface.

Water corrosivity depends on, as well pH value and its oxygen content (Table.2.).

Table 2.

pH and O_2 values in distillate and circulating water.

Indices names					
Replenishment distillate			Circulating water		
pH	O_2, mg /l	Fe, mg/l	pH	O_2, mg/l	Fe, mg/l
8,9-9,5	0,35-0,80	0,2-1,2	8,8-9,3	3,45-11,2	4,6-12,0

Values of pH are practically the same in both waters and according to this index are favourable for carbon steel.

Data comparison on soluble oxygen content in replenishment distillate and distillate converted into circulating water show rapid O_2 concentration increase in circulating water. It is connected with air-tightnessles of plant circulating water-supply system. It has jet gaps promoting water enrichment by oxygen that rapidly increase medium corrosivity. Oxygen action destruction is also shown by a fact that general iron content in circulating water (and it is a product of steel materials corrosion) is greatly more (more than one order) than replenishment distillate (see Table 2). Steel sample (steel 3) gravimetric test in circulating water (16-24°C) at different exposition times (from 16-18 up to 100-120 hours) showed that corrosion values rate is in a range ~ 0,3-0,9 mm/year that is corresponding to the field of low-resistance metals and to 6-7 amount of corrosion resistance [2]. Here corrosion character is uniform at full lack of point and pitting damage traces.

Influence over corrosion of such factors as exposition time, medium mixing, temperature was determined by electrochemical measurement on potentiostat and electrochemical cell by procedure [3].

Corrosion potential φ_{cor}. with time increase is removed initially up to 0,03-0,04 V, then is stabilized, and cathodic and anodic polarization curves practically do not change and it shows stability of corrosion rate in time (Figure 1).

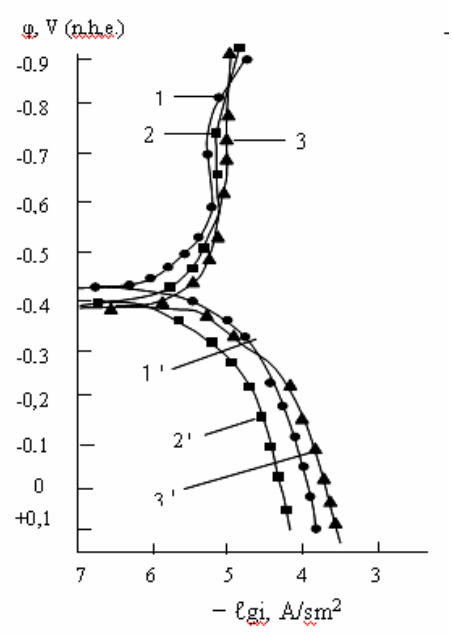

Fig.1. Cathodic (1-3) and anodic (1'-3') potentiodynamic (*V*=20 mV/min.) polarized curves of steel 3 in motionless circulating water (25°C) at different time exposition: 1-1'-2h.; 2-2'-22 h.; 3-3'-66 h; *φ,V* (normal hydrogen electrode, n.h.e.)

Time of specimen-electrode exposition practically has no influence upon steel 3 corrosive electrochemical behaviour in mixing water.

Absolutely other picture is observed at steel 3 electrochemical behaviour study in motionless (statical state) and mixing (dynamical state) water (Figure 2). In this case cathodic and anodic polarizational curves are significantly different. In case of medium mixing rapid efficiency in crease is observed in both cathodic and anodic processes. It is explained by significant facilitation of oxygen access to cathodic and anodic areas of metal surface and corrosion process takes place mainly by oxygen polarization. Water temperature increase from 25 up to 50°C (actually water temperature is no more than 30°C) practically has no influence upon steel cathodic and anodic polarization (Figure 3). Only small displacement of φ_{cor}. to ~ 0,05 V into negative side is observed. Value of top cathodic current and corrosion rate (i) remains practically unchanged.

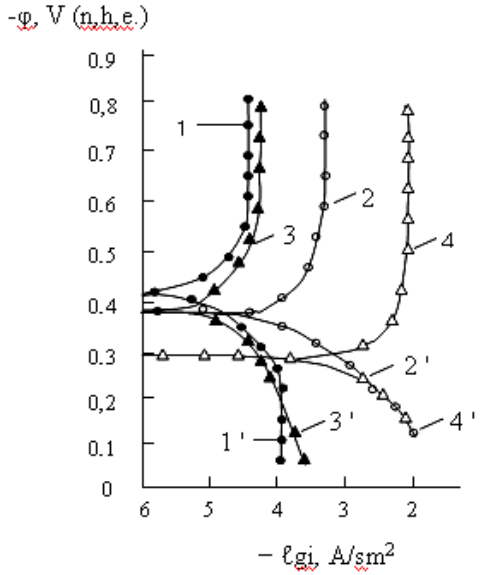

Fig.2. Influence of circulating water (25°C) upon cathodic (1-4) and anodic (1 '- 4') potentiodynamic (υ = 20 мV/min) polarization of steel 3:
1-1' and 2-2' – exposition time –2 h.
3-3' and 4 - 4'– exposition time –70 h.
1-1' and 3 -3' – motionless water.
2-2' and 4 - 4'– mixing.

To protect carbon steel from corrosion in demineralized water in conditions of work of water-supply circulating system a number of corrosion inhibitors had been tested on the basis of phosphates $Na_3PO_4 \cdot 12H_2O$; $(NaPO_3)_6$; $Na_5P_3O_{10}$ and surfactant RAS (refined alkylarylsulphonate).

Out of phosphate inhibitors the most efficient was hexamethhaphosphate of natrium $(Na\ PO_3)_6$. Using 40-60 mg/l (by general mass) provides full protection of carbon steel in distillate. However it is known [4] that polyphosphates getting into open reservoir promotes development of blue-green water-plants (phenomenon of autrofication) decreasing oxygen content in water and causes fishes death. At present tendency of polyphosphate using limitation each taken separately and transition to their use in mixture with organic combinations is observed.

A large group of corrosition inhibitor preparations as in known from literature including patent literature are different inhibitor mixtures, in particular, with surfactants. Multicomponent mixtures for obtaining effect of synergetic inhibitors more often are formed by proper corrosion inhibitors.

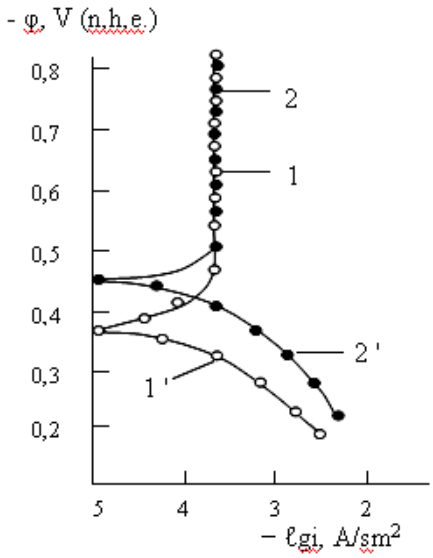

Fig.3. Cathodic (1-2) and anodic (1 '- 2 ') potentiodinamic (υ = 20 мV/min) polarized curves of steel 3 in mixing circulating water at different temperatures: 1-1 ' – 25°C; 2-2 ' – 50°C.

Their efficiency is significantly higher than initial ingredients.

The quantity of every possible combination is rather too much.

As an example "Composition for metal corrosion protection in neutral medium (authors certificate No. 280163 of USSR") consisting of four [4] components is showed and each of them separately is corrosion inhibitor.

However using of such complex inhibitor is more efficient than using of its components separately.

Two-component composition of polyphosphates with surfactants are of special interest and as is known they can show excellent synergetic effect.

A large number of surfactants are known, however only some their varieties are produced by industry. Besides, surfactant use in the system of circulating water-supply requires intoxicate, availability and low cost. Anodic surfactant RAS met all these requirements.

As a results of numerous experiments and test a new highly efficient way of carbon steel protection in a demineralized water had been developed for using in closed water-supply work conditions, i.e. introduction of polyphosphate and surfactant into composition system.

Composition components natrium hexamethophosphate and RAS are untoxic and permissible for use in industrial scale. Optimum protective dose of composition is 6mg/l (according to PO_4^{3-}) of natrium hexamethophosphate and 50mg/l of RAS active part.

[1] GOST 2874-85 "Portable water".
[2] GOST 13819-85 "Metal corrosion resistance scale".
[3] *L.I. Freyman, V.A. Makarov, I.E. Bryksin.* "Potentiostatical methods in corrosive study and electrochemical protection". Publishing house "Chemistry", L., 1972.
[4] *V.A. Panov, A.A. Emkov, G.N. Pozdnyshev, N.M. Baikov.* Inhibitors of inorganic salt deposits. Review of field main directions, series «Nefteprомyslovoe delo», M.VNIIOENG, 1978. (in Russian).

A.F. Əliyev

MİNERALSIZLAŞDIRILMIŞ SUDA KARBONLU POLADIN KORROZİYA MEXANİZMİNİN ELEKTROFİZİKİ TƏDQİQİ

Karbonlu poladın atomlu şirinləşdiriçi qurğuda distillyatın korroziya mexanizminin tədqiqi nəticələri araşdırılıb. Suya daxil edilən ikikomponentli kompozisiyalı polifosfat və anionlu SAM (Səthi Aktiv Maddə) ilə korroziyanın qarşısının alınmasının effektli üsulu işlənib. Texnologiya Aktau ş. (Kazaxıstan) plastmass zavodunda istehsala tətbiq edilib.

А.Ф. Алиев

ЭЛЕКТРОФИЗИЧЕСКИЕ ИССЛЕДОВАНИЯ МЕХАНИЗМА КОРРОЗИИ УГЛЕРОДИСТОЙ СТАЛИ В ДЕМИНЕРАЛИЗОВАННОЙ ВОДЕ

Приводятся результаты исследований механизма коррозии углеродистой стали в дистилляте атомной опреснительной установки. Разработан эффективный способ предотвращения коррозии - введение в воду двухкомпонентной композиции полифосфата и анионного ПАВ. Технология внедрена в производство на заводе пластмасс г. Актау (Казахстан).

Received: 19.10.05

THE ABSORBENTS OF MWF RADIATION ON THE BASE OF HIGH DISPERSION MATERIALS

S.T. AZIZOV, M.A. SADICHOV
Institute of Physics of NASA
Azerbaijan, AZ-1143, Baku, Javid av., 33

The possibility of the use of the composition material in the capacity of the microwave absorbent on the base of the epoxy resin with the inputted water in it in the capacity of the high dispersion filler is investigated.

Introduction

The problem of the creation of non-reflective absorbents of electromagnetic radiation on the base of the accessible composition materials and simple technology of their production has been presented the big interest from immemorial times and has been attracted the attention of many investigators. Firstly it was connected with the neediness of treatment of the coverings for the population defense from harmful influence of the microwave radiation on them. Last time the investigations were carrying out in this direction in USA, Russia, Great Britain, Japan and in other industrially developed countries [1,2]. The absorbents of microwave radiation, created in the result of these investigations presented mainly multi-layer composition materials, marked on the metallic surfaces containing the high dispersion metallic and ferromagnetic particles in its composition. The absorbents of this class seemed usable in the long-wave region of microwave range. The efficacy of selective absorption of radiation of such absorbents on more high frequencies strongly decreased. Besides, the coverings of such type were needed to lead to relative big width even on the low frequencies for the achievement of total absorbent, that significantly charged the defended objects, and use of more effective ferromagnetic materials in the capacity of the fillers made these absorbents mechanically less strong.

At the same time, as it was established in the refs [3,4,5] the dielectric materials, which have the significant absorption in the range of super-high frequencies, can be used in the capacity of the absorbent microwave coverings. Thus, the treated microwave absorbent on the base of polyformaldegide and polyamide, introduced in it in the capacity of absorbent filler, supplied total slaking of electromagnetic radiation with wave length λ=1,5 cm in it [6]. However, the obtaining covering had the bigger width in the comparison with covering, forming with use of metallic or ferromagnetic particles, because of the low value of dielectric constant of composition material.

The main content

In this connection it is more preferably the use of microwave coverings of polar liquids in the capacity of fillers, having in this wave range the high values as dielectric loss ε'', so dielectric constant ε'. The polar liquid can be used in the capacity of the filler of some solid-body material, having good adgeoz properties for the technical realization of such absorbent coverings. The obtaining absorbents could have the need constructive rigidity at low volume of such encapsulated liquid inclusions, and they could supply the realization of the condition of total absorption of falling radiation in them at definite set of inclusion concentrations.

The inclusions themselves are possible in the form of capsule of liquid polar substances, closed into defense polymeric film membranes. As ε''=0 of the nonpolar matrix substance of absorbent, and ε' doesn't depend on frequency, then at the given temperature *T* and wave length λ of falling electromagnetic radiation, the choice of resonance values ε_0' and ε_0'' of absorbents is achieved by the variety of concentrations of it liquid phase.

The probability of realization of absorbents of electromagnetic radiation at the given *T* and λ on the base of composition materials, containing the high dispersion encapsulated polar liquids, is illustrated by the following example. The additive character of the connection of dielectric properties of absorbent with dielectric properties of it components and the smallness of the dimension of liquid capsules in the comparison with wave length of radiation is supposed for the comfort of the concept of results.

In the correspondence with data of the ref [5], the conditions of total or nonreflective absorption of electromagnetic radiation in two-layered system of dielectric-metal are described by the following equations:

$$\pi(2N-1)+arctg\frac{2\pi y}{n^1(1+y^1)-1}=\frac{1}{y}\ell n\sqrt{\frac{(1+n)^2+(ny)^2}{(1-n)^2+(ny)^2}} \quad (1)$$

$$\frac{\ell_o}{\lambda_o}=\frac{1}{4\pi n}\left[\pi(2N-1)+arctg\frac{2ny}{n^2(1+n^2)-1}\right], \quad (2)$$

where l_0 is layer width, *N* is number of zero minimum of dependence wave reflection coefficient on width of substance layer.

The coefficient of refraction of waves *n* and factor of dielectric loss *y* of covering material, introducing into equation (1) and (2) connect with it ε', ε'' by known ratios:

$$\varepsilon'=n^2(1-y^2);\varepsilon''=2n^2y. \quad (3)$$

The values ε' and ε'', introducing into equation (3), connect with dielectric constant ε_1' and dielectric loss ε_1'' of liquid phase and ε_2 of matrix substance by additive equations:

$$\varepsilon'=\varepsilon'_1(\varphi_o)+\varepsilon_2(1-\varphi_o) \quad \varepsilon''=\varepsilon''_1\varphi_o, \quad (4)$$

where φ is concentration of liquid phase in covering substance.

The joint solution of equations (1)-(4) allow to calculate the selective values of concentration φ of liquid phase and l_0 layer width of covering at given values N, wave length λ of falling radiation and dielectric coefficients of useable liquid phases ε', ε'' and matrix material.

Solution of simultaneous equations at the given values ε_1', ε_2'', ε_2, λ, N is carried out by the iteration mean. The selective values of liquid phase concentration and thickness l_0 of the coating layer are results of this calculation.

At the existence of the inclination of ε' and ε'' filler from additivity the graphoanalytic method of solution of initial equation system is used.

Below the calculation results φ and l on equations (1)-(4) of microwave absorbent at λ=1,5 cm, forming on the base of epoxy resin, introducing of the encapsulated water in it in the capacity of the filler.

The epoxy resin has dielectric constant ε=2,7. For water λ=1,5 cm and T=20C ε'=36.8, ε''=36.4 [7]. At the additive character of the connection between dielectric properties of the filler and its components, we have from the joint solution of equation system (1)-(4), that conditions of nonreflective absorption of radiation carry out at the volume concentration of liquid phase at φ=0.077 and l=0.173 cm width of absorbent layer on the value, which is closer to $\lambda_g/4$ (at N=2). The total absorption takes place also at less concentrations of liquid phase, but at the widths of covering layer, which is closer to $(2N\text{-}1)\lambda_d/4$.

Conclusion

Thus the conditions of total slaking of microwave radiation in the covering marked on metal, by the composition from epoxy resin and introduced water in it in the capacity of high dispersion filler.

[1] *I.P. Kozlov.* Normalnoe padenie ploskoy elektromagnitnoy volni na ploskosloistiy dielektrik. Vesti Mosk. aviats. inst-t 1997, t. 4, № 2, s. 37-41.

[2] *N.M. Volkov i dr.* Elektromagnitnoe izluchenie i volni. Moskva, 1992.

[3] *R.M. Kasimov.* İnjenerno-fizicheskiy jurnal, Moskva, 1994, t.6, №5-6, s.489.

[4] *G.R. Kasimov, S.T Azizov, R.M. Kasimov, Ch.O.Kadjar.* Izvestiya AN Azerbaijana, ser. Fiz-tex.i mat. nauk, 1995, t.16, № 5-6, s. 22-29.

[5] *R.M. Kasimov, M.A. Kalafi, G.R. Kasimov, Ch.O.Kadjar.* İnjenerno-fizicheskiy jurnal, t. 71, № 2, 1998, s. 282-285.

[6] *S.T. Azizov, M.A. Sadıxov, S.R. Kasimova, R.M. Kasimov, Ch.O.Kadjar.* Fizika, №1-2, t.10, s.3-5, 2004.

[7] *Ya.Yu. Akhadov.* Dielektricheskie parametri chistikh jidkostey. M, Izd. MAI, 1999, s. 285.

S.T. Əzizov, M.A. Sadıxov

YÜKSƏK DISPERSIYALI MATERIALLAR ƏSASINDA ƏYT ŞÜALARIN UDUCULARI

Məqalədə mikrodalğalı diapazonda epoksid qatranın əsasında kompozit materiallara yüksək dispersiyalı maddə kimi su daxil etməklə uducuların yaradılması mümkünlüyü tədqiq olunur.

С.Т. Азизов, М.А. Садыхов

ПОГЛОТИТЕЛИ СВЧ ИЗЛУЧЕНИЯ НА ОСНОВЕ ВЫСОКОДИСПЕРСНЫХ МАТЕРИАЛОВ

Исследуется возможность использования в качестве микроволнового поглотителя композиционного материала на основе эпоксидной смолы с введенной в него воды в качестве высокодисперсного наполнителя.

Received: 16.06.05

THE EXACT SOLUTIONS OF KANE EQUATIONS WHICH HAVE BAND EDGE GAP POTENTIAL WITH RING-SHAPED NON-SPHERICAL OSCILLATOR POTENTIAL IN EXTERNAL NON-UNIFORM ELECTRIC FIELD

A.M. BABAYEV [1,2]

[1]Institute of Physics, Azerbaijan Academy of Sciences, 370143, Baku,
[2]Department of Physics, University of Suleyman Demirel,
Isparta 32260, Turkey

The energy spectrum of electrons in narrow band gap semiconductor nanocrystals which have position dependence band-gap in an external non-uniform electric field which compensate the position dependence of the band edge of the valence band potential is studied theoretically taking into account the nonparabolicity of electrons in dispersion laws. The exact solutions of the Kane equations with strong spin-orbital interaction are determined with via the band-gap changes as a function of the position. The band edge gap potential is taken as the ring-shaped non-spherical oscillator potential $V(r)=\frac{\gamma r^2}{2}+\frac{a}{r^2}+\frac{b}{r^2\sin^2\theta}$.

1. Introduction

In recent years there has been a great interest to the nanostructures, which was developed from narrow-gap semiconductors. In these nanostructures much smaller effective mass of electrons results higher size quantization energy. In order to investigate the optical and kinetic properties of nanostructures it will be possible to observe size quantization energy states. On the other hand in narrow-gap semiconductors (InSb, InAs) the spin-orbit interaction and the non-parabolicity energy spectrum of carriers must be taken into account. Kane model was derived to prove the non-parabolicity of the energy spectrum of carriers. Parabolic potential $V(r)=\frac{1}{2}m\omega^2 r^2$ is often used to describe confined quantum dot [1].

Confinement potentials which are in the form of $V(r)=a\cdot r^2+br^{-2}$ describe a quantum dot, an antidot, or a quantum ring, depending on the values of *a* and *b* [2].

In the work [3] the eigenfunctions and eigenvalues of the Schrödinger equation with a ring-shaped non-spherical oscillator were obtained.

For electronic devices, one of the most important semiconductor parameter is the value of the energy gap between the valence band maximum and the conduction band minimum. Many applications, particularly those that depend on optical properties, depend crucially on the value of the fundamental gap. The fundamental gap is indeed modified in compositional quantum wells, wires and dots as position dependent [4,5].

In [6] the exact solutions of the Dirac equation with a linear scalar confining potential in uniform electric field are given. A scalar potential in the Dirac equation is equivalent to a dependence of the rest mass upon position.

In the present study, the energy spectrum and the wave functions of the electrons in Kane-type semiconductor quantum dots with strong spin-orbital interaction is determined with via the band-gap changes as a function of the position**.** The position dependence of the band gap implies the position dependence of the effective mass of electrons and is taken ring-shaped non-spherical oscillator potential.

In the Kane model [7, 8, 9, 10], the k.p interactions within the valence and conduction band complex are considered in an exact manner, while the interactions with remote bands are accounted for in second order perturbation theory. This eight-band model, which simultaneously takes into account the nonparabolicity of the electron- and light hole dispersion and the complex structure of the valence band , describes the energy band structure around the Γ point of the Brillouin zone very well.

In the three-band Kane's Hamiltonian the valence and conduction bands interaction is taken into account via the only matrix element *P* (so called Kane's parameter). The system of Kane equations for the case of strong spin-orbital interaction $\Delta >> E_g$ have the from [7, 8]:

$$\left(\varepsilon_c(r)-E\right)C_1-\frac{Pk_+}{\sqrt{2}}C_3+\sqrt{\frac{2}{3}}Pk_zC_4+\frac{Pk_-}{\sqrt{6}}C_5=0 \quad (1)$$

$$\left(\varepsilon_c(r)-E\right)C_2-\frac{Pk_+}{\sqrt{6}}C_4+\sqrt{\frac{2}{3}}Pk_zC_5+\frac{Pk_-}{\sqrt{2}}C_6=0 \quad (2)$$

$$-\frac{Pk_-}{\sqrt{2}}C_1+\left(\varepsilon_v(r)-E\right)C_3=0 \quad (3)$$

$$\sqrt{\frac{2}{3}}Pk_zC_1-\frac{Pk_-}{\sqrt{6}}C_2+\left(\varepsilon_v(r)-E\right)C_4=0 \quad (4)$$

$$\frac{Pk_+}{\sqrt{6}}C_1+\sqrt{\frac{2}{3}}Pk_zC_2+(\varepsilon_v(r)-E)C_5=0 \tag{5}$$

$$\frac{Pk_+}{\sqrt{2}}C_2+(\varepsilon_v(r)-E)C_6=0 \tag{6}$$

Here P is the Kane parameter, and $k_\pm=k_x\pm ik_y$, $\vec{k}=-i\vec{\nabla}$, $\varepsilon_c(r)$ is the band edge potential for conduction band and $\varepsilon_v(r)$ is the band edge potential for valence band and C_i are envelope functions. Let's introduce an external electric field $V(r)$ to compensate the position dependence of the band edge of valence band potential $\varepsilon_v(r)$, where $V(r)=-\varepsilon_v(r)$. Thus the Kane equations will be as follows:

$$(\varepsilon_c(r)-\varepsilon_v(r)-E)C_1-\frac{Pk_+}{\sqrt{2}}C_3+\sqrt{\frac{2}{3}}Pk_zC_4+\frac{Pk_-}{\sqrt{6}}C_5=0 \tag{7}$$

$$(\varepsilon_c(r)-\varepsilon_v(r)-E)C_2-\frac{Pk_+}{\sqrt{6}}C_4+\sqrt{\frac{2}{3}}Pk_zC_5+\frac{Pk_-}{\sqrt{2}}C_6=0 \tag{8}$$

$$-\frac{Pk_-}{\sqrt{2}}C_1-EC_3=0 \tag{9}$$

$$\sqrt{\frac{2}{3}}Pk_zC_1-\frac{Pk_-}{\sqrt{6}}C_2-EC_4=0 \tag{10}$$

$$\frac{Pk_+}{\sqrt{6}}C_1+\sqrt{\frac{2}{3}}Pk_zC_2-EC_5=0 \tag{11}$$

$$\frac{Pk_+}{\sqrt{2}}C_2-EC_6=0 \tag{12}$$

If we eliminate the expressions (9) -(12) into formulas (7) and (8) we obtain:

$$\left\{-E-\varepsilon_v(r)+\varepsilon_c(r)-\frac{2P^2}{3E}\Delta_3\right\}C_{1,2}=0 \tag{13}$$

where Δ_3 three dimensional Laplacien and $-\varepsilon_v(r)+\varepsilon_c(r)=E_g(r)$ the band gap potential energy. Let's assume that the band gap potential is $E_g(r)=E_g(0)+\frac{\gamma r^2}{2}+\frac{a}{r^2}+\frac{b}{r^2\sin^2\theta}$. Where a and b are constant have the dimensions of Joule ·m^2 Equation (13) can be written as follows according to the above expressions.

$$\left\{-E+E_g(0)-\frac{2P^2}{3E}\Delta_3+\frac{\gamma r^2}{2}+\frac{a}{r^2}+\frac{b}{r^2\sin^2\theta}\right\}C_{1,2}=0 \tag{14}$$

Since the problem has a spherical symmetry, we seek a solution to the differential equation in the form

$$C_{1,2}(r,\theta,\varphi)=\frac{1}{r}F_{1,2}(r)\Theta(\theta)\exp(im\varphi) \qquad m=0,\pm1,\pm2,.. \tag{15}$$

Substituting equation (15) into Eq. (14) allows us to obtain the angular wave function and the radial one as

$$\left(\frac{d^2}{dr^2}-\frac{\gamma r^2}{2}\frac{3E}{2P^2}+\frac{3E(E-E_g(0))}{2P^2}-\frac{a}{r^2}\frac{3E}{2P^2}-\frac{\lambda}{r^2}\right)F_{1,2}(r)=0 \tag{16}$$

$$\frac{1}{\sin\theta}\frac{\partial}{\partial\theta}\left(\sin\theta\frac{\partial\Theta(\theta)}{\partial\theta}\right)+\left(\lambda-\frac{m^2}{\sin^2\theta}-\frac{b}{\sin^2\theta}\frac{3E}{2P^2}\right)\Theta(\theta)=0 \tag{17}$$

with the constant λ to be determined below.

Let's introduce a new notation;

$$\xi = \sqrt{m^2 + \frac{3Eb}{2P^2}}, \quad \lambda = \ell'(\ell'+1), \quad x = \cos\theta \tag{18}$$

Substitution of Eq. (18) into Eq. (17) leads to

$$(1-x^2)\frac{d^2\Theta(x)}{dx^2} - 2x\frac{d\Theta(x)}{dx} + \left[\ell'(\ell'+1) - \frac{\xi^2}{1-x^2}\right]\Theta(x) = 0 \tag{19}$$

whose normalized solution can be obtained as [11]

$$\Theta_{\ell'\xi}(\theta) = \sqrt{\frac{\ell'+1}{2}\frac{\ell'-\xi}{\Gamma(\ell'+\xi+1)}}(\sin\theta)^{\xi}\sum_{k=0}^{\left[\frac{\ell'-\xi}{2}\right]}\frac{(-1)^k\Gamma(2\ell'-2k+1)}{2^{\ell'}k!(\ell'-2k-\xi)\Gamma(\ell'-k+1)}(\cos\theta)^{\ell'-2k-\xi} \tag{20}$$

with

$$\ell' = \xi + k, \quad k = 0,1,2,.. \tag{20}$$

If we introduce the following notation

$$b^2(E) = \frac{3E(E - E_g(0))}{2P^2} \tag{21}$$

$$\chi^2 = \frac{\gamma}{2}\frac{3E}{2P^2} \tag{22}$$

$$\alpha = a\frac{3E}{2P^2} \tag{23}$$

$$\alpha + \lambda = L(L+1) \tag{24}$$

equation (16) can be written as

$$\frac{d^2F_{1,2}(r)}{dr^2} + \left(b^2(E) - \chi^2r^2 - \frac{L(L+1)}{r^2}\right)F_{1,2}(r) = 0 \tag{25}$$

Taking into account the asymptotic behavior of $F_{1,2}(r)$ for $r \to 0$ and for $r \to \infty$, we look for a solution $F_{1,2}(r)$ in the form of [12]:

$$F_{1,2}(r) = r^{L+1}\exp\left(-\frac{\chi}{2}r^2\right)u(r) \tag{26}$$

Substituting (26) into (25), we get the following equation for the function *u(r)*:

$$\frac{d^2u}{dr^2} + 2\left(\frac{L+1}{r} - \chi r\right)\frac{du}{dr} - \left\{2\chi\left(L+\frac{3}{2}\right) - b^2(E)\right\}u = 0 \tag{27}$$

Introducing a new independent variable $\xi = \chi r^2$, we obtain the following differential equation from (27):

$$\xi\frac{d^2u}{d\xi^2} + \left(L+\frac{3}{2}-\xi\right)\frac{du}{d\xi} + \left\{\frac{1}{2}\left(L+\frac{3}{2}\right) - \frac{1}{2}s\right\}u = 0 \tag{28}$$

where

$$s = \frac{b^2(E)}{2\chi} = \frac{E - E_g(0)}{2P}\sqrt{\frac{3E}{\gamma}} \tag{29}$$

The solution of equation (28) is a confluent hypergeometric function

$$u =_1 F_1\left\{\frac{1}{2}\left(L+\frac{3}{2}-s\right), L+\frac{3}{2}; \xi\right\} \tag{30}$$

The condition that $F_{1,2}(r)$ decreases for $r \to \infty$ gives us

$$\frac{1}{2}\left(L+\frac{3}{2}-s\right) = -n_r \qquad (n_r = 0,1,2,...) \tag{31}$$

and consequently the energy levels are given by

$$\frac{E-E_g(0)}{2P}\sqrt{\frac{3E}{\gamma}}=\left(L+2n_r+\frac{3}{2}\right). \tag{32}$$

Where L is found from equation (24) as follows:

$$L=\frac{1}{2}\sqrt{1+4\left(a\frac{3E}{2P^2}+\left(\sqrt{m^2+\frac{3Eb}{2P^2}}+k\right)\left(\sqrt{m^2+\frac{3Eb}{2P^2}}+k+1\right)\right)}-\frac{1}{2} \tag{33}$$

The Kane parameter P is expressed by the effective mass m_n of electrons as the following relation for strong spin-orbital interaction [9]:

$$\frac{2P^2}{3E_g}=\frac{\hbar^2}{2m_n} \quad \text{and} \quad \gamma=m_n\omega^2 \tag{34}$$

$$\left(E-E_g(0)\right)\sqrt{\frac{E}{E_g(0)}}=\left(\frac{1}{2}\sqrt{1+4\left(\frac{2m_n}{\hbar^2}\frac{Ea}{E_g(0)}+\left(\sqrt{m^2+\frac{2m_n}{\hbar^2}\frac{Eb}{E_g(0)}}+k\right)\left(\sqrt{m^2+\frac{2m_n}{\hbar^2}\frac{Eb}{E_g(0)}}+k+1\right)\right)}-\frac{1}{2}+2n_r+\frac{3}{2}\right)\hbar\omega \tag{35}$$

Equation (35) can be useful for analyzing the influence of nonparabolicity on the energy spectrum of electrons in quantum dots and determines only the energies of electrons in quantum dots.

For the parabolic case $\left(E-E_g(0)\right) << E_g(0)$, we obtain

$$E=E_g(0)+\left(\frac{1}{2}\sqrt{1+4\left(\frac{2m_n a}{\hbar^2}+\left(\sqrt{m^2+\frac{2m_n b}{\hbar^2}}+k\right)\left(\sqrt{m^2+\frac{2m_n b}{\hbar^2}}+k+1\right)\right)}-\frac{1}{2}+2n_r+\frac{3}{2}\right)\hbar\omega \tag{36}$$

If $a=b=0$ we obtain

$$E=E_g(0)+\left(\ell+2n_r+\frac{3}{2}\right)\hbar\omega \tag{37}$$

from (36) where $\ell=m+k$.

The equation (37) is the same as the solution of the Schrödinger equation for the harmonic oscillator potential.

The radial eigenfunctions are:

$$R_n^L(r)=N_n^L\frac{1}{r}F_{1,2}(r)=N_n^L r^L\exp\left(-\chi r^2/2\right){}_1F_1\left\{\frac{1}{2}\left(L+\frac{3}{2}-s\right),L+\frac{3}{2};\xi\right\} \tag{38}$$

with a normalized factor N_n^L to be determined below.

The confluent hypergeometric functions can be expressed by the associated Laguerre polynomials [13]:

$$L_n^\alpha(x)=\frac{\Gamma(\alpha+n+1)}{n!\Gamma(\alpha+1)}\cdot{}_1F_1\{-n,\alpha+1;x\} \tag{39}$$

from which, together with the following important formula [13]:

$$\int_0^\infty x^\alpha e^{-x}L_n^\alpha(x)L_m^\alpha(x)=\frac{\Gamma(\alpha+n+1)}{n!}\delta_{nm} \tag{40}$$

we can finally obtain the orthonormality relation for the radial wave functions as

$$\int_0^\infty R_n^L(r)R_m^L(r)r^2dr=\delta_{nm} \tag{41}$$

where the radial wave function is given by

$$R_n^L(r)=N_n^L r^L\exp\left(-\chi r^2/2\right)\cdot L_n^{L+\frac{1}{2}}\left(\chi r^2\right) \tag{42}$$

with

$$N_n^L=\chi^{\frac{2L+3}{4}}\cdot\sqrt{\frac{2n!}{\Gamma\left(L+n+\frac{1}{2}\right)}} \tag{43}$$

2. Conclusion

The exact solutions of Schrödinger equation for the electrons which have Kane spectrum, in the spherical potential well considering the position dependence of the edge of the valence and the conduction bands are studied. The results which are found can be used to describe the energy spectrum of electrons in the quantum dots which are growth from narrow band-gap semiconductors A^3B^5 (InSb, InAs etc.).

[1] *T. Chakraborty*. Quantum Dots, Elsevier 1999

[2] *N. Kim, G. Ihm, H.-S. Sim, and T. W. Kang*. Phys. Rev B, Vol. 63, 235317, (2001).

[3] *Shi-Hai Dong , Guo-Hua Sun , M. Lozada-Cassou*. Physics Letters A 328 (2004) 299–305

[4] *K Barnham, D. Vredansky*. "Low-dimensional semiconductor structures", Cambridge University Press 2001.

[5] *Edward Chen, O.Voskoboynikov, C.P.Lee.* Solid State Communications 125, 381-385, (2003)

[6] *Su Ru-keng and Zhang Yuhong* . J. Phys. A: Math.Gen.17 851-857,(1984)

[7] *E. O. Kane.* J. Phys. Chem. Solids 1, 249, (1957)

[8] *T.Darnhofer and U.Rössler*. Phys. Rev B, v47, p16020 (1993)

[9] *W. Zawadzki, S. Klahn and U. Merkt*. Phys. Rev B, v33, p16916 (1986)

[10] *B. R:Lassing*. Phys. Rev B, v31, p8086 (1985)

[11] *C.Y. Chen, D.S. Sun, Y.W. Liu.* Acta Phys. Sinica 51 (2002) 468 (in Chinese)

[12] *I.I. Goldman and V.D. Krivchenko*. Problems in quantum mechanics, Dover Publications, New York.

[13] *I.S. Gradshteyn, I.M. Ryzhik.* Tables of Integrals, Series, and Products, fifth ed., Academic Press, New York, 1994.

A.M. Babayev

QEYRİ-BİRCİNS ELEKTRİK VƏ HƏLQƏŞƏKİLLİ QEYRİ SFERİK OSSİLYATOR POTENSİALI SAHƏSİNDƏ KEYN TƏNLİKLƏRİNİN DƏQİQ HƏLLİ

Qadağan zolağın eni koordinatdan asılı olan darzolaqlı yarımkeçirici nanokristallarda elektronların dispersiya qanununun qeyri-parabolikliyi nəzərə alınmaqla, valent zonasının kənarının koordinatdan asılılığını kompensasiya edən xarici qeyri-bircins elektrik sahəsində elektronların enerji spektri nəzəri olaraq öyrənilmişdir. Qadağan zolağının koordinatdan asılı olduğu Keyn tənliyinin dəqiq həlli tapılmışdır. Zonanın kənarları üçün potensial kimi həlqəşəkilli, qeyri-sferik ossilyator potensialı götürülmüşdür: $V(r) = \frac{\gamma r^2}{2} + \frac{a}{r^2} + \frac{b}{r^2 \sin^2 \theta}$.

A.M. Бабаев

ТОЧНОЕ РЕШЕНИЕ УРАВНЕНИЯ КЕЙНА В УЗКОЩЕЛЕВЫХ ПОЛУПРОВОДНИКОВЫХ НАНОКРИСТАЛЛАХ С ПОЗИЦИОННО ЗАВИСЯЩЕЙ ЩЕЛЬЮ, ВО ВНЕШНЕМ НЕОДНОРОДНОМ ЭЛЕКТРИЧЕСКОМ ПОЛЕ, КОМПЕНСИРУЮЩЕМ ПОЗИЦИОННУЮ ЗАВИСИМОСТЬ КРАЯ ВАЛЕНТНОЙ ЗОНЫ

Теоретически изучен энергетический спектр электронов в узкощелевых полупроводниковых нанокристаллах с позиционно зависящей щелью во внешнем неоднородном электрическом поле, компенсирующем позиционную зависимость края валентной зоны, с учетом непараболичности закона дисперсии электронов. Найдено точное решение уравнений Кейна с позиционно зависящей энергетической щелью. Потенциал для краев зон выбран в виде кольцеобразного несферического осцилляторного потенциала $V(r) = \frac{\gamma r^2}{2} + \frac{a}{r^2} + \frac{b}{r^2 \sin^2 \theta}$.

Received: 16.12.05

THE MODERN PROBLEMS OF THERMO-ELECTRIC MATERIALS SCIENCE

F.K. ALESKEROV
Scientific-Production Association "Selen" NASA
Baku-1143, F. Agayev, 14

The analysis shows, that the crystals on the base of Bi and Sb chalcogenides, obtained by the method of molecular-beam epitaxy, are the more perspective materials for thermo-electrical cooling. However, the thermo-electric cooling devices on the materials, produced by the method of powder metallurgy are still realized practically. This is the more profitable economically technological operation. The standard thermo-batteries on the base of AIN ceramic with the use of polycrystals are realized and treated over the World.

The modern problems of material treatment for thermo-electric solid-state cooling and electro-generation have been discussed. The data, published during 10 years are given. The following questions had been included in the base of the review:

1. The technology of the obtaining (synthesis, metalo-ceramic method, extrusion) and growing up of the crystals (methods of Chochralsky, Bridgmen and directed crystallization);
2. The homogeneity of complex doped solid solutions, the heterogeneity of impurity segregation on interlayered borders;
3. Thermo-electric efficacy in the interconnection with structure changes;
4. The artificially anisotropic materials with different layers;
5. The nano-structural film thermoelectrics.

The present paper is dedicated to the analysis of the literature data on the above mentioned problems and choice of more technological methods of thermo-element production (TE).

The considered methods. The main methods of material obtaining on the base Bi and Sb chalcogenides are:

- the obtaining of perfect monocrystals by Chochralsky method;
- the growing up of directed crystals (DC) by the method of vertically directed crystallization, and also by HF-heating;
- crystallization from the solutions by Bridgmen method;
- the obtaining of the samples by the method of powder metallurgy;
- the obtaining of the samples by extrusion method;
- the evaporation by thermal method
- the growing up of nano-structural elements by the method of electron-beam epitaxy.

The monocrystals of above mentioned layered crystals and their solid solutions are better grown up by Chochralsky method with alloy replenishment of liquid phase from floating crucible. They have high thermo-electric efficacies ($Z \geq (3{,}2\text{-}3{,}5)10^{-3}$ K^{-1}) and are used mainly for the study of physical properties of monocrystals of complex solid solutions. The termo-elements on their base are etalons as on maximal temperature overfalls, so on minimal temperatures of cool junctions of thermo-element (TE).

(DC), obtained by the vertical crystallization don't let to them on the efficacy. The crystals, obtained at the growing velocities are well used for TE (2-3)cm/h. At smaller velocities (less than 1 cm/h) it is possible to obtain the doped crystals Bi_2Te_3, Sb_2Te_3, Bi_2Se_3, Bi_2Se_3 and their solid solutions and eutectics. They are easily pricked on the basis plane (0001); on these layers at easy pricks the steps of different complexes are clearly seen (unnecessary, inclined from component stoichiometry, and also introduced impurities).

This method unites in itself not only obtaining of the crystals for the investigations, but the growing up of the complex high-effective alloys of half-manufacturing scale.

Bridgmen method. Many semiconductor crystals $A^{IV}B^{VI}$, $A_2^{III}B_3^{VI}$ are obtained by this method. This method has the set of advantages [1]: the experiment simplicity, the possibility of crystal obtaining with micro-structural characteristics and sizes of monocrystal regions, accessible for the study of physical properties. The monocrystal ingots by diameter 10-30mm can be obtained by the given method. On the investigation results [1] the microstructures of grown up crystals (for, example $A^{IV}B^{VI}$) at variation of the form of conic bottom of ampoule of alloy overheating ΔT^{+} relatively the furnace liquids temperature, the axes temperature gradient in stove ΔT_4 of velocity of ampoule broach √ has been established, that the creation of the monocrystalline seed crystal is more possible at the conditions: $\Delta T \leq 20$ K/cm, $\Delta T^{+} < 30$K, √ < 0,4 mm/h. The conic bottom of the ampoule should have the walls of equal width [1]. Indeed, the given method is seemed ineffective one at the serial manufacturing.

The widely-known metal-ceramic method and the extrusion of sample storages by the extrusion are the more technological ones for the manufacturing mastery. The ingots directly after synthesis in ampoule are obtained by these methods. The refs, in which the technologies of alloy obtaining of bigger volume (more 5kg) without quartz ampoules (for example in dielectric crucibles) are described, demand the special attention. The investigators prefer not to publish the processes of such type. The samples, obtained by cool (heat) pressing and extrusion are mainly used in all produced thermo-electric batteries (TB). It is need to note, that alloys of p-type are less effective ones ($\leq 2{,}6 \cdot 10^{-}3 \cdot K^{-1}$).

The influence of obtaining technology on the branch homogeneity TE (BTE). Let's compare and analyze (DC, pressed streaks-extrusions) on the heterogeneity of the composition in materials on the base of Bi and Sb tellurides, obtained by different methods after synthesis and from samples from them. The publications in this region are given in the following refs [2-5]. Not only thermo-electric properties of alloys in wide temperature intervals are discussed in them, but the parameters, influencing on the formation of micro- and macro-heterogeneities in growing crystals. The longitudinal and transversal heterogeneities, which are character for the considered alloys, homogenization questions and impurity introduction, are

such ones. The qualitative analysis of distribution curves of Se and Te shows on the presence in solid solutions, obtained by directed crystallization from the alloy and by extrusion method, longitudinal layered heterogeneity. Solid solutions, prepared by the methods of powder metallurgy reveal the micro-heterogeneities, statistically distributed on the volume. The size of micro-heterogeneities, observable in all samples was bigger ≥150mcm [2]. (DC) are more homogeneous ones; the samples, obtained by cool and heat pressing are less homogeneous ones.

The composition of n-type has the most homogeneity.

$Bi_2(Te_{0,94}\ Se_{0,06})_3$<0,01% CuBr>). These crystals in temperature interval 298-433°K have high value of parameter ZT (0,91). The decrease of concentration micro-heterogeneity in alloys is observed $Sb_{2-x}\ Bi_xTe_3$ at their obtaining by extrusion method in the conditions of superplasticity in the comparison with metaloceramic samples [2,5]. The high diffusion velocity in deformation hearth and micro-crystal structure of extruded samples cause to quick regulation of the composition.

The distribution of micro-thermo-electromotive force (α) on the length of the samples (for p-$Sb_{2-x}\ Bi_x\ Te_3$ (x=0,2 и x=0,5) qualitatively shows the bigger dispersal of the values from average in metaloceramic samples). The least dispersal in values of micro-electro-motive force is observed on extruded annealed samples [2,4].

The analysis of component distribution in crystals $Bi_x\ Sb_{2-x}\ E_{3+y}$ at x=0-2,0 y=0,03 by grown method of vertical band recrystallization shows, that solid solutions have non-equal homogeneity of element distribution on cross-section. The increase of Te content in alloy increases the homogeneity of Sb distribution on sample cross-section [6]. The decrease of quantity of excess Te leads to the appearance of the streaks of pure Te between grains of phases and to the appearance of grains of the given phases.

The monocrystals of more effective solid solutions of systems n-(Bi_2Te_3-Bi_2Se_3) and p-(Sb_2Te_3-Bi_2Te_3), grown up by Chochralsky method with alloy replenishment by liquid phase from floating crucible, are characterized by most homogeneity. The homogeneous content of Bi, Sb, Te on the cross-section and monocrystal length, doped by Se in the correspondence with cut $Sb_{1,5}\ Bi_{0,5}\ Te_3$-Bi_2Se_3 (Bi_2Se_3 till 15 mol%) is proved in [7], the effective distribution coefficient of Se in Sb_2Te_3-Bi_2Te_3 system has been defined. Its value is defined by the ratio Sb_2Te_3 and Bi_2Te_3 in the system and decreases from 1.25 till 0.70 with the increase of stibium telluride content [7].

Thus, the more homogeneous samples on length and cross-section are obtained by the methods: Chochralsky, Bridgmen and directed crystallization. The samples, obtained by methods of extrusion and powder metallurgy are less homogeneous ones.

Structure and electro-physical parameters of thermo-electric monocrystals Sb_2Te_3 and Bi_2Te_3

The thermo-electric properties are defined not only by impurity atoms, but by electrically active own defects. For the growing up of формула it is need to establish as the dependence of structure unsoundness from obtaining method, so its influence on the different properties. In this direction in the capacity of example can be investigations [8] of defects of crystalline structure and dislocation structure of monocrystals of bismuth telluride and its solid solutions by method of fairy electron microscopy. These investigations [8] show, that dislocation in basis plane are main type of defect: the presence of hexonal nets and parallel sets of dislocations has been established. The presence of packing defects, situated parallelly to the chip plane and very small dislocation loops has been revealed from contrast of electron-microscopic photos. The observable defects don't significantly influence on electric properties. However, some impurities, being in basis plane (0001) can significantly influence on anisotropy of crystal properties. That's why electron-microscopic photos always visually demonstrate the surface of glide plane (0001). It is possible to make the following conclusions about desirability of the presence in interlayered space the electroactive additions (as Cu and Ni), leading to the increase $Z_{opt.} \geq 3{,}2\cdot10^{-3}\cdot K^{-1}$ and hardening (BTE).

Anisotropic thermo-electric devices

Last years on the base of anisotropic crystals the transversal transformers, in which non-diagonal tensor component of thermo-electro-motive (α) force is used, have been created and treated. Moreover, the transversal voltage (besides thermo-electric parameters) strongly depends on the ratio of geometric sizes of thermoelement (TE) and because of this can achieve the bigger value. The anisotropic materials are created artificially with the aim of the increase of thermo-electric good quality. They present themselves the system of alternating parallel layers with different parameters [9]. The high-grade semiconductors of n- and p-type with significantly differed electro- and heat conductivities are the most initial components of such layered material.

Thus in the ref [9] the calculation of characteristics artificially anisotropic material, consisting on semiconductor and super-conductive layers (HTSC) was carried out by the authors. It is shown, that the use of the streaks from (HTSC) changes the optimization conditions of geometrical parameters of layered structure (layer angle of inclination and the ratio of their widths) in the comparison with normal semiconductors. Thermal-electrical efficacy and sensitivity (TE), prepared from the material with superconducting streaks, increases the corresponding parameters of the structure with the layers from the metal in 2-3 times [9].

The use of HTSC increases the sensitivity of the heat flow probe more than in three times. Thus, the treatment of strongly anisotropic heterophase TE is the actual task; also the results of author ref's are interest in this respect [10].

Multi-layer film hetero-structures for TE

The thin films of Bi and Sb chalcogenides and their multi-layer hetero-structures have the highest value (Z). The epitaxial films $(Bi,Sb)_2\ (Te,Se)_3$ with high values of power parameter $\eta=\alpha^2\delta$ are grown up with the help of the method of heat wall and method of molecular-beam epitaxy MBE [11]. The chemical method (MOCVD) for the obtaining of thin textured layers Bi_2Te_3 has been successfully used by authors of the ref. [12]. According to [13] the significant increase of Z can be achieved in the films with width α in several lattice constants; this increase of Z can be supplied as because of the η, so in the result of the decrease of lattice heat conductivity. Thin layers $(Bi, Sb)_2\ (Te, Se)_3$ with width or size of crystal grains in 50-20 nm can have the significant bigger value of Z, than corresponding monocrystals [11]. The plane-parallel hetero-structures, in which the layers of

thermo-electrical material are divided by thin barrier streaks from the material with excellent physico-chemical parameters are investigated experimentally [13]. The Bi_2Te_3 was used in hetero-structures on the base of the films Sb_2Te_3, obtained with the use of MOCVD in the capacity of the material of barrier streaks. This direction is significantly perspective from the point of view of the creation of new high-effective thermo-electrical materials with the use of micro-electron technologies.

What is the real picture, which is connected with the serial production of thermo-electrical batteries on the base of the created high-effective branches of TE.

The samples, "obtained by the method of powder metallurgy, extrusion and further directed polycrystals" are firstly the most economic TE for the industrial aims. The leading world firms (China, USA, Russia, Germany, France and others) use these samples at the assemblage of the thermo-electrical batteries on the base of AIN ceramic.

The conclusions: nowadays the metalo-ceramic processes, which are brazed on AIN ceramic, are the most economically technological ones for the serial production of thermo-batteries. The samples, obtained by epitaxial grafting of hetero-structural layers on the base of the same Bi and Sb chalcogenides will be more perspective for the future.

[1] *V.I. Shtanov*. J. Kristallographiya. 2004, t.49, №2, s. 343-349.

[2] *I.V. Gasenkova, V.A. Chubarenko, E.A. Tyavlovskaya, T.E. Svechnikova*. J. Poverkhnost. Rentgenovskie. Sinkhrotronnie I neytronnie issledovaniya. 2003, №3, s. 32-41.

[3] *Boo Yang, Jung, Tae Sung, Dow-Bin Hyun and Jae Dong*, Thermoelectric Properties of $(Bi_{0,25}, Sb_{0,75})_2Te_3$ Prepared by Mechanical Alloyind and Hot Pressing, Journal of the Korean Physical, Vol.31, №1, July 1997, p. 219-222.

[4] *Osamu Vamashita and Shoichi Tomiyoshi*, High performance n-tipe bismuth telluride with higly stable thermoelectric figure of merit, Journal of Applied PHYSICS, V. 95, №11, 2004, p. 6277-6283.

[5] *V.A. Chubarenko, I.V. Gasenkova, E.A. Tyavlovskaya, E.A. Kukharenko*. II Poverkhnost. Rentgenovskie. Sinkhrotronnie I neytronnie issledovaniya , 2001, №8, s.18.

[6] *G.A. Ivanov, V.A. Kulikov, T.N. Novgorodova*. II Materiali dlya termoelektricheskikh preobrazovateley. S.Peterburg: FTI im. A.F. Ioffa RAN, 1995, s.34.

[7] *L.D. Ivanova, Yu.V. Qranatkina, N.V. Polikarpova, E.I. Smirnova*. II Izv. AN, J. Neorganicheskie materiali, 1997, t.33, №6, s.669.

[8] *I.V. Gasenkova, T.E. Svechnikova*. Neorganicheskie materiali, 2004, t. 40, №6, s. 663-668.

[9] *D.A.Pshenay-Severin, Yu.I.Ravich, M.V.Vedernikov*. Fizika i tekhnika poluprovodnikov, 2000, t.34, v.4, s.1265-1269.

[10] *A.A Asheulov, I.V. Qutsul, A.A. Snarskiy*. Anizotropnie optikotermoelementi, sb. trudov Termoelektriki i ikh primeneniya, S.-Peterburg, 2002, s. 403-405.

[11] *Yu.A. Boykov, V.A. Danilov*. Ot tonkikh plyonok $(Bi_2Sb_2)_2(Te,Se)_3$ k mnoqosloynim geterostrukturam na ikh osnove: osobennosti rosta i effekti na mejfaznikh qranitsakh, sb.trudov «Termoelektriki i ikh primeneniya», S.-Peterburg, 2002, s. 231-236.

[12] *A. Giani, A. Boulouz, F. Pascal-Dellanoy, A. Foucaran*, Boyer., Thin Solid Films, 315,99,1999.

[13] *W.E. Bies, H. Ehrenreich, H. Runge*. J. Appl. Phys. 91,2033,2002.

F.K. Ələsgərov

TERMOELEKTRİK MATERİALŞÜNASLIĞIN MÜASİR PROBLEMLƏRİ

Bərk cisimlərin əsasında olan termoelektrik soyuducular və elektrogenerasiyalı materialların müasir problemləri müzakirə olunub, son 10 ildə çap olunmuş məqalələr göstərilib. Müzakirəyə aşağıdakı məsələlər çıxarılıb:

1. Texnoloji proseslər və kristalların göyərdilməsi (Çoxralski, Bridjmen və yönəlmiş kristallizasiya metodları);
2. Legirə olunmuş bircinsli çox komponentli bərk məhlulları; fəza aralığında aşqarların qeyri-bircinsliyin seqreqasiyası;
3. Struktur dəyişilməsi ilə əlaqədə olan termoelektrik effektivliyi;
4. Laylı süni anizotropik materialları;
5. Nanostrukturlu nazik təbəqəli termoelektriklər.

Ф.К. Алескеров

СОВРЕМЕННЫЕ ПРОБЛЕМЫ ТЕРМОЭЛЕКТРИЧЕСКОГО МАТЕРИАЛОВЕДЕНИЯ

Анализ показал, что наиболее перспективными материалами для термоэлектрического охлаждения являются кристаллы на основе халькогенидов висмута и сурьмы, полученные методом молекулярно лучевой эпитаксией. Однако практически пока реализованы термоэлектрические охлаждающие устройства на материалах, изготовленных методом порошковой металлургии. Это наиболее выгодная экономически технологическая операция. Во всем мире разработаны и реализуются в продаже стандартные термобатареи на основе AlN керамики с использованием поликристаллов.

Received: 16.11.05

PHOTOLUMINESCENT PROPERTIES OF GLASSES IN THE SYSTEM La_2O_3 - Ga_2S_3- $Ln^I{}_2O_3$ (WHERE Ln^I-Ce, Er)

S.A. ABUSHOV, H.B. GANBAROVA
Institute of Physics of National Academy of Sciences of Azerbaijan
Az-1143, Baku, H. Javid av., 33

I.B. BACHTIYARLI, O.Sh. KERIMLI
Institute of Chemical Problems of National Academy of Sciences of Azerbaijan
Az-1143, Baku, H. Javid av., 31

The photoluminescent properties of glasses $(Ga_2S_3)_{0,80}(La_2O_3)_{0,10}(Ce_2O_3)_{0,10}$, $(Ga_2S_3)_{0,65}(La_2O_3)_{0,33}(Er_2O_3)_{0,02}$, $Ga_2S_3)_{0,65}(La_2O_3)_{0,28}(Er_2O_3)_{0,07}$ and $(Ga_2S_3)_{0,65}(La_2O_3)_{0,30}(Er_2O_3)_{0,05}$ have been investigated. It is established, that glasses of given composition have the photoluminescent properties, intensity of which depends on quantitative content of Er_2O_3.

The glasses on the base of complex lanthanoid oxisulphides are used in the capacity of matrix, in which the 4 *f*-membranes are totally present or absent and the rest corresponding lanthanoid ions are applied in the capacity of activator, presenting the interest as from position of the revealing of common regularities of chemistry of rare elements, physics and chemistry of solid body, so in the plan of the creation of new materials with special properties.

That's why the aim of present paper was the investigation of photoluminescent properties of glasses $(Ga_2S_3)_{0,80}(La_2O_3)_{0,10}(Ce_2S_3)_{0,10}$, $(Ga_2S_3)_{0,65}La_2O_3)_{0,33}(Er_2O_3)_{0,02}$, $(Ga_2S_3)_{0,65}(La_2O_3)_{0,28}(Er_2O_3)_{0,07}$ and $(Ga_2S_3)_{0,65}(La_2O_3)_{0,30}(Er_2O_3)_{0,05}$.

Experimental part

In the capacity of initial components *β*- Ga_2S_3, *A*- La_2O_3, *A*-Ce_2O_3 and *C*- Er_2O_3 were used. *β*- Ga_2S_3 has the monoclinic syngony, which analogical to literature data [1]. *A*- La_2O_3 and *A*-Ce_2O_3 are crystallized in hexanal syngony, *C*- Er_2O_3 - in cubic syngony, corresponding to the lattice parameters in [2].

The synthesis of the samples of glasses, consisting from the given components, was carried out under the pressure of sulfur steams at 1425K in glass-graphite crucible, put into quartz reactor [3]. The synthesis was continued during 2,5 hours; further tempering was carried out at the temperature from 1425K by the means of the putting into the water at room temperature.

The photoluminescent (PL) spectrums of the investigated glasses were fixed on manufacture installation SDL-1. The sample excitation was carried out by helium-cadmium laser by the type LPM-11 (λ-441,6nm). The photoelectron multiplier FEU-39A was used as radiation receiver. The luminescence registration was carried out on the single-beam scheme with the help of the electron self-recording potentiometer KSP-4.

The results and their discussion

The photoluminescent properties of glasses in temperature range 77÷300K were investigated.

The PL spectrums of glasses $(Ga_2S_3)_{0,80}(La_2O_3)_{0,10}(Ce_2S_3)_{0,10}$ at different temperatures (1 - 77K, 2 - 190K, 3 - 300K) are presented on the fig.1. It is seen, that PL spectrum captures the region of wave lengths 460÷700nm. The pronounced three maximums at 537, 550 and 590 nm are observed on the spectrum at the temperature 77K. The observable pronounced maximums are joint and become insignificant at 190K, the spectrum has the bell-shaped form with one maximum at 540nm at 300K.

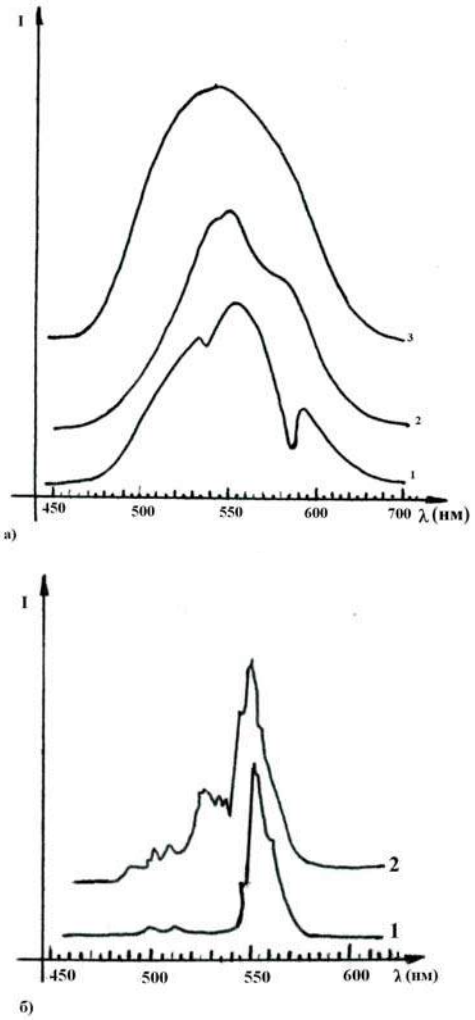

Fig.1. The PL spectrums of glass $(Ga_2S_3)_{0,80}(La_2O_3)_{0,10}(Ce_2O_3)_{0,10}$ at 1-77, 2-190, 3-300K (a), $(Ga_2S_3)_{0,65}(La_2O_3)_{0,33}$ at 1-77 and 2-300K (b).

The observable broadband radiations on PL spectrum are connected probably with matrix defects (fig.1). The PL spectrum broad-band form at 300K is connected with quazi-conrtinuous distribution of the levels of radiation

recombination in the forbidden band of the given material. The emphasizing of the maximums in PL spectrums at 537, 550 and 590 nm in the temperature range 77 and 190K probably connects with the decrease of temperature widening of the bands, connected with matrix defects.

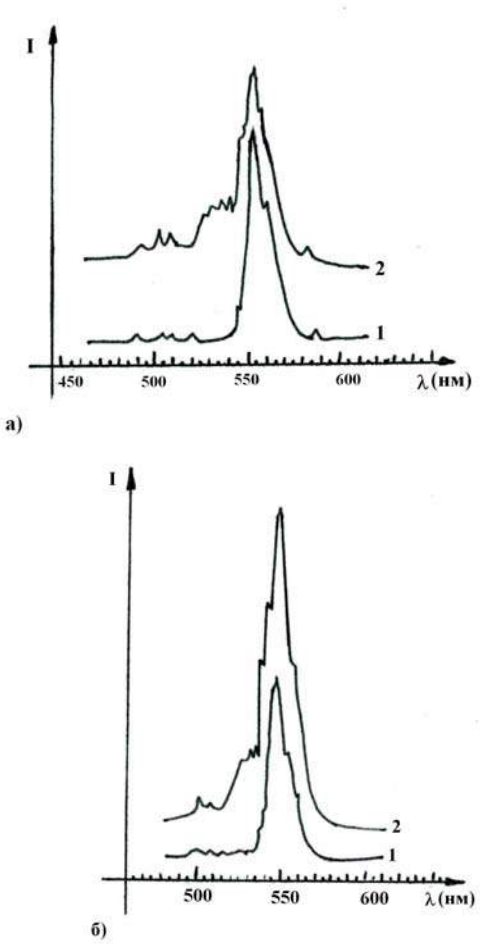

Fig.2. The PL spectrum of glass $(Ga_2S_3)_{0,60}La_2O_3)_{0,35}(Er_2O_3)_{0,05}$ (a), $(Ga_2S_3)_{0,65}(La_2O_3)_{0,28}(Er_2O_3)_{0,07}$ (b) at 1-77K and 2-300K.

The PL spectrums of glass $(Ga_2S_3)_{0,65}(La_2O_3)_{0,33}(Er_2O_3)_{0,02}$ at 77 and 300K are presented on the fig. 1b. These spectrums capture the spectral region 450÷580 nm. The two weak peaks at 500 and 512 nm at 77K are observed on the spectrum, the one intensive peak at 550 nm and the step at 562 nm, and new weak peaks appear on the spectrum at 300K in short-wave region at 490, 500, 502, 511 nm, the relative intensive peaks - at 528, 533, 537 nm and intensive peaks – at 545, 550 and 555 nm.

The observable intensive peak at 550 nm and the step at 562 nm on PL spectrum of glass at 77K are connected with internal-centered transfers $^4S_{3/2}$- $^4I_{15/2}$ of Er^{3+} ion [4,5]. This fact also proves by that at the temperature change from 77 till 300K the energetic state of maximums of these bands doesn't change (fig.1b).

The appearance of new weak bands of PL in the region 525÷537 nm at 300K and the increase of the value of peak half-width 550nm probably are connected with transfer $^4H_{11/2} \rightarrow {}^4I_{15/2}$ of ion Er^{3+} (fig.1b) [4,6].

The Pl spectrums of glass $(Ga_2S_3)_{0,65}(La_2O_3)_{0,28}(Er_2O_3)_{0,07}$, $(Ga_2S_3)_{0,65}(La_2O_3)_{0,30}(Er_2O_3)_{0,05}$ at 77 and 300K are presented on the fig.2 a, b.

From the picture it is seen, that PL spectrums of both glasses are almost similar. The revealed new bands in the spectrums of glass compositions $(Ga_2S_3)_{0,80}(La_2O_3)_{0,10}(Ce_2O_3)_{0,10}$, $(Ga_2S_3)_{0,65}(La_2O_3)_{0,33}(Er_2O_3)_{0,02}$, $(Ga_2S_3)_{0,65}(La_2O_3)_{0,28}(Er_2O_3)_{0,07}$, which are absent in spectrums $(Ga_2S_3)_{0,65}(La_2O_3)_{0,30}(Er_2O_3)_{0,05}$.are connected with the fact, that ions Er_2O_3 in these glasses are in different surroundings.

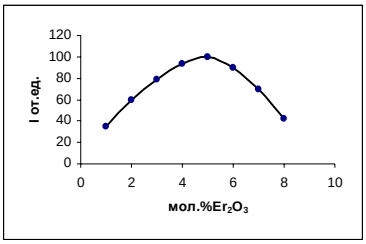

Fig.3. The dependence of radiation intensity on the $(Er_2O_3)_x$ content for glasses $(Ga_2S_3)_{0,65}La_2O_3)_{0,35}(Er_2O_3)_x$ at 300K.

Thus, the photoluminescence, the intensity of which depends on percent content of erbium oxide in them is observed in glasses of the compositions $(Ga_2S_3)_{0,80}(La_2O_3)_{0,10}(Ce_2O_3)_{0,10}$, $(Ga_2S_3)_{0,65}(La_2O_3)_{0,33}(Er_2O_3)_{0,02}$, $(Ga_2S_3)_{0,65}(La_2O_3)_{0,28}(Er_2O_3)_{0,07}$ and $(Ga_2S_3)_{0,65}(La_2O_3)_{0,30}(Er_2O_3)_{0,05}$, i.e. the intensity increases and further increase of Er_2O_3 content decreases with the increase of percent content Er_2O_3 till 5%.

[1]. *I. Goodyear, G.A. Steigmann.* Acta crist. 1963. v.16. N10. p.946.

[2]. *V.B. Glushkova*. Polimorfizm okislov redkozemel-nikh elementov. L. Nauka, 1967. 133s. (In Russian).

[3]. *I.B. Bakhtiyarov, O.Sh. Karimov*. Kimya problemlari jurnali. 2003.№3. s.27. (in Azerbaijan).

[4]. Spektroskopiya kristallov. Pod. red. *A.A. Kaminskiy, Z.L. Mortenshtern, D.T. Sviridov*. Izd., «Nauka». Moskow 1975. 384s. (in Russian)

[5]. *B.G. Tagiyev, O.B. Tagiyev, S.A. Abushov, F.A. Kyazimova, P.Benaloun, K. Bartau*. Luminescenciya kristallov $EuGa_2S_4$:Er. Trudi V mejdunarodnoy konferencii. Optika, optoelektronika I tekhnologii. 2003. 125s. (in Russian).

[6]. *Ch.Barthou, P.Benalloul, B.G.Tagiev, O.B. Tagiev, S.A.Abushov, F.A.Kazimova and A.N.Georgobiani*. J.Phys: Condens. Matter 16, 2004, p. 8075-8084.

S.A. Abuşov, X.B. Qənbərova, İ.B. Bəxtiyarlı, O.Ş. Kərimli

La_2O_3 - Ga_2S_3- $Ln^I_2O_3$ SİSTEMLƏRİNDƏ ŞÜŞƏLƏRİN FOTOLÜMİNESSENSİYA XASSƏLƏRİ

$Ga_2S_3)_{0,80}(La_2O_3)_{0,10}(Ce_2O_3)_{0,10}$, $(Ga_2S_3)_{0,65}(La_2O_3)_{0,33}(Er_2O_3)_{0,02}$, $Ga_2S_3)_{0,65}(La_2O_3)_{0,28}(Er_2O_3)_{0,07}$ və $(Ga_2S_3)_{0,65}(La_2O_3)_{0,30}(Er_2O_3)_{0,05}$ tərkibli şüşələrin fotolüminessensiya xassəsi tədqiq edilmişdir. Müəyyən olunmuşdur ki, bu tərkibli şüşələr fotolüminessensiya xassəsi göstərir və intensivlik tərkibdəki Er_2O_3 miqdarından asılıdır.

С.А. Абушов, Х.Б. Ганбарова, И.Б. Бахтиярлы, О.Ш. Керимли

ФОТОЛЮМИНЕСЦЕНТНЫЕ СВОЙСТВА СТЕКОЛ В СИСТЕМЕ $La_2O_3 - Ga_2S_3 - Ln^I_2O_3$ (где Ln^I-Ce, Er)

Исследованы фотолюминесцентные свойства стекол $(Ga_2S_3)_{0,80}(La_2O_3)_{0,10}(Ce_2O_3)_{0,10}$, $(Ga_2S_3)_{0,65}(La_2O_3)_{0,33}(Er_2O_3)_{0,02}$, $Ga_2S_3)_{0,65}(La_2O_3)_{0,28}(Er_2O_3)_{0,07}$ и $(Ga_2S_3)_{0,65}(La_2O_3)_{0,30}(Er_2O_3)_{0,05}$. Установлено, что стекла вышеуказанного состава обладают фотолюминесцентными свойствами, интенсивность которых зависит от количественного содержания Er_2O_3.

Received: 05.10.06

$TlIn_{1-x}Se_2$ TİP KRİSTALLARIN PYEZOELEKTRİK XASSƏLƏRİ

E.M. QOCAYEV, K.C. GÜLMƏMMƏDOV, G.S. CƏFƏROVA, H.S. ORUCOV, S.S. OSMANOVA

Azərbaycan Texniki Universiteti,
Baku, 370073, H. Javid av.

Təqdim olunan işdə $TlIn_{1-x}Ln_xSe_2$ tip kristalların pyezoelektrik xassələrinin tədqiqinin nəticələri verilmiş və baza birləşməsi olan $TlIn_{1-x}Se_2$-nin zona quruluşuna əsasən alınmış nəticələrin müzakirəsi aparılmışdır. Müəyyən edilmişdir ki, $TlInSe_2$ -nin kristallik qəfəsində üçvalentli indium atomlarının üçvalentli lantanoidlərlə əvəz edilməsi ilə bu kristalların tenzohəssaslıq əmsalını artırmaq və idarə etmək olar.

Məlum olduğu kimi TlSe tip çoxkomponentli birləşmələr yüksək tenzohəssaslıq əmsalına malik olmaları ilə fərqlənirlər [1-5]. Bu tip birləşmələr içərisində $TlInSe_2$ kristalı xüsusi yer tutur [6,7]. Bu onunla əlaqədardır ki, tenzorezistorların hazırlanması zamanı meydana çıxan çətinliklər, yəni nümunələrin kəsilməsi və emal edilməsi, onların səthinin cilalanması, xüsusi kimyəvi üsulla səthinin mexaniki qüsurlu hissəsinin yox edilməsi və s. $TlInSe_2$ kristalından istifadə edildikdə çox sadələşir və böyük zəhmət tələb etmədən həyata keçirilir. $TlInSe_2$ birləşməsinin və onun əsasında bərk məhlulların monokristalları təbii düzbucaqlı formaya və güzgü səthlərə malik olurlar. Belə ki, göstərilən tip monokristallar, en kəsiklərinin sahəsi təxminən $0,1\div0,2mm^2$, uzunluqları 1-50mm olmaqla müxtəlif ölçülərdə olurlar. Bu kristallardan iti uclu kəsici alətlə, çox asanlıqla tenzoötürücü hazırlamaq üçün nümunələr seçmək mümkün olur. Bu nümunələrə etibarlı mexaniki kontakt, kondensator boşalması ilə təsirsiz qaz mühitində naqillərin birbaşa nümunəyə lehimlənməsi ilə vurulur. Ötürücülərin hazırlanmasında altlıq olaraq 45 markalı, qalınlığı $0,5\div1$mm, uzunluğu 20-100mm olan polad lövhələrdən istifadə edilir. Səthinin işlənməsinə görə altlıq 7-ci sinifdən aşağı olmamalıdır. Altlıq əvvəlcə toluol vasitəsilə diqqətlə təmizlənir, sonra isə etil spirti ilə yuyulur. Bu üsulla təmizlənmiş altlığın üzərinə epoksid-krezol lak (EP-96) təbəqəsi çəkilir. Bu təbəqənin qalınlığı 10-15 mkm tərtibdə olmalıdır. Altlıq üzərinə lak çəkilərkən onun səth üzərində bərabər paylanmasına nail olmaq lazımdır. Altlıq otaq temperaturunda 1 saat saxlandıqdan sonra yüksək temperaturlu polimerləşməni həyata keçirmək üçün quruducu şkafda yerləşdirilir. Temperatur tədricən 470 K-ə qədər qaldırılır və bu temperaturda altlığın 1 saat saxlanılması tam polimerləşməni təmin edir. Bu prosesdən sonra altlıq üzərinə nümunənin həndəsi ölçüsündən böyük ölçüdə 2-ci lak təbəqəsi çəkilir. Yuxarıda qeyd etdiyimiz qaydada kontakt vurulmuş kristal altlığın ikiqat lak təbəqəsi ilə örtülmüş hissəsində yerləşdirilir və ehmalca sıxılır. Bundan sonra kristalın səthi tamamilə lakla örtülür. Bu proses həyata keçirilərkən altlıq üzərində nümunəni ixtiyari istiqamətdə yönəltmək olar. Nümunənin altlıq üzərində stabil vəziyyətini təmin etmək üçün o, nazik (eni 1.5 mm olan) ftoroplast lentlə bağlanılır. Nümunə ilə altlıq arasındakı bağlayıcı təbəqələri tam qurutmaq üçün bu sistem əvvəlcə 290-300K temperaturda 1 saat saxlanılır və bundan sonra 1.5 saat müddətində 460K temperaturda tabalma həyata keçirilir. Bu prosesdən sonra lentin açılması nümunənin halına heç bir mənfi təsir etmir və nümunə ölçmə üçün yararlı sayılır.

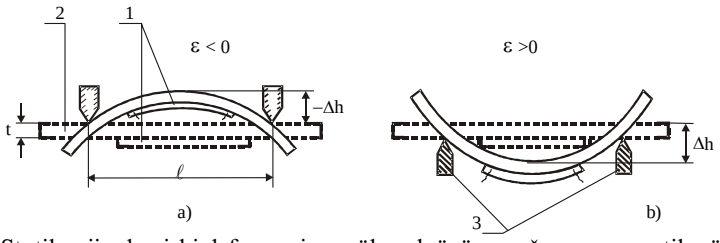

Şəkil 1. Statik rejimdə nisbi deformasiyanı ölçmək üçün qurğunun sxematik görünüşü: 1-kristal nümunə; 2-polad altlıq; 3-kənar dayaqlar.

$TlIn_{1-x}Ln_xSe_2$ kristallarından bu qayda üzrə hazırlanmış nümunələrin tenzohəssaslığı [8] işində təsvir olunan qurğuda statik rejimdə ölçülmüşdür. Kristala deformasiya şəkil 1-də təsvir olunan xüsusi qurğu ilə ötürülür. Güzgü üzlü, düzbuğaqlı «sap şəkilli» kristallar (1) yapışdırılmış, qalınlığı t olan polad tircik (2) bir-birindən l qədər məsafədə yerləşən iti uclu (3) dayaqları üzərində yerləşdirilir. Əyilmə zamanı tirciyin orta hissəsinin yerdəyişməsi Δh olur. Bu zaman nisbi deformasiyanın qiyməti

$$\varepsilon = \frac{4t}{l^2}\Delta h \qquad (1)$$

düsturu ilə, nümunənin tenzohəssaslıq əmsalı isə

$$K = \frac{R_\varepsilon - R_0}{R_0\varepsilon} = \frac{\Delta R_{\varepsilon,0}}{R_0\varepsilon} \qquad (2)$$

kimi təyin edilir. Burada R_ε- deformasiya olduqda, R_0 isə deformasiya olmadıqda nümunənin müqaviməti, $\varepsilon = \frac{\Delta l}{l_0}$ - nisbi deformasiyadır. R_ε- və R_0- müqavimətləri VK7-9 lampalı voltmetrin köməyilə təyin edilir.

Böyük müqavimətli kristalların tenzohəssaslıq əmsalının

$$K = \frac{\Delta R_{\varepsilon,0}}{R_0 \cdot \varepsilon} = -\frac{\Delta V_{\varepsilon,0}}{V_\varepsilon \cdot \varepsilon} \qquad (3)$$

kimi təyin edilməsi daha əlverişlidir. Beləliklə, şəkil 2-də göstərilən sxem əsasında tenzohəssaslıq əmsalını təyin etmək üçün deformasiya olmadıqda (V_0) və olduqda (V_ε) gərginlik düşgülərini ölçmək kifayətdir.

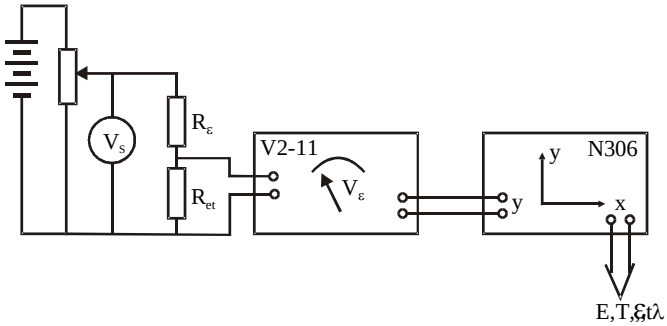

Şəkil 2. Statik rejimdə tenzohəssaslıq əmsalını təyin etmək üçün prinsipial sxem.

Bu üsulla tenzohəssaslıq əmsalı təyin edilir və qənaətləndirici nəticələr alınır.

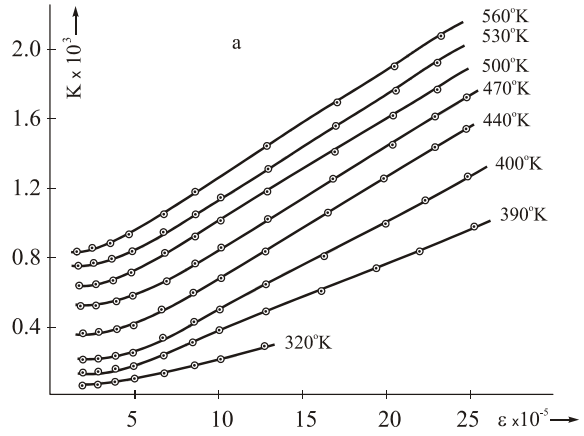

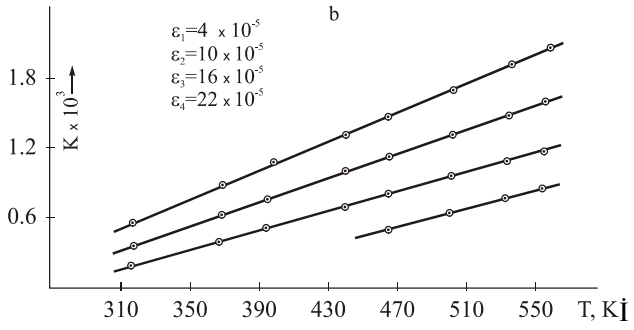

Şəkil 3. $TlIn_{0.98}Nd_{0.02}Se_2$ kristallarında tenzohəssaslıq əmsalının deformasiyadan (a), və temperaturdan (b) asılılığı

lkin tədqiqatlarla müəyyən edilmişdir ki, $TlInSe_2$ birləşməsi əsasında alınmış $TlIn_{1-x}Ln_xSe_2$ ($0 \le x \le 0.04$) bərk məhlulları [9,10] böyük tenzohəssaslıq əmsalına malikdirlər.

Müxtəlif texnoloji rejimlərdə alınmış və hazırlanmış tenzoötürücülərin xarakteristikalarının qismən fərqlənməsinin səbəbi polimerləşmə dərəcəsinin, nümunələrin qalınlıqlarının müxtəlif olması və digər amillərlə əlaqədar olması müəyyən edilmişdir.

Məlumdur ki, yarımkeçirici tenzometrik materialların əsas göstəricisi onların başlanğıc müqavimətlərinin və tenzohəssaslıqlarının temperatur asılılığı hesab olunur. Yarımkeçirici tenzometrlərdən dəyişən temperaturlu konstruksiyalarda istifadə olunduqda məhz bu əlamət nəzərə alınır. Mövcud tenzometrlərin həssaslığı adətən temperatur artdıqca azalır. Bu da onların tətbiq olunma imkanlarını məhdudlaşdırır. Bu baxımdan bizim tədqiqat obyektimiz olan $TlInSe_2$ və onun əsasında alınan bərk məhlullar xüsusi diqqətə layiqdirlər. Belə ki, bu kristalların temperaturu artdıqca onların deformasiyaya görə həssaslıqları artır. Məsələn, $TlIn_{1-x}Pr_xSe_2$ kristalları üçün aparılmış tədqiqatların nəticələri şəkil 3-də verilir. Şəkildən göründüyü kimi temperatur artdıqca tenzohəssaslıq əmsalı xətti qanunla artır.

Ümumən, bu tip kristallarda müşahidə edilən pyezoelektrik effekt aşağıdakı kimi izah edilə bilər. Məlumdur ki, deformasiya zamanı kristalın həm uzunluğu, həm en kəsiyinin sahəsi, həm də xüsusi müqaviməti dəyişir və bu halda ümumi elektrik müqavimətini

$$R(\varepsilon) = \frac{\rho(\varepsilon) l(\varepsilon)}{S(\varepsilon)}$$

kimi ifadə edə bilərik.

Əgər

$$\rho(\varepsilon) = \rho_0(1+\pi\varepsilon),\ \ l(\varepsilon) = l_0(1+\varepsilon),\ \ S(\varepsilon) = S_0(1-\nu\varepsilon^2)$$

olduğunu qəbul etsək, onda müəyyən sadələşdirmədən sonra tenzohəssaslıq əmsalı

$$K = \frac{\rho_0 l_0 + \rho_0 l_0 \pi\varepsilon + \rho_0 l_0 \varepsilon + \rho_0 l_0 \pi\varepsilon^2}{S_0 - 2S_0\nu\varepsilon + S_0\nu^2\varepsilon^2} \qquad (4)$$

olur. Kiçik nisbi deformasiyalar üçün ε^2 daxil olan hədləri atsaq və sadələşdirmələr aparsaq tenzohəssaslıq əmsalı üçün

$$K = 1 + 2\mu + m_e \qquad (5)$$

tapılır. Puasson əmsalı təxminən 0,3-ə bərabər olan metallardan fərqli olaraq, m_e-əmsalının qiymətindən asılı olan ümumi müqavimətin dəyişməsi (ΔR) bu halda cəmisi 20% təşkil edir. Yarımkeçiricilərdə ΔR praktiki olaraq xüsusi elektrik keçiriciliyinin dəyişməsindən asılı olur.

Bizim apardığımız tədqiqatlar göstərmişdir ki, $TlIn_{1-x}Nd_xSe_2$ kristalları da ilkin $TlInSe_2$ kimi çox yüksək tenzohəssaslıq əmsalına malikdirlər və tərkibdən asılı olaraq həmin əmsalın qiymətini idarə etmək mümkündür (şəkil 4). Müəyyən edilmişdir ki, həndəsi ölçüləri 0.25x0.1x10 $мм^3$ olan

kristallar əyrilik radiusu 4-6 mm olan əyilməyə tab gətirir, deformasiyanın limit qiyməti isə 1.5% təşkil edir. Tədqiq olunan kristalların tenzometrik xarakteristikaları zamandan və deformasiya dərəcəsindən asılı olaraq da tədqiq edilmişdir. Mexaniki deformasiyadan sonra xüsusi müqavimətin dəyişməsi

$$\frac{\Delta\rho}{\rho_0} = \pi_e \cdot E\varepsilon = m_e\varepsilon \qquad (6)$$

düsturu ilə təyin edilmişdir.

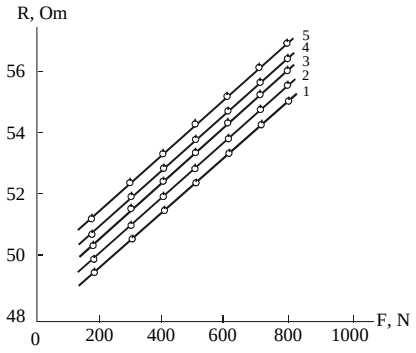

Şəkil 4. $TlIn_{1-x}Nd_xSe_2$ krisitallarının müqavimətlərinin deformasiya qüvvəsindən asılılığı:
1-x=0; 2-x=0,01; 3-x=0,03; 4-x=0,04; 5-x=0,05.

Burada π_e -deformasiya və xüsusi müqavimət arasında mütənasiblik əmsalı, *E*- Yunq moduludur.

Beləliklə, aşkar olur ki, yarımkeçirici üçün tenzohəssaslıq əmsalı hər şeydən əvvəl materialların müəyyən kristalloqrafik istiqamət üzrə elastiki sabitlərindən asılıdır. İlkin ölçmələrə görə [001] kristalloqrafik istiqamət üzrə 300K-də $TlIn_{1-x}Ln_xSe_2$ monokristallarında Yunq modulu onların tərkibindən asılı olaraq $E=(13\text{-}160)\cdot10^{10}N/m^2$ intervalında dəyişən qiymətlər alır. Bu qiymət artıq yarımkeçirici tenzometriyada məlum materiallar üçün alınmış qiymətlərdən çox böyükdür. Bizim qənaətimizə görə bu, əsasən $TlIn_{1-x}Ln_xSe_2$ kristallarının mürəkkəb energetik quruluşa malik olması ilə əlaqədardır. Doğrudan da $TlInSe_2$ birləşmsinin modifikasiya olunmuş Habbard Şam modeli ilə yük sıxlığının aralıq qiymətlərilə hesablanmış zona quruluşu üçün hesablamalarından aşağıdakı nəticələr alınır (şəkil 5).

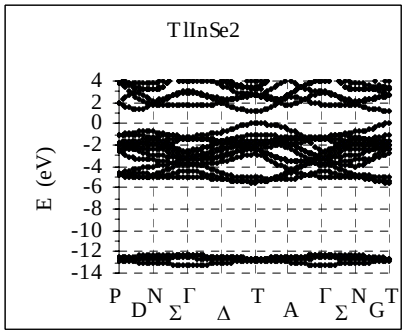

Şəkil 5. $TlInSe_2$ birləşməsinin zona quruluşu.

Valent zonalarını üç qrupa bölmək mümkündür. On zonadan ibarət ən yuxarı əsas qrup ~3.5eV enə malikdir. AOXK metodu istifadə olunmaqla və qrup nəzəriyyəsi analizi aparmaqla müəyyən edilmişdir ki, bu zonalar, valent zonanın tavanı və ona yaxın hissələr istisna olmaqla, əsasən Tl, In və Se atomlarının p-hallarından törəyir. Bu qrupun ən yuxarı hissələri, yəni valent zonanın tavanı və yaxın hissələr isə əsasən Tl ionlarının 6s-hallarından törəyir. Sonuncu nəticəni həmçinin ayrıca tavan hallarının iştirakı ilə aparılan yük sıxlığı hesablamaları da təsdiq edir. Əsas qrupdan aşağı ~2.0eV enində dörd zonadan ibarət qrup yerləşir. Bu zonalar əsasən Tl və In atomlarının s-hallarından törəyir. Dörd zonadan ibarət ən aşağı qrup –12.5eV ətrafında yerləşir ki, bu zonalar da Se atomlarının s-hallarından törəyir.

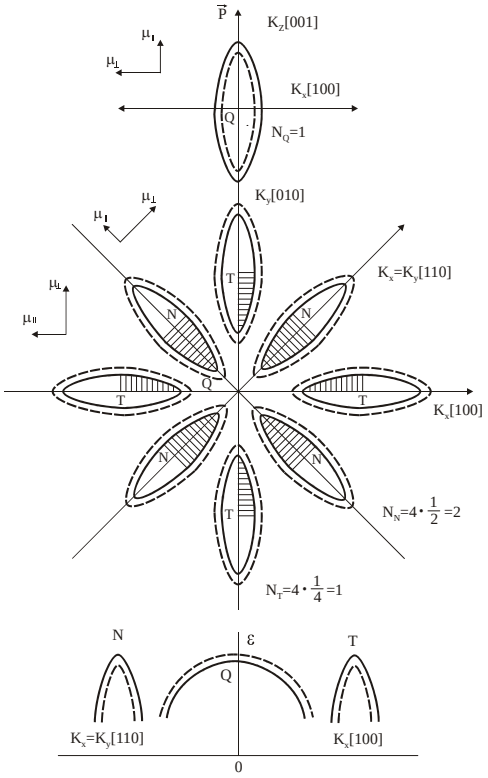

Şəkil 6. Dördellepsoidli model.

Valent zonanın maksimumu və həmçinin keçirici zonanın minimumu Brilluen zonasının sərhəddində yüksək simmetriyalı *T* nöqtəsində yerləşir və uyğun olaraq T_3 və T_4 gətirilməyən təsvirlərinə aiddir.

Keçirici zonanın digər minimumu 0.17 eV yuxarıda olmaqla Brilluen zonasının səthində *D* xətti üzərində yerləşir və D_1 gətirilməyən təsvirinə aiddir.

Minimal düz zolaq *T* nöqtəsində dipol yaxınlahmasında qadağan $T_3 \rightarrow T_4$ keçidlərlə formalaşır. Düz keçidlərin aktivləşmə enerjisi $Eg\ T_3 \rightarrow T_4$ =1.20eV olur.

$TlIn_{1-x}Ln_xSe_2$ tip kristallar tetraqonal sinqoniyada kristallaşan $TlInSe_2$ -in elementar qəfəsində indium atomlarının lantanoidlərlə əvəz olunmasından alındığından həmin kristallar halında valent zonasının ~3.5eV enə malik olan qrup Tl, In və Se atomlarının -hallarından, əsas qrupdan aşağı 2.0eV enə malik zonalar isə Tl, In və Pr-un s-hallarından törəyir.

Qrup nəzəriyyəsinə görə [11] TlSe tip kristallarda sabit enerji səthi özünü 3 oxlu elipsoid kimi biruzə verir (şəkil 6). $TlInSe_2$ kristallarında aşkar edilmiş pyezorezistiv effekt ekstremumları $Q(N_Q$=0.1ellipsoid), $T(N_T$=4·1/4=1-ellipsoid) və $T(N_N$=4·1/2=2-ellipsoid) nöqtələrində yerləşən 4 ellepsoidli model əsasında keyfiyyətcə izah oluna bilir.

Vadilərdəki daşıyıcılar üçün olan müstəvilərdə dispersiya qanunu aşağıdakı kimi ifadə olunur:

$$N-\varepsilon=\frac{\hbar^2}{2}\left(\frac{K_x^2}{m_{||}}+\frac{K_x^2}{m_{\perp}}\right) \quad (7)$$

$$T-\varepsilon=\frac{\hbar^2}{2}\left(\frac{K_x^2}{m_{||}}+\frac{K_y^2}{m_{\perp}}\right) \quad (8)$$

$$Q-\varepsilon=\frac{\hbar^2}{2}\left(\frac{K_x^2}{m_{\perp}}+\frac{K_z^2}{m_{||}}\right) \quad (9)$$

burada $m_{||}$ və $m_{\perp}$ yükdaşıyıcıların müvafiq olaraq ellepsoidin uzununa və eninə oxları üzrə effektiv kütləleridir. Burada yükdaşıyıcıların yürüklükləri müvafiq olaraq

$$\mu_{||}=\frac{q\tau}{m_{||}} \quad (10)$$

$$\mu_{\perp}=\frac{q\tau}{m_{\perp}} \quad (11)$$

kimi ifadə edilir.

Əgər vadilərdə yükdaşıyıcıların sayı n_0 olarsa, onda Q,T, və N vadilərində həmin daşıyıcıların sayı müvafiq olaraq, $n_0/4$, $n_0/4$ və $2\cdot n_0/4$ olmalıdır. Tetraqonal oxa paralel istiqamətdə həmin vadilərdə keçiriciliyə təsir edən toplananlar müvafiq olaraq $\sigma_Q^{||}=\frac{en_0}{4}\cdot\mu_{||}$, $\sigma_T^{||}=\frac{en_0}{4}\cdot\mu_{\perp}$ və $\sigma_N^{||}=\frac{e2n_0}{4}\cdot\mu_{\perp}$ kimi təyin edilir. Onda /001/ oxu boyunca ümumi elektrik keçiriciliyi

$$\sigma_0^{||}=\sigma_z=en_0\frac{3\mu_{\perp}+\mu_{||}}{4} \quad (12)$$

lakin /001/ oxu boyunca bir tərəfli deformasiya zamanı keçiricilikdə iştirak edən «ağır» (yürüklüyü $\mu_{//}$ olan) və «yüngül» (yürüklüyü $\mu_{\perp}$ olan) deşiklərin nisbəti dəyişir. Göstərilən dəyişmə yükdaşıyıcıların bir vadidən digərinə axmasının nəticəsi olub, qeyd olunan pyezorezistiv effektin meydana çıxmasına səbəb olur.

$TlIn_{1-x}Ln_xSe_2$ kristallarının /001/ oxu boyunca dartılması zamanı həmin istiqamətdə həərkət edən ağır deşiklərin nisbi sayı artır, və bununla əlaqədar olaraq keçiricilik azalır. Analoji qaydada nümunən sıxılması zamanı isə əksinə, keçiricilik artır. Vadilərdə daşıyıcıların yenidən paylanmasının səbəbi bir istiqamətli deformasiya zamanı ekstremumların müxtəlif şəraitlərdə olması ilə əlaqədardır. Yəni, kristalın /001/ oxu istiqamətdə dartılması zamanı /100/ və /110/ istiqamətlərdə sıxılmaları baş verdiyindən, nəticədə /001/ oxu üzərində olan Q ekstremumu yuxarıya qalxır və buna müvafiq olaraq /100/ və /110/ oxları üzərindəki minimumlar aşağıya düşür, bu zaman müvafiq vadilərin ümumi elektrik keçiriciliklərinə /001/ istiqamətdə verdikləri paylar da dəyişir. Beləliklə, kristalların /001/ oxu istiqamətdə dartılması zamanı keçiricilikləri

$$\sigma_{dar}^{||}=\frac{en_0}{4}\cdot(3\mu_{\perp}+\mu_{||})+\frac{e\Delta n}{4}(\mu_{||}-\mu_{\perp}) \quad (13)$$

kimi təyin edilir.Bununla əlaqədar olaraq $\mu_{\perp}>\mu_{||}$ olduğundan nümunələrin dartılması zamanı elektrik keçiriciliyinin dəyişməsi mənfi

$$\Delta\sigma_{dar}^{||}=\frac{e\Delta n}{4}\cdot(\mu_{||}-\mu_{\perp})<0 \quad (14)$$

olur.

Nümunənin sıxılması zamanı isə elektrikkeçiriciliyinin dəyişməsi müsbət olur. Deməli /001/ oxu istiqamətində nümunənin dartılması zamanı elektrikkeçiriciliyi azalır, sıxılması zamanı isə artır ki, bu da təcrübələrin yuxarıda qeyd olunan nəticələri ilə yaxşı uzlaşır.

[1]. *Q.D. Quseynov, Q.B. Abdullaev*. Pğezorezistivnıe efektı na monokristallax $TlInSe_2$-TlInTe. DAN SSSR. 1973, t.208, №5, s.1052-1054.

[2]. A.S. 401208 (SSSR). Poluprovodnikoviy tenzodatchik . *Q.D.Quseynov i Q.B.Abdullaev*. (Rusca)

[3]. A.S.539215 (SSSR). Sposob requlirovaniya çuvstvitelnosti tenzodatçikov. *Q.B.Abdullaev, V.D.Rustamov, M.Z.İsmaylov, K.M.Bannayev, S.M.Bidzinova*. Opubl. v M.İ., 1976, №46. (Rusca)

[4]. *E.M. Qodjaev, E.A. Allaxərov, X.O. Sadıxova.* Tenzometriçeskiye svoystva monokristallov $TlInTe_2$. İzv.RAN, Neorqaniçeskiye materialı, 1994, t.30, №6, s.859. (Rusca)

[5]. *E.M. Qodjaev, Q.S. Djafarova*. Diaqramma sostoyaniya i svoystva faz sistemı $TlInSe_2$-$TlPrSe_2$. İzv. RAN, Neorqaniçeskiya materialı, Moskva, 2003, t.39, №1, s.11-13. (Rusca)

[6]. *Q.G. Quseynov*. Poisk i fiziçeskie issledovaniə novıx poluprovodnikov – analoqov. Avtoref.diss. d.f.-m.n., Vilğnös, 1972, 60 s. (Rusca)

[7]. *E.M. Kerimova*. Fiziçeskiye osnovı materialovedeniya nizkorazmernıx poluprovodnikov. Diss. dok. fiz.-mat.nauk. Baku, İFAN, 1991, s.449. (Rusca)

[8]. *X.S. Xalılova*. $TlIn_{1-x}Nd_xSe_2$ kristallarının elektron və istilik xassələri. Diss.f.-r.e.n., Bakı, BDU, 2003, 134s. (Rusca)

[9]. *E.M. Qodjaev, I.R. Nuriev, A.M. Nazarov, Ç.I. Rustamov, X.S. Xalilova, A.M. Suleymanova*. Pezoelektriçeskiye svoystva soyedineniy tipa $A^{III}B^{III}C_2^{VI}$ i tverdıx rastvorov na ix osnove. Deponirovan v AzNİİTİ. Deponirovannıe nauçnıye rabotı №3 (25) s.8, 1999 q., 15.07.99. za № Az.2624. (Rusca)

[10]. *E.M. Qodjaev, S.X. Xalilov, X.S. Xalilova, M.A. Quseynov, A.M. Suleymanova*. Pezoelektriçeskiye

svoystva kristallov $TlIn_{1-x}Nd_xS_2$ İnjenerno-Fiziçeskiy Jurnal 2003, tom 76, №2, s.76-79. (Rusca)

[11]. *F.M. Qaşimzade, G.S. Orudjev*. Rasçet gnerqetiçeskoqo spektra elektronov troynıx poluprovodnikovıx soedineniy so strukturoy selenida talliya. Doklad AN Azerb.SSR, 1980, t.36, №12, s.18-23. (Rusca)

Э.М. Годжаев, К.Дж. Гюльмамедов, Г.С. Джафарова, Г.С. Оруджев, С.С. Османова

ПЬЕЗОЭЛЕКТРИЧЕСКИЕ СВОЙСТВА КРИСТАЛЛОВ $TlIn_{1-x}Ln_xSe_2$

В предъявленной работе изложены результаты исследования пьезоэлектрических свойств кристаллов типа $TlIn_{1-x}Ln_xSe_2$ и обсуждения результатов на основе зонной структуры исходного соединения $TlInSe_2$. Выявлено, что при замещении трехвалентного индия трехвалентными лантаноидами в решетке $TlInSe_2$ можно увеличить и управлять коэффициент тензочувствительности этих кристаллов.

E.M. Qojaev, K.J. Gulmamedov, G.S. Djafarova, G.S. Orudzhev, S.S. Osmanova

PIEZOELECTRIC PROPERTIES OF CRYSTALS $TlIn_{1-x}Ln_xSe_2$

In the present work the results of investigations of piezoelectric properties of $TlIn_{1-x}Ln_xSe_2$ type crystals and its discussion on the basis of band structure initial compound $TlInSe_2$ are presented. It is revealed that at replacement trivalent Indium with trivalent Lanthanoid in lattice $TlInSe_2$ it is possible to increase and operate the tenzosensitivity of these crystals.

Received:15.12.05

ROTATIONAL CONSTANTS AND COMPONENTS OF DIPOLE MOMENTS OF TRANS-TRANS-TRANS AND TRANS-TRANS-GOSH CONFORMERS OF BUTYL SPIRIT

Ch.O. KADJAR, S.A. MUSAYEV, S.B. KAZIMOVA,
A.A. ABDULLAYEV, E.Ch. SAIDOV
Institute of Physics of National Academy of Sciences of Azerbaijan
H.Javid av., 33, Baku AZ-1143 Azerbaijan

The calculated rotational constants, main inertia moments, asymmetry parameters and components of dipole moments of trans-trans-trans and trans-trans-gosh conformers of N-butanol molecule are given in the paper.

N-butanol is related to the set of one-atom spirits. The complexity of the structure, internal rotation relative three axes simultaneously, the existence of the different barriers, the presence of hydroxyl group leads to many different conformers and the complex rotational spectrum of this molecule is expected. The wide use of butyl spirit in organic chemistry causes the increased interest as from scientific, so from practical points of view, the investigation of the spectrum of this molecule.

The internal rotation and rotational isomerism in N-butanol molecule had been investigated in refs [1-4]. The conformational analysis of the internal rotation round single connections C-C-C and C-O in N-butanol molecule is given in these refs, that allows to estimate the stability of possible isomeric forms. Authors show, that in molecule spectrum of normal butyl spirit the absorption line is expected, connected with *trans-trans-gosh*, *trans-gosh-trans* and *trans-gosh-gosh* isomers.

Table 1

Structural parameters of some one-atom spirits

Spirits / Parameters	Methyl [2]	Ethyl [5]	Propyl [6]	Isopropyl [7]	Average value
$R(C-C)A^0$		1,519	1,505	1,505	1,509
$R(C-O)A^0$	1,428	1,437	1,466	1,466	1,449
$R(O-H)A^0$	0,960		0,968	0,968	0,965
$R(C-Ha)A^0$	1,095	1,096	1,104	1,104	1,099
<CCC			$114^0 27'$	$114^0 59'$	$114^0 43'$
<CCO		$107^0 74'$	$106^0 38'$	$110^0 19'$	$108^0 11'$
<COH			$101^0 40'$	$105^0 48'$	$103^0 44'$
<CCHa		$109^0 61'$	$108^0 06'$	$109^0 28'$	$108^0 98'$
Ω				$2^0 95'$	$2^0 95'$
ω				$120^0 32'$	$120^0 32'$

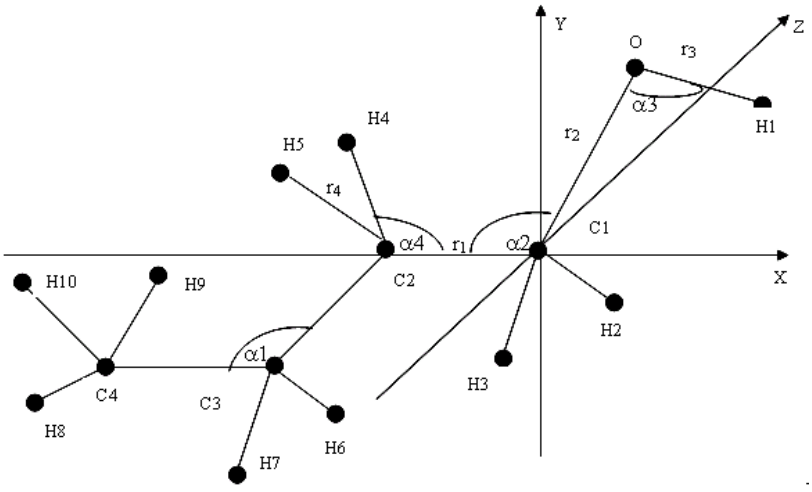

a)

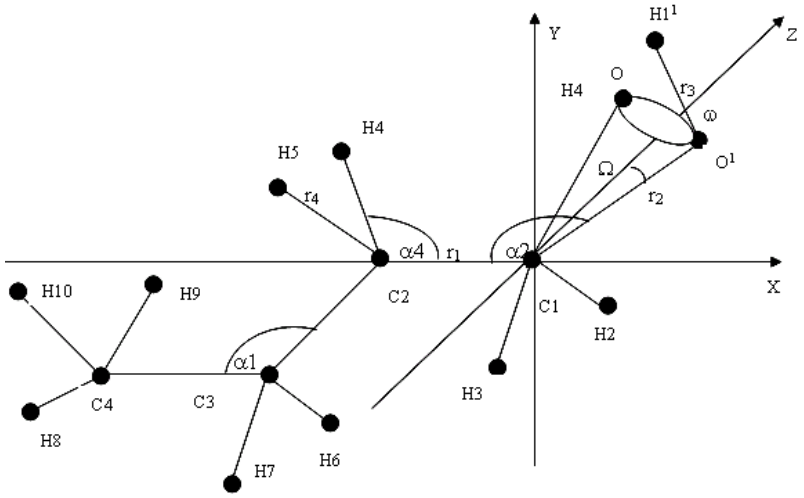

b)

Fig.1. Structures *trans-trans-trans* (*a*) and *trans-trans-gosh* conformers of N-butanol molecule (*b*).

For the calculation of rotational constants and component of dipole moments of normal butyl spirit and its conformers the structural parameters of related molecules had been taken as the base. For more right choice of structural parameters the structural parameters of molecules of methyl, ethyl, propyl and isopropyl spirits, investigated in the refs [2,5,6-8] had been analyzed.

The co-ordinates for *trans-trans-trans* had been chosen thus, that C1 atom was in the beginning of the co-ordinate, H1, O, C1, C2, C3, C4, H8 atoms were in plane XOY, H2, H3, H4, H5, H6, H7, H8, H10 laid on the equal distances from this plane (fig.1, a.).

The *trans-trans-gosh* conformer, considered by us, was obtained in the result of precession atoms O and H1 round axes, going through C1 atom and center of gravity of O and C1 atoms. The expression of coordinates of all atoms, besides H1 and O stay the same, besides H1 and O.

For the comfort the following designations had been pointed: R(C – C) – r_1: R(C – O) – r_2: R(O – H) – r_3: R(C – H) – r_4: <CCC - α_1: <CCO - α_2: <COH - α_3: <CCH - α_4: rotation angle of atoms O and H1-ω: precession angle – Ω.

The mathematic expressions for calculation of coordinates of atoms *trans-trans-trans*, *trans-trans-gosh* conformers of N-butanol molecule had been mentioned in such co-ordinate (tab.2).

Table 2

The expression for the definition of coordinates of atoms of N-butyl spirit molecule and its gosh-conformer in arbitrary co-ordinates

№		X	Y	Z
1	C_1	0	0	0
2	C_2	$-r_1$	0	0
3	C_3	$-r_1- r_1*\cos(\pi-\alpha_1)$	0	$-r_1*\sin(\pi-\alpha_1)$
4	C_4	$X(C_3) - r_1$	0	$Z(C_3)$
5	H_2	$X(H_3)$	$-Y(H3)$	$Z(H_3)$
6	H_3	$r_3*\cos(\pi-\alpha_4)$	$r_3*\sin(\pi-\alpha_4)$*КОРЕНЬ(3)/2	$-r_3*\sin(\pi-\alpha_4)/2$
7	H_4	$X(C_2)- r_3*\cos(\pi-\alpha_4)$	$r_3*\sin(\pi-\alpha_4)$*КОРЕНЬ(3)/2	$-Z(H_3)$
8	H_5	$X(H_4)$	$- Y(H_4)$	$Z(H_4)$
9	H_6	$X(C_3)- X(H_3)$	$Y(H_2)$	$Z(C_3)+ Z(H_2)$
10	H_7	$X(H_6)$	$-Y(H_6)$	$Z(H_6)$
11	H_8	$X(C_4)- X(H_2)$	0	$Z (C_4)- r_3*\sin(\pi-\alpha_4)$
12	H_9	$X(C_4)- X(H_3)$	$Y(H_2)$	$Z (C_4)- Z(H_2)$
13	H_{10}	$X(H_9)$	$-Y(H_9)$	$Z(H_9)$
14	O	$r_2*\cos(\pi - \alpha_2)$	0	$r_2*\sin(\pi - \alpha_2)$
15	H_1	$X(O)+ r_4*\cos(\alpha_2-\alpha_3)$	0	$Z(O)- r_4*\sin(\alpha_2-\alpha_3)$
16	O^1	$X(O)+ r_2*\sin\Omega*(1+ \cos(\pi-\omega))*\sin(\pi-\alpha_2-\Omega)$	$r_2*\sin\Omega*\sin(\pi-\omega)$	$Z(O)-r_2*\sin\Omega*(1+\cos(\pi-\omega))*\cos(\pi-\alpha_2-\Omega)$
17	H_1^1	$X(H_1)-(r_4*\sin(\pi-\alpha_3-\Omega))- r_2*\sin(\Omega)*(1+\cos(\pi-\omega))*\sin(\pi-\alpha_2-\Omega)$	$(r_4*\sin(\pi-\alpha_3-\Omega))-r_2*\sin(\Omega))*\sin(\pi-\omega)$	$Z(H_1)+(r_4*\sin(\pi-\alpha_3-\Omega))- r_2*\sin(\Omega)*(1+\cos(\pi-\omega))*\cos(\pi-\alpha_2-\Omega)$

The rotational constants trans-trans-trans and trans-trans-gosh of butanol conformers and also components of dipole moments relative them were calculating on the base of the obtained structure.

The rotational constants, main inertia moments, asymmetry parameters and components of dipole moments of N-butyl spirit and its gosh-conformer are given in the table 3.

At the study of molecule structures the program "RASMOL" (molecular visualization program) is used. Molecular visualization program "RASMOL" is used for the clearness of atom situation in molecule (fig.2).

Table 3

Rotational constants, main inertia moments, asymmetry parameters and dipole moments of N-butyl spirits and its gosh-conformers

Parameters	trans-trans-trans	gosh-trans-trans
A	19069.852	19087.051
B	1980.781	1952.240
C	1881.827	1870.899
μ_a	0	0
$\mu_в$	1.1085	1.1086
μ_c	1.1042	1.1044
$\mu_{об}$	1.5647	1.5649
X	-0,98849	-0,98823
I_A	26,50943468	26,4855483
I_B	255,2179651	256,323263
I_C	268,6384636	270,207531

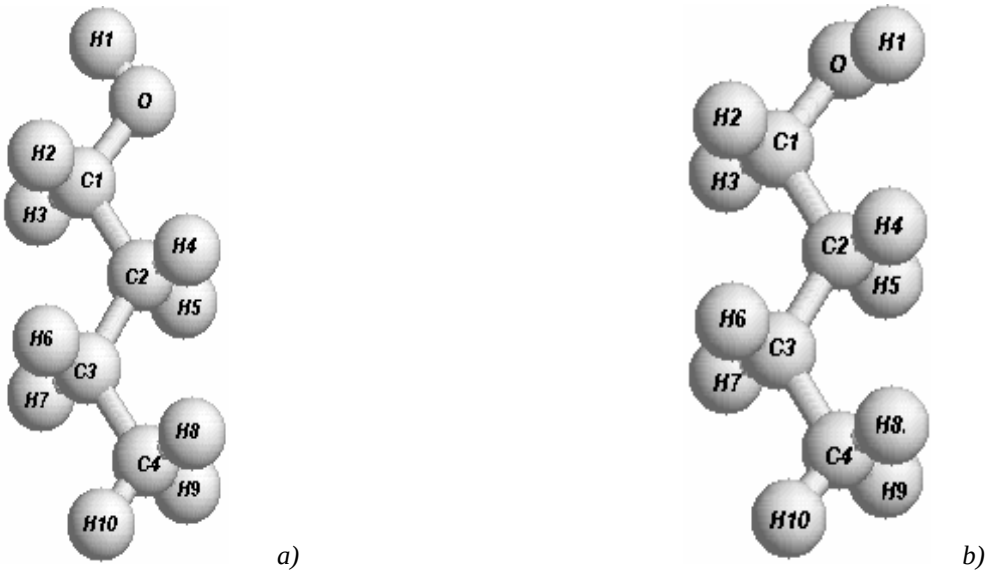

Fig.2. The visual images of molecules: butyl spirit (a) and its gosh-conformer (b).

[1] *A.A. Abdurakhmanov, E.I. Veliyulin*. Izv. AN Azerb. SSR, ser. FTMN, 1970, № 3, s. 101-105.

[2] *Ch.O. Kadjar*. Mikrovolnovaya spektroskopiya nekotorikh odnoatomnikh spirtov i ikh zameshennikh. Dissertatsiya d.f.m.nauk. 1972, Baku, IFAN Azerb. SSR.

[3] *A.A. Abdurakhmanov, E.I. Veliyulin, L.M. Imanov*. J. Strukt. khimii, 1972, t. 13, № 2, s. 251-255.

[4] *L.M. Imanov, A.A. Abdurakhmanov, R.A. Ragimova, E.I. Veliyulin*. Izv. AN. Azerb. SSR, ser. FTMN, 1970, № 6, s. 81-83.

[5] *R.T. Kadjarov*. Mikrovolnoviy spektr i struktura *ON-trans-trans* konformera molekuli propanola. Kand. fiz.-mat. nauk, 1990, Baku, Filial NII Fotoelektroniki.

[6] *R.A. Ragimova*. Issledovanie mikrovolnovogo vrashatelnogo spektra i strukturi normalnogo propilovogo spirta. Kand. fiz.-mat. nauk, 1967, Baku, IFAN Azerb. SSR.

[7] *S.A. Musaev*. Tsentrobejnoe vozmushenie i dvoynie MV-MV i RCh-MV rezonansi vo vrashatelnikh i vrahatelno-kolebatelnikh spektrax molekul $(SN_3)_2SNON$ i $(SD_3)_2CDOH$. 1983. Kand. fiz.-mat. nauk, Baku, Filial NII Prikladnoy fiziki.

[8] *S.A.Musaev.* Tsentrobejnoe vozmushenie i vnutrennee vrashenie v molekulax etilovogo i izopropilovogo spirtov. Dissertatsiya d.f.m.nauk. BAKU - 2003, IFAN.

Ç.O. Qacar, S.A. Musayev, S.B. Kazımova, A.A. Abdullayev, E.Ç. Səidov

BUTİL SPİRTİ MOLEKULUNUN TRANS - TRANS - TRANS VƏ TRANS - TRANS - QOŞ KONFORMERLƏRİNİN FIRLANMA SABİTLƏRİ VƏ DİPOL MOMENTLƏRİ

Məqalədə normal butil spirti molekulasının trans – trans – trans və trans – trans – qoş konformerinin fırlanma sabitlərinin, baş ətalət momentlərinin, asimmetriya əmsallarının və dipol momentlərinin komponentlərinin hesablanmasından bəhs olunur.

Ч. О. Каджар, С. А. Мусаев, С. Б. Кязимова, А. А. Абдуллаев, Э.Ч. Саидов

ВРАЩАТЕЛЬНЫЕ ПОСТОЯННЫЕ И КОМПОНЕНТЫ ДИПОЛЬНОГО МОМЕНТА ТРАНС – ТРАНС – ТРАНС И ТРАНС – ТРАНС – ГОШ КОНФОРМЕРОВ БУТИЛОВОГО СПИРТА

В статье приводятся рассчитанные вращательные постоянные, главные моменты инерции, параметры асимметрии и компоненты дипольных моментов транс – транс – транс, транс – транс – гош конформеров молекулы Н – бутанола.

Received: 08.11.05

THERMO-ELECTROMOTIVE FORCE AND HALL EFFECT IN $FeGa_2S_4$

N.N. NIFTIYEV, F.M. MAMEDOV
Azerbaycan State Pedagogical University Az-1000, Baku, U. Hajibeckov, str.,4.

O.B. TAGIYEV
Institute of Physics of NAS of Azerbaycan, Az-1143, Baku, H. Javid av., 33

The thermo-electromotive force and Hall effect have been investigated in the different temperatures in $FeGa_2S_4$ semiconductors. On sign of the thermo-electromotive force it is established, that $FeGa_2S_4$ has p or n type of the conductivity in the different temperature intervals, The coefficient of the thermo-electromotive force, concentration and Hall mobility of current carriers have been defined.

$FeGa_2S_4$ is related to the class of the compounds $A^{II}B_2^{III}X_4^{VI}$ (A-Mn, Fe, Co, Ni; B-Ga, In; X-S, Se, Te), having elements with thin *d*-membranes [1-5]. These compounds are perspective for the creation of the lasers, light modulator, photodetectors and other functional devices on their base, directed by the magnetic field. The physical properties of $FeGa_2S_4$ had been studied in some refs. [6-8].

In the given ref. The results of the investigation of thermo-electromotive force and Hall effect in $FeGa_2S_4$ crystals are given.

The crystals $FeGa_2S_4$ have been obtained by the direct alloying of elements of high frequency (99, 999%) in stoichiometric quantities. By the roentgenographical method it has been established, that $FeGa_2S_4$ has rhombic structure by формула $ZnAl_2S_4$ type with parameters of crystalline lattice a=12.89; b=7.51; c=6.09Å [6].

The samples were prepared by the way of the mechanical treatment of the ingot in the form of the parallelepiped with average sizes ~ 5×6×7mm^3. The investigations were carried out on the constant current in the constant magnetic field on $FeGa_2S_4$ samples.

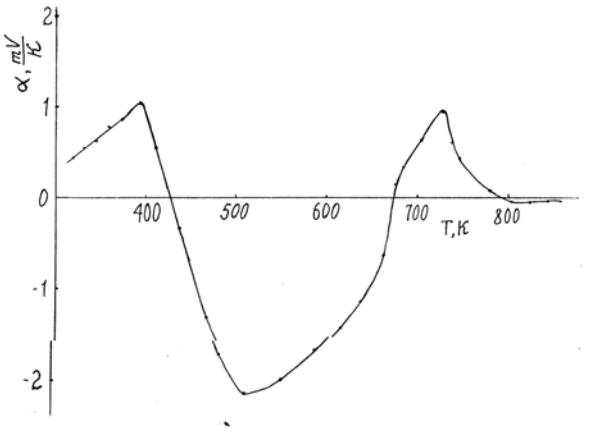

Fig.1. The temperature dependence of the coefficient of thermo-electromotive force for $FeGa_2S_4$ crystals.

The temperature dependence of the coefficient of thermo-electromotive force (α) for $FeGa_2S_4$ crystals is given on the fig.1. It is seen, that in the temperature interval 300÷850K the curve of the coefficient of thermo-electromotive force has easy character. At low temperatures (up to ~420K) the coefficient of thermo-electromotive force shows on the hole conductivity. The thermo-electromotive force in the interval 300÷400K weakly increases and achieves ~1mV/K. On the sign of the thermo-electromotive force it is seen, that in the temperature interval 300÷420K $FeGa_2S_4$ has p type of the conductivity. The positive sign of the coefficient of thermo-electromotive force till ~420K evidences about the fact that in this temperature interval in $FeGa_2S_4$ crystals $n_D\mu_D > n_e\mu_e$. It can be proposed, that extrinsic levels in $FeGa_2S_4$ crystals at ~420K aren't ionized totally. Ionizing they with temperature increase lead to the increase of electron concentration and higher ~420K till 670K $n_e\mu_e$ become more, than $n_D\mu_D$. It is seen, that in this temperature interval $FeGa_2S_4$ has *n* type of the conductivity. In the temperature interval 425÷510K the negative coefficient of thermo-electromotive force strongly increases and its value achieves ~ 2.1mV/K. The part, where α increases with the temperature increase is one $\alpha \sim In(T)^{3/2}$, that corresponds to the following expression [9]:

$$\alpha = \frac{k}{e}\left(In\frac{N_c}{n} + r + 2 \right)$$

(Effective state density $N_c \sim T^{3/2}$). Further, in the temperature interval 510÷675K the negative coefficient of thermo-electromotive force decreases with temperature increase and higher ~675K the conductivity transfers into hole one.

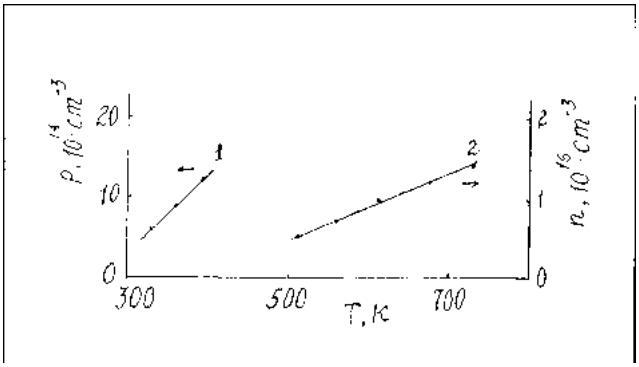

Fig.2. The temperature dependence of the concentration of current carriers for $FeGa_2S_4$ crystals.

The temperature dependencies of the concentration of current carriers, defined from the measurements of Hall effects for $FeGa_2S_4$ crystals are given on the fig.2. It is seen, that the concentrations of the current carriers in the low-temperature and high-temperature regions have different values. The concentration of the current carriers (curve 1) in the low-temperature region in the investigated temperature interval P=(6÷12)·10^{14}cm^{-3} changes. It is need to note, that the same values of the concentration of the current carriers

for $FeGa_2S_4$ have been obtained from the measurements of the dependence of the electroconductivity of these samples from electric field [8]. In the high-temperature region the value of the concentration of current carriers (curve 2) in the temperature interval 500÷730K almost doesn't change and its value is equal to $(1\div3)\cdot10^{16}cm^{-3}$.

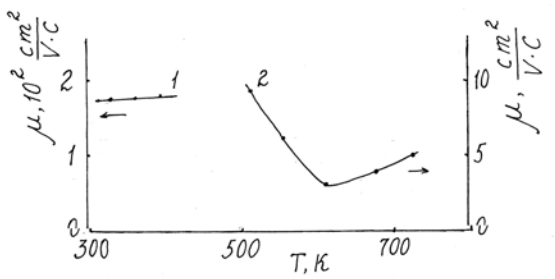

Fig.3. The temperature dependence of the mobility of the current carriers for $FeGa_2S_4$ crystals.

The temperature dependence of Hall mobility of current carriers for $FeGa_2S_4$ crystals is given on the fig.3. It is seen, that the mobility of current carriers (curve 1) in the temperature interval 300÷400K weakly increases and its value achieves $\mu\approx180cm^2/B\cdot s$. In the high-temperature region 500÷740K the value of the mobility of current carriers changes in the interval $\mu=(4\div9)cm^2/B\cdot s$. We know, that the mobility of the current carriers depends on the composition and perfection of the crystalline structure of the semiconductor, on concentration temperature of current carriers [10]. As at the high temperatures the scattering on the thermal vibration of the lattice is the main mechanism of the scattering and the mobility of current carriers decreases with temperature increase. The mobility also decreases with the increase of the concentration of current carriers. In our case in high-temperature region the mobility of the current carriers in $FeGa_2S_4$ becomes lower, that in the low-temperature region.

Thus, in $FeGa_2S_4$ crystals the thermo-electromotive force and Hall effect at the different temperatures have been investigated. The coefficient of the thermo-electromotive force and conductivity type have been defined. The concentration and Hall mobility of the current carriers have been found.

[1]. *B.K. Babayev.* V. sb.: Troyniye poluprovodniki i ikh primeneniye. Kishinyov, Shtiinca, 1976. (in Russian).
[2]. *R.N. Bekimbetov, Yu.V. Rud, M.A. Tairov*. FTP, 1987, 21, s. 1051. (in Russian).
[3]. *G. A. Medvedkin, yu.V. Rud, M.A. Tairov*. Phys.Stat.Sol. (a), 1989, 3, 289.
[4]. *N.N. Niftiyev, O.B. Tagiyev, G.M. Niftiyev*. Neorganicheskiye materiali, 1996, 32, 291. (in Russian).
[5]. *N.N. Niftiyev, O.B. Tagiyev*. Pisma v JETF, 2003, 29, 49. (in Russian).
[6]. *M.P. Pardo*. Mater. Res.Bull. 1981, 16, 1375.
[7]. *O.Gorechov, C.C. Levy, S. Doggiu, M.P. Pardo*. Mater. Res. Bull. 1981, 16, 1493.
[8]. *N.N. Niftiyev, M.A. Alidzhanov, O.B. Tagiyev, M.B. Muradov, F.M. Mamedov*. Ukr. J. Phys., 2004, 49, 579.
[9]. *A.I. Ancelm.* Vvedeniye v teoriyu poluprovodnikov. M. Nauka, 1978, 420. (in Russian).
[10]. *B.L. Bonch-Bruyevich, C.G. Kalashnikov*. Fizika poluprovodnikov. M. Nauka, 1990, 685. (in Russian).

N.N. Niftiyev, O.B. Tağıyev, F.M. Məmmədov

$FeGa_2S_4$-DƏ TERMO-E.H.Q. VƏ XOLL EFFEKTİ

$FeGa_2S_4$ yarımkeçirijisində müxtəlif temperaturlarda termo-e.h.q. və Xoll effekti tədqiq edilmişdir. Termo-e.h.q.-nin işarəsinə görə müəyyən edilmişdir ki, $FeGa_2S_4$ müxtəlif temperatur intervallarında *p* və ya *n* tip keçirijiliyə malik olur. Termo-e.h.q. əmsalı, jərəyan yükdaşıyıjıların konsentrasiyası və Xoll yüyürüklüyü təyin edilmişdir.

Н.Н. Нифтиев, О.Б. Тагиев, Ф.М. Мамедов

ТЕРМО-Э.Д.С. И ЭФФЕКТ ХОЛЛА В $FeGa_2S_4$

В полупроводниках $FeGa_2S_4$ исследованы термо – э.д.с. и эффект Холла при различных температурах. По знаку термо- э.д.с. установлено, что $FeGa_2S_4$ обладает *p* и *n* типом проводимости в разных температурных интервалах. Определены коэффициент термо-э.д.с., концентрация и холловская подвижность носителей тока.

Received: 12.10.06

PIEZORESISTIVE EFFECT IN THE NONORDERED SYSTEM POLYMER-SEMICONDUCTOR

A.I. MAMMADOV
Institute of Physics of NAS of Azerbaijan
Baku, AZ-1143, H. Javid av.,33

In this work the results of investigations of piezoresistive properties of the composition system polymer-semiconductor are presented. Also, the influence of the electroconductance, concentration and mobility of the charge carriers of the filler, the upper mentioned properties and the dielectric characteristics of the composite components had been investigated.

It is shown that the electroconductance in composites due to tunneling charge carriers between particles of filler through polymer layer.

Till recently variety of active composite materials and sphere of their usage were limited. There were basically electret, pyroelectric, piezoelectric and photoelectric composites [1-3]. But lately the figure was suddenly changed; now there are new active composites – posistors, varistors (bipolar non-linear transducer) and piezoresistors. One of the main features of the above mentioned composites are extreme big and invertible dependence of resistance on tension of the electric field, temperature and mechanic tension. This promotes their wide usage in electronic technique [4-7]. Composite limiter of current, tension and no- contact switches are very perspective elements for usage in electrotechnical, chemical and petroleum industry. Composites-semiconductor, polymer-piezoelectric allow to create nonlinear elements on their base for different purposes, particularly piezoresistors.

However, receiving necessary and what is an important, reproducible feature of the mentioned composite abruptly get complicated by their structural features:

Presence of difficultly regulated interphased limits, heterogeneity, potential barrier on the verge of phase disengagement and hysteresis effect. Depending on the limits' type and geometry, phase interaction character and potential barrier, the features of piezoresistive composite may noticeably differ. It cannot be doubted that electronic features of piezoresistive composite are mainly defined by energetic levels laid in the forbidden gap of polymer phase, which appear because of heterogeneity of its physical and chemical structures, availability of the interfacial phase, structure of which differs from structures of the other (separated) phases.

There is conflicting data about the nature of localized states and their role in the formation of different effects, including piezoresistive. That's why establishment of the structure contribution and electrophysical parameters of the separated phases and limiting electronic effects gains very important meaning in formation of piezoresistive effect in composite – polymer-semiconductor.

Let us examine the influence of pressure (P) on electroconductivity (ρ), i.e.

Piezoresistive effect in composites on the base of non-polar polyethylene (PEHD), polypropylene (PP) and polar polyvinylidene fluoride (PVDF), filled with semiconductors (Si and Ge). Dependence of $lg\rho$ from the pressure P composites on the base of PEHD, PP and PVDF silicon and germanium is shown in the plate (table) 1.

Table 1

Dependence of $lg\rho$ of various composites

P,MPa	$Lg\rho$, Om·m					
	PEHD+Si	PP+Si	PVDF+Si	PEHD+Ge	PP+Ge	PVDF+Ge
0	4,8	4,44	3,7	5,08	4,77	4,92
0,5	3,7	3,1	2,7	4,15	4,15	3,38
1	2,55	2,22	2	3,38	3,61	2,85
1,5	2,1	1,8	1,44	3,15	3,15	2,62
2	1,78	1,44	1,22	3	2,85	2,46
2,5	1,56	1,22	0,89	2,92	2,54	2,38
3	1,33	1,11	0,67	2,85	2,46	2,31
3,5	1,22	0,89	0,56	2,85	2,35	2,23
4	1,22	0,89	0,56	2,77	2,27	2,19

As may be seen from the table 1, as the pressure is boosted, the resistance of the compositions is decreased, and what is more, the level of decrease depends on the features of polymer and filler, also very much from the quantity of filler content in the composite. Level of resistance change at pressure change may be defined by the expression $lg\rho_0/\rho$, where ρ_0 and ρ specific resistance of composites at normal pressure which we consider as 0 and terminal pressure (in our case 4 MPa). On table 2 there dependence $lg\rho_0/\rho$ on the content of semiconductor filler C for compositions with silicon and germanium is presented. With the increase of the quantity (C) of the filler the magnitude $lg\rho_0/\rho$ is increased at first, reaching the maximum at C = 50% mass, and afterwards it is decreased.

Dependence $lg\rho$ on electroconductivity of filler $lg\sigma_и$ for composites on the base of PEHD и PVDF is shown in the tables 3 и 4.

Table 2

Dependence $lg\rho/\rho_o$ on the content of semiconductor phase

C,%. *d*=75mcm	$lg\rho/\rho_o$			
	PVDF+Si	PEHD+Si	PVDF+Ge	PEVP+Ge
20	2,6	2,3	2	1,8
30	3,2	2,9	2,6	2,3
50	3,5	3,2	2,7	2,4
60	3,4	2,9	2,4	2,2
80	3,2	2,2	1,8	1,7

Table 3

Dependence $lg\rho$ on electroconductivity Si for PEHD

$lg\sigma_н$, $Om^{-1}m^{-1}$	$lg\rho_o$, Om·m			
	C=7%	C=33%	C=40%	C=60%
0,5	8,5	5,875	4,375	1,75
1,2	8,5	5,325	4	1,75
1,8	8,5	4,375	3,25	1,625
2,5	8,5	3	2,25	1,625

Table 4

Dependence $lg\rho$ on electroconductivity Si for PVDF

$lg\sigma_н$, $Om^{-1}m^{-1}$	$lg\rho_o$, Om·m			
	C=7%	C=33%	C=40%	C=60%
0,35	9	4,2	2,8	1,25
1	9	3,9	2,5	1,17
1,4	8,5	3,6	2,3	1,17
1,9	8,5	3,1	1,83	1,08
2,75	8,5	1,33	1,08	1

At little contents of the filler ($C<C_{кр1}$) resistance of the composites reach the level at which it doesn't depend on the filler's electroconductivity. At big contents of the filler ($C>C_{кр2}$) resistance of the composites also doesn't depend on $\sigma_н$. At medium contents C ($C_{кр1}<C<C_{кр2}$) there is strong dependence of $lg\rho$ on $\sigma_н$.

It is known that the electroconductivity of the filler is defined by two factors:

Concentration of he current carrier (*N*) and their mobility (μ). That's why let's view the influence of these factors on the electroconductivity of the composites. As it's seen on the table.5, influence $lg\rho$ from *N* has the same form as $lg\rho$ from $\sigma_н$, while the electroconductivity of the carriers practically doesn't affect on the electroconductivity of the composites (fig.1). That's why we can say that the electroconductivity of the composite is basically connected with the concentration of the current carriers in the semiconductor filler.

Table 5

Dependence of the specific resistance $lg\rho$ and $lg\rho_1/\rho$ from the carrier concentration *lgN* particles of the semiconductive phase

lgN	$lg\rho$, Om·m		$lg\rho_1/\rho$	
	on the base of PEHD	on the base of PVDF	on the base of PEHD	on the base of PVDF
17	8,86	6,14	1,55	1,05
17,25	-	-	1,8	1,45
17,75	8,29	6,14	2,05	1,7
18,25	7,71	5,71	1,7	1,85
18,75	7,14	5,28	1,35	1,7
19,25	5,71	4,29	-	1,35
19,5	4,43	3,43	0,65	0,75
19,75	2,86	2,43	0,3	0,4

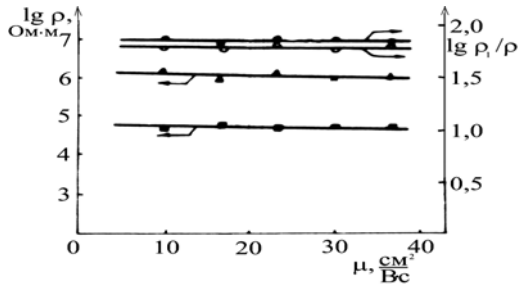

Fig.1. Dependence of the specific resistance and composite sensitivity on the base of PEHD and PVDF from the mobility μ charge carrier of the particles semiconductive phase, C=33%: 1,3 – PEHD, 2,4 –PVDF.

In the composite piezoresistor between semiconductive particles very thin layers of the polymer are placed, and that's why each pair of the contacting layers form the micropiezoresistor. The composite piezoresistor is the difficult chain of the parallel and in series connected micropiezoresistors.

On fig. 2 the simple model of the composite is shown which allows us to explain the conductivity change of the composite polymer-semiconductor under the mechanic tension.

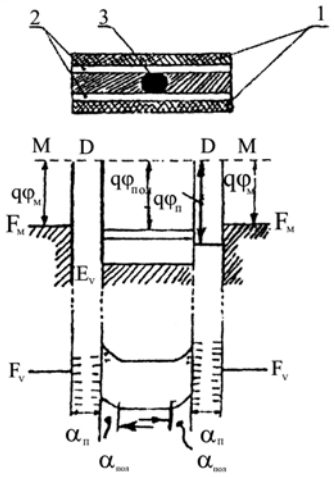

Fig. 2. Model and energy band structure of the piezoresistor: 1-metal electrodes, 2- polymer, 3- semiconductor. $q\varphi_м$, $q\varphi_{пол}$, $q\varphi_п$ – works of extraction, semiconductor and polymer, correspondingly, $\phi_м$, $\phi_{пол}$, $\phi_п$ – Fermy metal levels, semiconductor and polymer, $a_п$ – polymer layer, where the charges are localized, $a_{пол}$ – layer thickness of the semiconductor spatial charge.

It is known, that the tunneling possibility is practically defined by the expression:

$$W \approx \exp\left[-\frac{2}{\hbar}\sqrt{2m(\varphi_o - E)}d\right]$$

where $\hbar$ - quantum constant, φ_o - potential barrier height, d – barrier thickness.

As it is seen from this expression, the possibility of tunneling is less when the barrier width gets more and the energy of the tunneling particle gets less. As all these parameters stand in the index of exponent, the dependence of the possibility from them is very abrupt. The distance between the particles in the composites at which the tunneling is possible, may be achieved by variation of the volume content and by the size of the semiconductive filler. As it was already mentioned, on contact forming the phase composite, there happens the exchange of the charge which leads to the establishment of the thermodynamic equilibrium on the verge of phase separation. By this Fermy level is compared at both phases. We may assume, that from the semiconductor (e.f. type n – Si) the chargers go to the polymer phase and are stabilized on the different boundary traps. On semiconductive phase the equal-sized positive charge is formed. According to the charge concentration in the semiconductive particle and in the traps in polymer matrix on the verge, positive and negative charges will be distributed in accordance with the phases on some area near the verge of the phase separation. It is obvious, that the height of the barrier in this case is equal to the difference between the work function of the polymer and semiconductor or to the electronic сродством фаз. However, let's mention that in the composite this factor depending on the width of the polymer layers between semiconductive particles, which depends on the diameter and volume content of the semiconductive filler, may be somewhat different. In this connection, the formation of the potential barrier, appearance of the charge carriers and conductivity mechanism will be somewhat different. Carrier tunneling through the barrier may be accompanied by their hopping conductivity through thin polymer layer. The changes of the height and the width of the barrier on the verge of the phase separation with the increase of the content of the semiconductive particles at their diameter constancy (reduce) can be explained by the following way. At the increase of the content of the filler the width of polymer layers between the particles are reduced, that's why, in spite of the increase of number of traps on the verge the polymer-particle because of the strong on the boundary of the amorphousation, the number of ionized traps are reduced because of the increase of electrostatic электростатического repulsion between the boundary layers of polymer matrix (fig.2), bordering to two neighboring particles or to electrode and particle. That's why the reduce of the electroconductivity of the composite with the increase of the content is connected with the reduce of the barrier layer width and the height of the potential barrier on the verge of phase separation. From this point of view the examined effects, for example, piezoresistive effect in the composite polymer-semiconductor can be explained. By interaction of mechanic tension the thickness of polymer layers are reduced and it leads to the release of the charge carriers from the ionized traps on the verge of polymer- particle due to the increase of the electrostatic repulsion. If the energy disengaged from the traps of polymer layers of the charge carriers will be not enough to reach the zone of conductivity, the hopping mechanism is realized. In compliance with spatial and energy distance between separated traps the deformation of polymer layers and activation of the charge carriers under the influence of mechanic tension may lead to charge tunneling from one trap to another. Ionization of the traps on the verge of phases' separation and their charge transfer along the polymer layers by one of the mentioned mechanisms lead to further charge tunneling from semi-conductive particles to polymer and to decrease of height and width of the potential barrier, therefore, to increase of the conductivity of the composite, i.e. to appearance of piezoresistive effect.

[1] *A.I. Mammadov.* Elektronnaya tekhnika, 1988, ser.6, v.6, s.233.
[2] *A.I. Mammadov, M.A. Kurbanov, M.A. Ramazanov i dr.* Materials of 11 International conference "Yablona-86", Bulgaria, Varna, 1988, c.136-140.
[3] *A.I.Mammadov, M.G.Shakhtakhtinsky, M.A.Kurbanov, V.E. Yurkevich.* Compositive pyroelectric material. Patent N1745090, 01.03.1992.
[4] *A.I. Mammadov, O.A. Ragimov, E.M. Gamidov, M.A. Kurbanov.* Izvest. AN Azerb. Ser. mat. fiz. tekh., 1993, X1У, t.3-4, c.163.
[5] *M.G.Shakhtakhtinsky, A.I.Mammadov, M.A. Kurbanov* i *dr*. Dokl.AN Az.SSR, 1987,37,c.44-49.
[6] *M.G. Shakhtakhtinsky, N.A. Alieva, A.I. Mammadov.* Dokl. AN Az .SSR, 1986, №8, c.34-36.
[7] *M.G.Shakhtakhtinsky, M.A.Kurbanov, A.I.Mammadov. i dr*. Probl.Energ.AN Azerb., 2000, №2, c.58-63.

Ə.İ. Məmmədov

POLİMER – YARIMKEÇİRİCİ QEYRİ-NİZAMİ SİSTEMDƏ PYEZOREZİSTİV EFFEKTİ

Hazırkı işdə polimer-yarımkeçirici kompozit sistemin pyezorezistiv xassələrinin nəticələri təqdim edilmişdir. Yarımkeçirici maddənin yükdaşıyıcıların elektrikkeçiriciliyinin, konsentrasiyasının, yürüklüyünün və kompozitin dielektrik xarakteristikaların pyezorezistiv xassələrə təsiri öyrənilmişdir.

Müəyyən edilmişdir ki, kompozit sistemdə elektrik keçiriciliyi yükdaşıyıcıların polimer laylar vasitəsilə yarımkeçiricinin hissəcikləri arasında tunel effektinə əsasən baş verir.

А.И. Мамедов

ПЬЕЗОРЕЗИСТИВНЫЙ ЭФФЕКТ В НЕУПОРЯДОЧЕННОЙ СИСТЕМЕ ПОЛИМЕР-ПОЛУПРОВОДНИК

В настоящей работе представлены результаты исследования пьезорезистивных свойств композиционных систем полимер-полупроводник.

Изучено влияние на них электропроводности, концентрации и подвижности носителей заряда наполнителя и диэлектрические характеристики компонентов композита .

Установлено, что электропроводность в композитах осуществляется туннелированием носителей заряда между частичками наполнителя через полимерные прослойки.

Received: 05.01.06

DETERMINATION OF DEBYE SCREENING LENGTH FROM CONDUCTIVITY OF PbTe FILMS

M.M. PANAHOV, S.N. SARMASOV, M.Z. MAMEDOV
Baku State University
Baku, Az-1145, Z. Khalilov str, 23

In this paper the epitaxial layers of PbTe, which physical properties practically did not differ from properties of monocrystals were prepared. IR-lasers and receivers of radiation, optical filters and thermogenerators are created on the basis of such layers. However number of questions concerning growth of epitaxial layers of the given group materials is investigated insufficiently. The laws of oxygen molecules capture, during layers growth and influence of ferroelectric substrate polarization on conductivity of layers concern to such questions.

Measurement of film parameters, prepared on ferroelectric substrates, allows carrying out experimental determination of Debye screening length.

Introduction

In modern science and engineering with monocrystals of various semiconductors are widely applied also of thin films prepared by vacuum evaporation and other methods.

A huge success of physics of semiconductors has served as stimulus to development of semiconductor electronics and modern semiconductor technology. Application of semiconductors in various areas of cybernetics, automatics and telemechanics providing the successful decision of huge number of tasks of the large economic value, represents all growing requirements to essential expansion of nomenclature of a new semiconductor materials and increase of their quality.

The various methods for preparation of epitaxial films have enabled essential expansion of their application areas. The idea about an opportunity of use epitaxy for preparation monocrystalline films of semiconductors and creation on their basis *p-n* junctions was stated in 1954. The set of works is published in literature from that moment. The outstanding place among these works takes epitaxy of A^4B^6 group materials. These materials belong to narrow gap semiconductors and are widely used in engineering. In 1964 were prepared epitaxial layers of PbS and PbTe by S.A. Semiletov's group, which physical properties practically did not differ from properties of monocrystals. IR-lasers and receivers of radiation, optical filters and thermogenerators are created on the basis of such layers. However number of questions concerning growth of epitaxial layers of the given group materials is investigated insufficiently. The laws of oxygen molecules capture, during layers growth and influence of ferroelectric substrate polarization on conductivity of layers concern to such questions.

Films of PbTe were prepared on $LiNbO_3$ and Debye screening length is determined from conductivity of films.

Results and discussion

It is known, that at interaction of an external electrical field with the charge carriers in semiconductor are redistributed, therefore there is a volumetric charge $\rho(r)$ and electrical field *E* connected with a volumetric charge by the Poisson equation [1]:

$$div\varepsilon\varepsilon_0 E(r) = \rho(r) \qquad (1)$$

Expressing an electrical field *E* by potential we can write

$$\nabla^2\varphi(r) = -\rho(r) / \varepsilon\varepsilon_0 \qquad (2)$$

The potential energy of electrons *V(r)* bends zones so, that $E(r) = E + V(r)$ or,

$$E_c(r) = E_{(c)} + V(r) \qquad (3)$$

$$V(r) = V_S e^{-x/L_D} \qquad (4)$$

The zones bent downwards for the *p*-PbTe films. For the film prepared on negative, domains, the power zones are bent upwards (Figure 1).

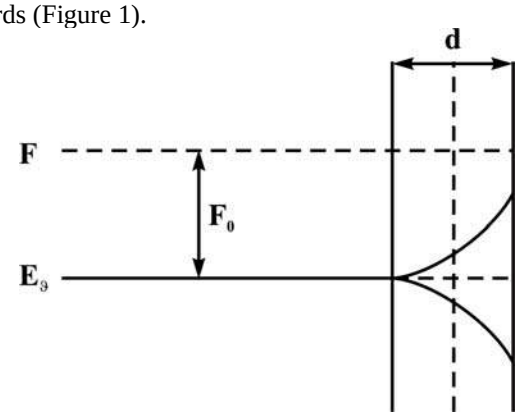

Fig. 1. The energetic zone diagram of *n*-PbTe films prepared on the negative and positive domain of $LiNbO_3$.

We shall consider the characteristics of conductivity change of the *p*-PbTe films prepared on different domains of $LiNbO_3$, for definition of Debye screening length (Figure 2). Let's on experimental curve allocate some points appropriate to thickness interval of *45-75 nm*, which where $tg\alpha < 1$, that is characteristic for *p*-PbTe films prepared $LiNbO_3$ with various polarization. Film of *p*-PbTe prepared on positive domains at small thickness $(d \le 50\ nm)$ has intrinsic conductivity about $\sim 10^{16}\ cm^{-3}$ and at $d \ge 50\,nm$ the structure was worsened. Therefore we have chosen some pairs of points in thickness interval of $50\,nm < d < 75\,nm$. The concentration of holes in samples with thickness of *60 nm*, prepared on positive and negative domains was:

$$P_+^1 = 3{,}8 \cdot 10^{16}\, cm^{-3} \quad , \quad P_-^1 = 1{,}4 \cdot 10^{17}\, cm^{-3} \, ,$$

and for the thickness of *70 nm* ,

$$P_+^2 = 6 \cdot 10^{16}\, cm^{-3} \quad , \quad P_-^2 = 2 \cdot 10^{17}\, cm^{-3}$$

The concentration holes in a source were ~ 10^{17} cm^{-3} at *300 K*, i.e. film is nondegenerate [2]. Then the formulas for concentration of charge carriers in semiconductors maybe write as [3; 4]

$$P_- \sim e^{-F_- / kt} \tag{5}$$

$$P_+ \sim e^{-F_+ / kt} \tag{6}$$

where P_- and P_+ - are the concentration of holes in PbTe films prepared on negative and positive domains of $LiNbO_3$, and F_- and F_+ - are the appropriate Fermi levels.

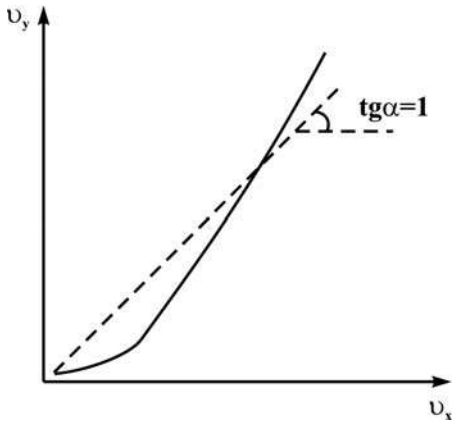

Fig. 2. Change of conductivity of the *n*-PbTe films on different domains of $LiNbO_3$.

As the semiconductor is in a thermodynamic balance condition and Fermi level in it is constant, distance between it and energy zones varies at change of carrier concentration. We spend readout of Fermi levels from edge of valence zone (Figure 1) and thus for Fermi levels of these two *p*-PbTe films we can write down:

$$F_- = F_0 - ue^{-d / L_D} \tag{7}$$

$$F_+ = F_0 + ue^{-d / L_D} \tag{8}$$

where u – is the potential energy connected to action by surface polarization. Substituting (7) and (8) in (5) and (6) and resulting in linear approximation $\left(L_D \geq d\right)$ averaging of a Fermi level by film thickness we can write for carriers concentration:

$$P_- \sim e^{-\frac{F_0 + ue^{-d/2L_D}}{kt}} \tag{9}$$

$$P_+ \sim e^{\frac{F_0 - ue^{-d/2L_D}}{kt}} \tag{10}$$

Further having divided (9) on (10) and taking the logarithm we have

$$\ln(P_- / P_+) = 2ue^{-\frac{d/2L_D}{kT}} \tag{11}$$

The expression for curve points appropriate to film thickness of $d_1 = 60\, nm$ and $d_2 = 70\, nm$, can be write as,

$$\ln(P_-^1 / P_+^1) = 2ue^{-\frac{d_1/2L_D}{kT}} \tag{12}$$

$$\ln(P_-^2 / P_+^2) = 2ue^{\frac{d_2/2L_D}{kT}} \tag{13}$$

Having divided the equation (12) on (13) and take the logarithm, we have,

$$\ln \frac{\ln\left(P_-^1 / P_+^1\right)}{\ln\left(P_-^2 / P_+^2\right)} = \frac{d_2 - d_1}{2L_D} \tag{14}$$

Equation for calculation the Debye screening length can be written:

$$L_D = \frac{d_2 - d_1}{2\ln \frac{\ln\left(P_-^1 / P_+^1\right)}{\ln\left(P_-^2 / P_+^2\right)}} \tag{15}$$

Substituting experimental values of d_1, d_2 and hole concentration for investigated films we find value of L_D~*100 nm*. Designed on the formula of $L_D = \sqrt{\varepsilon \varepsilon_0 kT / ne^2}$, this parameter is about $107 \cdot 10^{-9} m$. Here for PbTe ε ~*400*, $n = 10^{17}\, cm^{-3}$, $T = 300K$.

Conclusion

Substituting experimental values of d_1, d_2 and hole concentration for investigated films we find value of L_D~*100 nm*. Designed on the formula of, this parameter is about $107 \cdot 10^{-9} m$. Here for PbTe ε ~*400*, $n = 10^{17}\, cm^{-3}$, $T = 300K$

Measurement of film parameters, prepared on ferroelectric substrates, allows carrying out experimental determination of Debye screening length.

[1] *P.S. Kireev*. Physics of semiconductors, M., 1975, p.454.

[2] *C. Miqnotte*. Structural studies of erbium-implanted $NiNbO_3$ single crystals. Nucl Instrum. And Meth Phys. Res. B. 2002, 187, №1, c.95-110.

[3] *P.Q. Mantas*. Dielectric response of materials: extension to the Debye model: J. Eur. Ceram. Soc. 1999. 19, №12, c. 2079-2086.

[4] *A.V. Novoselova, V.P. Elmonov* in: Current topics in Materials Science, Noth-Holland, 1981, v.7, p.643.

M.M. Pənahov, S.N. Sərməsov, M.Z. Məmmədov

PbTe TƏBƏQƏLƏRİNİN KEÇİRİCİLİYİ ƏSASINDA DEBAY EKRANLAŞMA UZUNLUĞUNUN TƏYİNİ

PbTe-un alınmış epitaksial layının fiziki xassələri monokristalın xassələrindən praktiki olaraq fərqlənmir. Təbəqənin parametrlərinin ölçülməsi Debayın ekranlaşma uzunluğunu təcrübi olaraq təyin etməyə imkan verir.

Bu cür laylar əsasında İQ – lazerlər, şüalanma qəbuledicisi, optik süzgəclər və termogeneratorlar yaradılmışdır.

М.М. Панахов, С.Н. Сармасов, М.З. Мамедов

ОПРЕДЕЛЕНИЕ ДЛИНЫ ЭКРАНИРОВАНИЯ ДЕБАЯ ИЗ ПРОВОДИМОСТИ ПЛЕНОК PbTe

Получены эпитаксиальные слои PbTe, физические свойства которых практически не отличились от свойств монокристаллов [1,2]. На основе таких слоев созданы ИК – лазеры и приемники излучения, оптические фильтры и термогенераторы. Однако, ряд вопросов, относящихся к росту эпитаксиальных слоев данных соединений, изучен недостаточно. К таким вопросам относятся закономерности захвата молекул кислорода в процессе роста слоев, влияние поляризации сегнетоэлектрической подложки на проводимость слоев.

Измерение параметров пленок, выращенных на сегнетоэлектрических подложках, позволяет проводить экспериментальное определение длины экранирования Дебая.

Received: 14.12.05

KÜTLƏ SPEKTROMETRİNİN İON – OPTİK XARAKTERİSTİKALARINA ANALİZATORUN PARAMETRLƏRİNİN KƏNARAÇIXMALARININ TƏSİRİ

A.M. HƏŞİMOV, T.K. NURUBƏYLİ,
Azərbaycan MEA Fizika İnstitutu

K.Z. NURUYEV
Azərbaycan Milli Aerokosmik Agentliyi

İşdə aksial-simmetrik elektrik sahəli uçuşmüddətli kütlə spektrometrlərin konstruktiv elementlərinin hesablanmış qiymətlərdən kənaraçıxmalarının onların texniki göstəricilərinə təsiri tədqiq etmək üçün hesablama üsulu təklif olunub. Bu vaxt nominal parametrdən kənaraçıxmaların iki tipi, müəyyən diapazonda diskret və kəsilməz kənaraçıxmalara baxılmışdır.

Konkret kütlə spektrometri misalında konstruktiv elementlərin hazırlanmasında yol verilən kənaraçıxmaların və gərginliklərin fluktasiyalarının onun ayırdetmə qabiliyyətinə təsiri araşdırılmışdır.

Kütlə spektrometrlərinin layihələşdirilməsində və hazırlanmasında əsas məsələlərdən biri onun konstruktiv elementlərinin parametrlərinin hesablanmış qiymətlərdən yol verilən kənaraçıxmaların düzgün qiymətləndirilməsidir. Çünki bu tələblərin həddən artıq sərt olması cihazın əsassız baha başa gəlməsinə, sərbəstliyi isə analizatorun ion-optik xarakteristikalarının pisləşməsinə gətirir [1-4]. Elektrik və (və ya) maqnit sahəli analizatorların bu cür kənaraçıxmalarının metodiki və nəzəri əsaslandırılması işlərində baxılmışdır. Məsələn, [4]-də radial elektrik sahəli analizatora daxil olan enerjiyə və bucağa görə dağınıqlığa malik ion dəstinin analizator daxilində üçqat fokuslanma şərtləri nəzəri baxılmış və bu parametrlərin analizatorun ion-optik xarakteristikasına və ionların zamana və məkana görə fokuslaşdırılmasına təsiri araşdırılmışdır.

Bu məqalədə konkret parametrlərə malik aksial-simmetrik sahəyə malik uçuşmüddətli kütlə-spektrometrlərinin konstruktiv parametrlərinin nominal qiymətlərdən kənaraçıxmalarının onun texniki göstəricilərinə təsiri araşdırılmışdır.

1. Hesablama metodikası

Şəkildə aksial-simmetrik sahəli uçuşmüddətli kütlə analizatorunun ion-optik sxemi verilmişdir. [5]-də bu cür analizatorun ionlarının trayektoriyalarının onun çıxışında kəsişmə (fokuslanma) nöqtəsinin koordinatları aşağıdakı şəkildə verilmişdir:

$$\Delta = \frac{y - r_0}{r_0}; \quad \Lambda = \frac{z}{r_0}, \qquad (1)$$

burada y - ionların fokus nöqtəsində orta trayektoriyadan nisbi kənaraçıxmalarının radial proyeksiyası; z - radial istiqamətdə bucağa görə dağınıqlığa malik ionların orta trayektoriyadan kənaraçıxması; r_0- orta trayektoriyanın radiusudur.

Bu koordinatların α_i kiçik parametrlərdən asılılığı aşağıdakı parametrik tənliklərlə ifadə olunur:

$$\Delta = \sum_{i=1}^{7} \Delta_i \alpha_i \quad \text{və} \quad \Lambda = \sum_{i=1}^{7} \Lambda_i \alpha_i, \qquad (2)$$

burada Δ_i və Λ_i - girişində və çıxışında elektrik sahəsi kəskin sərhədə malik analizatorun həndəsi və sahə parametrlərinin funksiyaları, kiçik α_i parametrləri isə

$$\alpha_1 = tg\,\alpha;\ \alpha_2 = tg\,\beta;\ \alpha_3 = \frac{S}{r_0};$$

$$\alpha_4 = \frac{h}{r_0};\ \alpha_5 = \frac{\Delta V}{V_0};\ \alpha_6 = \frac{\Delta M}{M_0};\ \alpha_7 = \frac{U_0}{V_0},$$

burada α və β - ionların radial və aksial istiqamətdə açılma bucaqları; S, h- giriş diafranmasının eni və hündürlüyü; ΔV, ΔM - ionun orta trayektoriya ilə hərəkətinə uyğun enerjisi və kütləsinin kənara çıxmaları, V_0 vəU_0 - ionun enerjisinə uyğun sürətləndirici gərginlik və orta trayektoriyanın potensiallarıdır.

Kütlə spektrometrinin parametrlərinin hesablanmış qiymətlərdən kənaraçıxmaları nəinki ionların trayektoriya tənliklərinin əmsallarına (Δ_i, Δ_i) həmçinin, kiçik parametrlərə də təsir edə bilir. Bu hal ion mənbəyinin eninə yerdəyişməsi və potensialların fluktasiyası zamanı baş verir. Bu halları [6]-dan istifadə etməklə araşdırmaq olar. Burada isə Δ_i və Λ_i əmsallarının dəyişməsi halına baxaq. Hesablanmanın sadəliyi xatirinə fərz edək ki, analizatorun parametrlərinin α_i kənaraçıxmaları kənar elektrik və maqnit sahələrinin paylanmasına təsir etmir. Onda (1)-dəki Δ_i əmsalının dəyişməsinin aşağıdakı şəkildə göstərmək olar:

$$\delta\Delta_i = \sum_{i=1}^{7} \Delta_i \alpha_i + \sum_{i=1}^{7} \left(\sum_{k=1}^{N} \frac{\partial \Delta_i}{\partial P_k} \beta_k \right) \alpha_i,$$

burada P_k -kənaraçıxmalara məruz qalmış parametrlər, $\beta_k = \delta P_k$ – k- cı parametrin kənaraçıxması; N-P_k parametrlərin sayıdır. P_k- parametrləri dedikdə analizatorun həndəsi ölçülərini xarakterizə edən r_0, λ_1, λ_2, ψ, χ_0, χ_k (şəkilə bax) və ya elektrik və maqnit sahələrinin paylanmasını götürmək olar.

α_i və β_k parametrləri bir-birindən asılı olmadığı üçün əmsalların maksimal dəyişmələrinni belə yazmaq olar:

$$\left|\delta\Delta_i\right|_{max} \le \sum_{k=1}^{N} \sum_{i=1}^{6} \left| \frac{\partial \Delta_i}{\partial P_k} \right| \left|\alpha_i\right|_{max} \left|\beta_e\right|_{max}. \qquad (3)$$

Buradan görünür ki, xarakteristikaları ikinci tərtib kiçik kəmiyyətlərlə təyin olunan analizatorun parametrlərinin kənaraçıxmaları hesabına Δ_i əmsallarının dəyişməsi heç olmasa bir tərtib kiçik olmalıdır.

2. Kənarçıxmaların ionların bucağa görə fokuslanmasına təsiri

İonların bucağa görə fokuslanması zamanı analizatorun parametrlərinin hesablanmış kənaraçıxmaları Δ_i əmsallarının aşağıdakı dəyişmələrinə gətirir:

$$\delta\Delta_i = \sum_{k=1}^{N} \left.\frac{\partial \Delta_i}{\partial P_k}\right|_{\lambda_2} \cdot \beta_k \ .$$

Bu zaman fokus nöqtəsi sistemin optik oxu boyu yerdəyişməsi belə ifadə olunur:

$$\left|\delta\lambda_2\right| = \frac{1}{J_1}\sum_{k=1}^{N}\frac{\partial\Delta_i}{\partial P_k}\left|\beta_k\right| \le \frac{1}{J_1}\sum_{k=1}^{N}\frac{\partial\Delta_i}{\partial P_k}\left|\beta_k\right|_{max} \ , \quad (4)$$

burada $J_1 = \dfrac{\partial\Delta_i}{\partial x_r}$- analizatorun çıxış qolunun $\left(\lambda_2 = \dfrac{l_2}{r_0}\right)$ fokusun yerdəyişməsinə verdiyi töhfəsidir.

Qeyd edək ki, analizatorun konstruktiv parametrlərinin icazə verilən kənaraçıxmaları elə seçilməlidir ki, Δ_i-nin dəyişməsinin yekun qiyməti ikinci tərtib aberrasiyadan böyük olmasın. Bu vaxt əgər arzu edilən nəticəni əldə etmək mümkün olmursa, ya cihazın konstruksiyasında müəyyən dəyişiklik etməli, və ya ion mənbəyinin dəliyinin yerini $\lambda_2 - \left|\delta\lambda_2\right|_{max}$-dan $\lambda_2 + \left|\delta\lambda_2\right|_{max}$ intervalda dəyişdirmək nəzərdə tutulmalı, ya da fokuslanma başqa parametrlərin dəyişməsi hesabına əldə olunmalıdır.

[3]-də göstərilmişdir ki, onların enerjiyə və radial bucağa görə dağınıqlıq hesabına fokuslanmanın pozulmasını korreksiya etmək üçün analizatorun üç parametrindən istifadə etmək kifayətdir. Buxdığımız halda bu üç parametrin (P_1, P_2, P_3) nominal qiymətdən kənaraçıxmaları zamanı fokuslanma şərti aşağıdakı tənliyi ödəməlidir.

$$\left.\frac{\partial\Delta_i}{\partial P_1}\right|_{\lambda_2}\beta_1 + \left.\frac{\partial\Delta_i}{\partial P_2}\right|_{\lambda_2}\beta_2 + \left.\frac{\partial\Delta_i}{\partial P_3}\right|_{\lambda_2}\beta_3 = -\sum_{k=1}^{N}\left.\frac{\partial\Delta_i}{\partial P_2}\right|_{\lambda_2}\beta_k \ .$$

Əgər fokuslanma zamanı β_1, β_2, β_3 parametrləri simmetrik dəyişməyə məruz qalırsa $\left(-\beta_{k,max} \le \beta_k \le \beta_{k,max}\right)$, onda fokuslanmanı əldə olunması üçün aşağıdakı bərabərsizlik ödənilməlidir.

$$\sum_{n=1}^{3}\left|\frac{\partial\Delta_i}{\partial P_n}\right|_{\lambda_2}\left|\beta_n\right|_{max} \ge \sum_{k=1}^{N}\left|\frac{\partial\Delta_i}{\partial P_n}\right|_{\lambda_2}\left|\beta_k\right|_{max} \ .$$

Bu zaman inamlı nəticə əldə etmək üçün hər bir parametrin tənzimləmə sərhədlərini elə seçmək lazımdır ki,

$$\beta_{n,max} \ge \left|\frac{\partial\Delta_i}{\partial P_k}\right|^{-1}_{\lambda_2}\sum_{k=1}^{N}\left|\frac{\partial\Delta_i}{\partial P_k}\right|_{\lambda_2}\left|\beta_k\right|_{max} \qquad (5)$$

olsun.

3. Kənaraçıxmaların analizatorun dispersiyasına və ayırdetmə qabiliyyətinə təsiri

Yuxarıda deyilənlərə və [6]-da alınan nəticələrə əsasən analizatorun parametrlərinin kənaraçıxmaları hesabına onun kütləyə görə ayırdetmə qabiliyyətinin (R) hesablanmış qiymətini aşağıdakı ifadə ilə təyin etmək olar:

$$\delta R \le \sum_{k=1}^{N}\left|\beta_k R^2 \sum_{i=1}^{7}\left(\frac{1}{\Delta_6}\frac{\partial\Delta_i}{\partial P_k} - \frac{\Delta_i}{\Delta_6^2}\frac{\partial\Delta_6}{\partial P_k}\right)\right| . \quad (6)$$

Analizatorun yol verilən maksimal kənaraçıxması əvvəlcədən verilmiş δR qiymətinin və hər bir β_k-nın bu dəyişməyə verə biləcəyi töhfələri nəzərə alsaq analizatorun konstruktiv parametrlərinin icazə verilən kənarıçıxmalarını təyin etmək olar.

Analoji olaraq dispersiya əmsallarının qiymətlərini dəyişməsini təyin etmək üçün

$$\delta\Delta_5 = \sum_{k=1}^{N}\left.\frac{\partial\Delta_5}{\partial P_k}\right|_{\lambda_2} ; \qquad \delta\Delta_6 = \sum_{k=1}^{N}\left.\frac{\partial\Delta_{65}}{\partial P_k}\right|_{\lambda_2}\beta_k$$

alarıq.

4. Sürətləndirici gərginliyin və sahələrin paylanmasının fluktasiyasının analizatorun xarakteristikalarına təsiri

Yuxarıda baxdığımız bütün halların hamısında fərz olunurdu ki, analizatorun hər bir parametri onların nominal qiymətləri ətrafında konkret qiymət alır. Bu halda isə baxılan parametrlər müəyyən diapazonda kəsilməz dəyişdiyi üçün bu dəyişmələrin analizatorun ion-optik xarakteristikalarına təsirini kompensə etmək olar.

[5, 6]-da göstərildiyi kimi sürətləndirici gərginliyin qeyri-stabilliyi ionların enerjiyə görə dağınıqlığına əlavə ekvivalent dağınıqlıq deməkdir. Gərginliklərin qeyri – stabilliyi ilə buna uyğun olan enerji və kütlənin ekvivalent dəyişmələri arasında əlaqə tənliyi zərrəciklərin orta trayektoriya ilə hərəkətini təmin edən tarazlıq şərtindən alınır

$$\frac{1}{2}(1-k)\varepsilon + \frac{1}{2}(1+k)\gamma = (1+k)\frac{\delta H_0}{H_0} - k\frac{\delta E_0}{E_0} , \quad (7)$$

burada $\varepsilon = \alpha_5$ və $\gamma = \alpha_6$- enerji və kütlənin nisbi kənaraçıxmaları, E_0 və H_0- elektrik və maqnit sahələrinin intensivliklərinin orta trayektoriyadakı qiymətidir. k=-1 (elektrik sahəsi) və ya k=1 (maqnit sahəsi) qiymətlərini yerinə qoysaq gərginliklərin dəyişmələrinin «yaratdığı» əlavə enerji və kütlə dağınıqları üçün uyğun olaraq

$$\varepsilon_{max} = \left(\frac{\delta E_0}{E_0}\right)_{max} ; \qquad \varepsilon_{max} = 2\left(\frac{\delta H_0}{H_0}\right)$$

yazmaq olar.

Hər iki sahənin birgə təsiri zamanı həmin fluktasiyalarını «kütləyə görə əlavə dağınıqlığı»

$$\gamma_{max} = 2_{max} = \left(\frac{\delta E_0}{E_0}\right)_{max} + _{max} = \left(\frac{\delta H_0}{H_0}\right)_{max}$$

olar. Axırıncı ifadədən görünür ki, başqa şərtlərin eyni olduğu elektrik və maqnit sahəsi analizatorların maqnit sahəsinin

stabilliyinə elektrik sahəsinin stabilliyinə nisbətən daha ciddi məhdudiyyətlər qoyulmalıdır. Başqa sözlə bu qeyri-stabilliklərin analizatorun işinə mane olmaması üçün onların yol verilən kənaraçıxmaları üçüncü tərtib kiçik kəmiyyət səviyyəsində olmalıdır.

5. Analizatorun parametrlərinin kənaraçıxmalarının onun ayırdetmə qabiliyyətinə təsirinin hesablanması

Hesablanmış parametrdəri r_0=240mm,$\lambda_1=\lambda_2=1$, ψ=254°44′, $\chi_0=\chi_k=\pi/2$, $\omega=1$, $k=-1$ (elektrostatik sahə) olan kütlə analizatoruna baxaq. Fərz edək ki, $V_0=1.2$kV, $\alpha_{max}=\beta_{max}=1.75\cdot10^{-2}$, $S=10$mm, $h=0.08$mm, $\alpha_5=5\cdot10^{-4}$.

Uyğun hesablamalardan sonra (6) aşağıdakı şəklə düşər:

$$\delta R \le \left(17{,}6\frac{\delta r_0}{r_0} + 8{,}7\delta\lambda_1 + 8{,}8\,\delta\lambda_2 + 17{,}6\,\delta\psi + \right. \\ \left. + \left(0\cdot\delta\chi_0 + 0\,\delta\chi_k + 45{,}3\,\delta\omega \right)\cdot 10^3 \right) \qquad (8)$$

Əgər fərz etsək ki, ayırdetmə qabiliyyətinin hesablanmış $R=1000$ qiymətindən yol verilən kənaraçıxması $\delta R=2.5q_0$ -dir və bütün parametrlərin bu dəyişməyə verdiyi töhfə eyni olub, uyğun olaraq $\delta r_0=0.07$, $\delta\lambda_1=\delta\lambda_2=5.6\cdot10^{-4}$, $\delta\psi=2.8\cdot10^{-8}$rad, δω=1.1·10-4 -dirsə onda (8)-dən $\delta\chi_0$ və $\delta\chi_k$ üçün 0,0175 alarıq. Onda parametrlərin yol verilən maksimal kənaraçıxmaları üçün aşağıdakıları alırıq:

İonların orta trayektoriyasının əyrilik radiusu (r_0)0,07 mm.

Analizatorun giriş və çıxış qolları (l_1 və $l_2 l_2$) 0,13mm.

Radial sahənin açılma bucağı (ψ)1′ bucaq dəqiqəsi. Elektrodların əyrilik radiusları (r_1 və r_2) 0,03

(8) ifadəsini araşdırarkən aşağıdakıları nəzərə almaq lazımdır:

1. Analizatorun parametrlərinin nominal qiymətlərdən yol verilmiş kənaraçıxmaları onların əvvəldə qəbul olunmuş kiçik kəmiyyət şərtinə uyğun gəlməsi xatirinə böyük götürülməməlidir.

2. Digər tərəfdən onların olduqca kiçik qəbul edilməsi qeyd olunduğu kimi cihazın hazırlanmasını mürəkkəbləşdirir, bəzən isə mümkünsüz edir. Nəzərə almaq lazımdır ki, yol verilən kənaraçıxmaların maksimum qiymətləri kütlə spektrometrinin ayırdetmə qabiliyyətini nəzərə çarpacaq dərəcədə azaltmasın. Burada da araşdırma iki istiqamətdə aparıla bilər. Birinci – parametrlərin kənaraçıxmaların qiymətlərini qabaqcadan qəbul edərək onların cihazın ayırdetmə qabiliyyətinə təsirini hesablamaq, beləliklə kənara çıxmaların qiymətini seçmək; ikincisi – ayırdetmə qabiliyyətinin yol verilən dəyişməsini və onun parametrlər arasında bölünməsini qabaqcadan bildikdən sonra analizatorun parametrlərini qiymətlərinin yol verilən maksimal kənaraçıxmalarını təyin etmək.

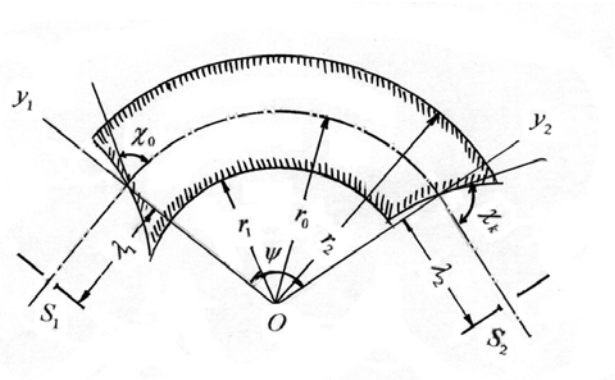

Şəkil 1. Aksial-simmetrik sahəli uçuşmüddətli kütlə analizatorunun ion-optik sxemi.

[1]. *M.L. Aleksandrov, L.N. Qaal, V.F. Denisov*. JTF, 1973 q., 43, vıp. 4, s.833. (Rusca).

[2]. *M.L. Aleksandrov, E.V. Sedunov*. Nauçnıne priborı, 1976, № 11, s. 16-21. (Rusca).

[3]. *A.F. Maqov, Q.M. Trubachov*. Nauçnıne priborı, 1978, № 18, s. 34-39. (Rusca).

[4]. *K.Z. Nuriyev, Z.K. Nurubeyli, T.K. Nurubeyli.* Energetikanın problemleri, 2005, № 3, s. 199.

[5]. *V.A. Oleynikov, A.A. Sısoev*. Metodika rasçeta i issledovanine fokusiruyushix po vremeni proleta svoystv sektornıx aksialno-simmetriçnıx poley. Dep. v VINITI, № 32792-80. (Rusca).

[6]. *A.A. Sısoev, Q.A. Samsonov*. Teoriya i rasçet statiçeskix mass-analizatorov, Ch. I, M. Izd-vo MIFI, 1972. (Rusca).

Hasimov A.M., Nurubeyli T.K., Nuruyev K.Z.

THE INFLUENCE OF PARAMETERS' DEVIATION ON ION-OPTICAL CHARACTER OF MASS-SPECTROMETER

The method was elaborated which allows to research the influence of the value deviation from nominal parameters of analyzer over the character of mass-spectrometer with axial symmetrical electrical field. Two types of deviation were considered: receiving discrete values and the values changing in some ranges uninterruptedly.

The influence of discrepancy of master field elements as well as the instability of accelerating and declinator fields over the mass-spectrometer characteristic researched.

Гашимов А. М., Нурубейли Т. К., Нуриев К.З.

ВЛИЯНИЕ ОТКЛОНЕНИЙ ПАРАМЕТРОВ АНАЛИЗАТОРА НА ИОННО-ОПТИЧЕСКИЕ ХАРАКТЕРИСТИКИ МАСС-СПЕКТРОМЕТРА

Разработана методика, позволяющая исследовать влияние отклонений значений от номинальных параметров анализатора на характеристики масс-спектрометра с аксиально-симметричным электрическим полем. Рассмотрены два типа отклонений: принимающие дискретные значения и меняющиеся непрерывно в некотором диапазоне.

Исследовано влияние неточности размеров полезадающих элементов, а также нестабильности ускоряющих и отклоняющих полей на характеристики масс-спектрометра.

Received: 15.12.05

PUTTING OUT OF LUMINESCENCE OF Nd^{3+} IONS IN SEMICONDUCTOR GLASSES

G.I. ABUTALIBOV, A.A. MAMEDOV
Institute of Physics of National Azerbaijan Academy of Sciences
Az-1143, Baku, H. Javid ave., 33

The processes of transfer and degradation of the energy of electron excitement in glassy matrix have been investigated. The microparameters of the interaction and minimal distance Nd-Nd have been defined by the different methods.

The several hundreds of active mediums of solid-state lasers have been found during the time of the formation of quantum electronics. These are mainly activated dielectric crystals and glasses. Their spectral-luminescent characteristics, fundamental properties of quantum transfers, are fundamental for laser crystals and glasses, defining the possibility of generation obtaining. That's why the luminescent properties present the most interest from all their properties. The methods of quantitative investigations of transformation processes of energy of electron excitement in collective of optically active centers, interacting with each other and field of the external radiation have been developed relatively recently. It is established, that we always have the situation $\Gamma >> W$ in laser crystal and glasses, where W is interaction possibility, Γ is line width [1]. By other words, the interaction is carried out by incoherent way that gives the possibility to use the possible approach for the describing of the energy processes in collective of interacting particles.

The energy relaxation of electron excitement in the collective of interacted particles in solid body presents itself the superposition of big number of elementary acts of energy transfer of two types. Firstly, these are elementary processes, leading to the excitement migration on metastable particle states, creating the donor (*D*) subsystem at their interaction with acceptors (*A*). There is the possibility of taking place of corresponding elementary acts [1]

$$W_{DD} = C_{DD} f_{DD}(R) \quad W_{DA} = C_{DA} f_{DA}(R) \ , \qquad (1)$$

where C_{DD} and C_{DA} are microparameters of interactions *D-D* and *D-A*; *R* is distance between couple of the interacted particles; $f_{DD}(R)$ $f_{DA}(R)$ are the functions, the form of which is defined by the nature of the interactions *D-D* and *D-A*. The dipole-dipole interaction and $f_{DD}(R)=f_{DA}(R)=R^{-6}$ take place in laser crystal and glasses.

The interaction processes in common case can be divided on three stages, revealing in the decomposition curve of the excited state, which can be expressed in general form [2]:

$$I(t) = I_0 \exp\left[-\frac{t}{\tau_0} + \Pi(t) \right] \qquad (2)$$

where τ_0 is life time of donor excited state in the absence of energy transfer from donors to acceptors, and $\Pi(t)$ function describes the kinetics of irreversible non-radiating energy transfer from excited donor state. The kinetics of first two stages, which are responsible for static transfer (the transfer in the absence of energy migration on donor subsystem), is described by common expression [3]

$$\Pi(t) = \sum_i In\left\{1 - x_a + x_a \exp\left[-(W_{DA})_i t\right]\right\} , \qquad (3)$$

where x_α is relative acceptor concentration, i.e. the part, accessible for acceptors of lattice nodes, captured by acceptors. The summation is led on all lattice nodes, accessible to the energy acceptors.

From the expression (3) in the capacity of the limits the expressions are followed, describing the static order decomposition at $t<t_1$ and static disorder decomposition at $t<t_1$:

$$t_1 \approx \left\{ \frac{x_a}{\left| In\,(1-x_a) \right|} \ \frac{C_{DA}}{R_0^6} \right\} , \qquad (4)$$

where R_0 is minimal distance between donor and acceptor of the energy. At $t<t_1$ the expression (3) is transformed in

$$\Pi(t) = -x_A c_{DA} \sum_i \frac{1}{R_i^6} t \ . \qquad (5)$$

From (4) it is seen, that at $x_a \to 1$, $t_1 \to \infty$, i.e. the expression (5) will have the place in all time scale. This is naturally, i.e. in this case each donor has the equal surroundings and all they disintegrate with equal velocity $C_{DA} \sum_i \frac{1}{R_i^6}$, which is equal to the sum of possibilities of transfer on all acceptors.

The summation exchange on *i* on integration on *R* in (5) gives

$$\Pi(t) = -\frac{4}{3} \pi \frac{c_{DA} n_A}{R_0^3} \ . \qquad (6)$$

The expression (3) has the form at low acceptor concentration ($x_\alpha \to 0$):

$$\Pi(t) = -x_a \sum_i \left[1 - \exp\left(-\frac{c_{DA}}{R_i^6} t \right) \right]. \qquad (7)$$

The summation exchange on I on integration on *R* in (7) at $t<t$ leads to the well-known Ferster result

$$\Pi(t) = -\gamma \sqrt{t} \ , \qquad (8)$$

where $\gamma = \frac{4}{3} \pi^{3/2} n_a \sqrt{c_{DA}}$.

The energy migration on the donor subsystem causes the process of migration-limited energy transfer from donor subsystem into acceptor one. It takes place at $t \rangle t_2 \sim (\gamma / \overline{W})^2$ and the decomposition law of excited state of donor subsystem has the form [1]:

$$I(t) = I_0 \exp\left[-\left(\frac{t}{\tau} + \overline{W}t + \Delta\right)\right] \qquad (9)$$

where $e^{-\Delta}$ is excitement part, not died by static way and

$$\overline{W} = f(n_A, n_D, c_{DA}, c_{DD}) \qquad (10)$$

(n_D is concentration of energy donors) – velocity of migration-limited relaxation. The form of function (10) is different in different models of migration-limited relaxation, which describe the different methods of excited transport in energy acceptor region [2]. At

$$\delta_{R_w} \rangle\rangle \overline{\lambda} \ , \qquad (11)$$

where $\overline{\lambda} = n_\partial^{-1/3}$ is character length of migration jump, $\delta_{R_W} = R_W / m$ (m is interaction multipolarity degree, in our case m=6, R_W is radius of sphere of strong stewing, defining as

$$\frac{c_{DA}}{R_W^6}\tau_W = 1, \qquad (12)$$

τ_W is passing time through sphere of radius R_w in the acceptor absence), mechanism of migration stewing is diffusion one.

As analysis shows [4], the condition (11) demands very strong demands on the ratio $C_{DA}/C_{DD} = z \geq 10^7$ [4] that makes it very doubtful: the possibility of the realization of diffusion model of energy transfer in laser crystals and glasses. The realization of mixed stewing mechanism, suggested in [2], is also unlikely, i.e. the potential form of dipole-dipole interaction doesn't leave the place for the region of this mechanism use:

$$R_W / m \langle\langle \lambda \langle\langle R_W . \qquad (13)$$

The jump mechanism of migration-limited relaxation is more often realized in practices [1,4]. It is supposed, that excitement enters (goes out) into (from) stewing sphere (s) for one jump, i.e.

$$R_W \leq \lambda , \qquad (14)$$

That on microparameter language means

$$C_{DA} \leq C_{DD} \qquad (15)$$

Concretesizing the time of one jump τ_W as the most possible one:

$$\tau_W^{-1} = (4/3\pi^{3/2} n_D C_{DD}^{1/2})^2 / 6 \qquad (16)$$

We can obtain the expression for R_W in jump model

$$R_W{}^j = (c_{DA} / 9 c_{DD} n_D{}^2)^{1/6} . \qquad (17)$$

The calculation of fundamental connection (10) of velocity of non-radiated relaxation because of the energy migration to the acceptor with microparameters of energy transfer for jump mechanism was carried out in [5]. This connection is defined by the formula

$$\overline{W} = 20 n_D n_A \sqrt{c_{DA}} \sqrt{c_{DD}} \sqrt{\rho_0} , \qquad (18)$$

where ρ_0 is possibility not to be in initial movement point at occasional passing along the lattice. In the case of simple three-dimensional passing $\rho_0 \approx 0.66$, i.e. taking under consideration the consequence, that the excitement can go out from the band of the acceptor action without dying, leads to the appearance of the numeral coefficient, very few differing from 1. The following is more significant one. At the calculation of ratio (18), the supposition about the fact, that distance donor-acceptor fluctuate in different stewing spheres was used. This supposition is right only at the small concentrations of active particles in crystal lattice, when acceptor donors exchange the one and the same base ion. By other words, it takes place, when the condition (14) has been carried out, but moreover in sphere R_W^j many seats are existed.

The concentration increase of donors leads to the decrease as $\overline{\lambda}$, so R_W . The ratio

$$R_W{}^j \langle\langle R_0 \qquad (19)$$

means the density constancy of donor excitements in space, which decreases in time on exponential law with decomposition constant, given by (5), i.e. the velocity of non-radiated. Decomposition in all time range is the single one and coincides with decomposition velocity on the initial part at small donor density. Such situation is called by kinetic limit.

The microparameters C_{DA} ,C_{DD} and value R_{min} had been defined by two methods. First method is the following one.

The expression for $\Pi(t)$ at dipole-dipole transfer mechanism has the form in limits of Zusman approach:

$$\Pi(t) = \frac{2}{3}\pi^2 n_A \sqrt{C_{DA}\tau_0}\left[\frac{1}{2}\Phi\left(\sqrt{\frac{t}{\tau_0}}\right) + \frac{t}{\tau_0}\Phi\left(\sqrt{\frac{t}{\tau_0}}\right) + e^{-\frac{t}{\tau_0}}\left(\frac{t}{\pi\tau_0}\right)^{\frac{1}{2}}\right] \ , \qquad (20)$$

where $n_A(n_D)$ is acceptor concentration (donors), $\tau_0 = \left(\frac{8}{27}\pi^3 n_D^2 C_{DD}\right)^{-1}$ - is more possible time of donor-donor transfer, and $\Phi(x) = \frac{2}{\sqrt{\pi}}\int_0^x e^{-y^2} dy$ is possibility integral.

Momentary stewing velocity $W(t)$ is equal at this

$$W(t) = \frac{d\Pi(t)}{dt} = n_A \int_0^\infty \frac{C_{DA}}{R^6} n(R,t) dV = \frac{2}{3}\pi^2 n_A \left(\frac{C_{DA}}{\tau_0}\right)^{\frac{1}{2}} \left\{\frac{1}{\sqrt{\pi}}\left(\frac{\tau_0}{t}\right)^{\frac{1}{2}} e^{-\frac{t}{\tau_0}} + \Phi\left(\sqrt{\frac{t}{\tau_0}}\right)\right\} \ , \qquad (21)$$

where *n(R,t)* is momentary excitement density on donor, being on *R* distance from acceptor. However, formulas (20) and (22) had been obtained in the supposition of the equality to the zero of minimal distance donor-acceptor, where the infinite big velocity of stewing at *t=0* was obtained from, that made the theory comparison with experiment in all time scale difficult. It is need to note, that at the consideration of minimal distance, not equaling zero, the analytic expression for *Π(t)* and *W(t)* can't be obtained, however, their asymptotic behavior can be analyzed, and also it is possible to study functions *Π(t)* and *W(t)* by numerical methods.

In ref. [7], the common expressions for *Π(t)* and *W(t)*, which have the form had been obtained with the use of the results [6], taking under consideration $R_0 \neq 0$:

$$W(t) = \frac{4\pi}{3} n_A \left(\frac{C_{DA}}{\tau_0}\right)^{\frac{1}{2}} \left\{ arctgb + e^{-\frac{t}{\tau_0}} \int_0^b e^{-\frac{t}{\tau_0}x^2} dx - e^{-\frac{t}{\tau_0}} \int_0^b \frac{e^{-\frac{t}{\tau_0}x^2}}{1+x^2} dx \right\} , \qquad (22)$$

$$\Pi(t) = \int_0^t W(t')dt'$$

where $b = \left(\frac{\tau_0}{\tau_1}\right)^{1/2}$, $\tau_1 = \left(\frac{C_{DA}}{R_0^6}\right)^{-1}$. The expression (22) describes the decomposition process of excited donor state in all time interval.

Thus, the microparameters C_{DA} , C_{DD} and value R_{min} can be obtained from the best coincidence of calculated and experimental curves.

The second method is the following one. According to Burshtein theory [6], kinetics of migration – rapid process, assigned by function *N(t)*, is described by integral equation

$$N(t) = N_0(t)R_e(t) - \int_0^t N_0(t-t')\dot{R}_e(t-t')N(t')dt' , \qquad (23)$$

where $R_e = e^{-\frac{t}{\tau_0}}$ (24) describes the kinetics at the end of excitement, and $N_0 = \langle e^{-Wt} \rangle$ is kinetics of static stewing of the excitement by acceptors. In particular, at dipole-dipole interaction N_0 has the form:

$$N_0 = \langle e^{-Wt} \rangle = e^{-\gamma\sqrt{t}} . \qquad (25)$$

It is need to note, that end kinetics of *R(t)* coincides with function (24) only on initial step $(t \le \tau_0)$, when the excitement return on initial center can't be considered, even in the case of order donor situation. At the dipole interaction the end kinetics at partial consideration of the return and dispersal on the distances between the donors has the form [8]:

$$R(t) = \exp\left(-\sqrt{\frac{t}{\tilde{\tau}}}\right), \qquad (26)$$

where $\tilde{\tau}$ is average holding time on the initial center. That's why in equation (23) R_e should be changed on *R*, after that instead (25) the following kinetic equation for the stewing will be obtained

$$N(t) = N_0(t)R(t) - \int_0^t N_0(t-t')\dot{R}(t-t')N(t')dt' . \qquad (27)$$

In the equation (27) the minimal distance donor-acceptor wasn't considered. As it was mentioned, the damping law of donor number with taking under consideration of "forbidden volume" differs from Ferster one (25) and has the form:

$$N_0^{'} = \exp\left\{ -\frac{4\pi}{3} n_A R_{\min}^3 \left(e^{-y_1} - 1 + 2\sqrt{y_1} \int_0^{\sqrt{y_1}} e^{-x^2} dx \right) \right\}, \text{ where } y_1 = \frac{tC_{DA}}{R_{\min}^6} . \qquad (28)$$

That's why in order to consider the minimal distance donor-acceptor, in equation (23) N_0 should be changed on N_0'. After that exchange we obtain the following equation

$$N(t) = N_0'(t)R(t) - \int_0^t N_0(t-t')\dot{R}(t-t')N(t')dt' . \qquad (29)$$

It is impossible to solve this equation in analytic form and *N(t)* can be investigated by only numerical methods. Thus, solving the equation (22), from the condition of the best coincidence of experimental and calculated curves it is possible to define the microparameters C_{DD}, C_{DA} and R_{min}.

It was shown in the previous chapter, that interaction microparameters, defined by different methods for neodymium ions in glass $La_2S_3{\cdot}2Ga_2O_3$ are very close. This is connected with the fact that in glass $La_2S_3{\cdot}2Ga_2O_3$-Nd^{3+} at the investigated neodymium concentrations the condition $\tau_1 \langle\langle t \langle\langle \tau_0$ is well carried out. If the given condition isn't carried out, it is impossible to define interaction microparameters, emphasizing the region of static disorder decomposition. That's why at the use of traditional analysis it is need to check the carrying out of the condition $\tau_1 \langle\langle t \langle\langle \tau_0$. If it isn't carried out, then the describing of the curves in all time scale is the only right step.

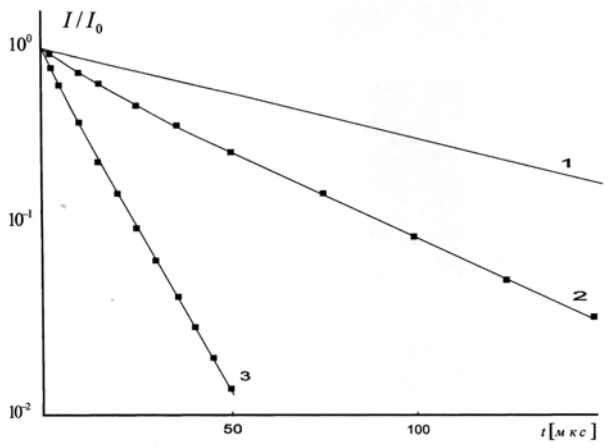

Fig.1. The experimental (continuous time) and calculated (points) of the decomposition of metastable state $^4F_{3/2}Nd^{+3}$ in glasses $(La_{1-x}Nd_x)_2S_3{\cdot}2Ga_2S_3$: 1-x=0.04; 2-x=0.14; 3-x=0.32; λ_b=0.591mcm.

In glass $La_2S_3{\cdot}2Ga_2S_3$-Nd^{3+} the condition $\tau_1 \langle\langle t \langle\langle \tau_0$ doesn't carried out and traditional analysis gives the result, strongly differing from the results, obtained on the describing of experimental curves in all time scale in Zusman theory limits. For the neodymium ions in glass $La_2S_3{\cdot}2Ga_2S_3$ the following parameters had been obtained on the describing of the experimental decomposition curves in all investigated interval (fig.1, point-calculation, total lines-experiment):

$$R_{\min} \approx (5{,}4 \pm 0{,}8)\,\text{Å}$$
$$C_{DA} \approx (2{,}5 \pm 1)\cdot 10^{-39}\, cm^6\, s^{-1}$$
$$C_{DD} \approx (1 \pm 0{,}5)\cdot 10^{-38}\, cm^6\, s^{-1}$$

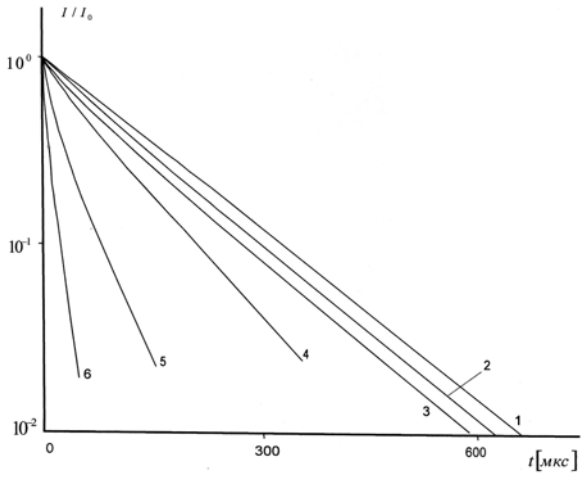

Fig.2. The time population evolutions of upper laser level of neodymium $^4F_{3/2}$ in glass $La_2S_3{\cdot}2Ga_2O_3$: 1-x=0.002; 2-x=0.01; 3-x=0.03; 4-x=0.05; 5-x=0.1; 6-x=0.156 λ_b=0.594mcm.

The decomposition curves of the excited state $^4F_{3/2}Nd^{3+}$ in glass $(La_{1-x}Nd_x)_2S_3{\cdot}2Ga_2O_3$($x$=0.002; 0.01; 0.03; 0.05; 0.1; 0.156) are presented on the fig.2. The measurements of quantum output at the resonance excitement on the glass samples with small concentration Nd^{3+} give the values $\eta \approx 1$. That's why the life time $^4F_{3/2}Nd^{3+}$, measured by us at the small concentration Nd^{3+}, which is equal 145 mcs, is the radiation one. The analysis of the non-exponential decomposition region, captured between the regions of static order and migration-limited decomposition, is given on the fig.3. The value $C_{DA}(Nd-Nd)$, calculated on the region of static disorder decomposition was $5{\cdot}10^{-40}cm^6s^{-1}$. The value $C_{DD}(Nd-Nd)$, defined from formula (36), was equal to $5{\cdot}10^{-40}cm^6s^{-1}$. At the high neodymium concentrations its concentration stewing usually takes place in the mode of kinetic limit [4], moreover, the stewing velocity coincides with the velocity of static order decomposition [9], i.e. significantly depends on minimally possible distance donor-acceptor R_{min} in the given matrix, being thus, the important parameter, characterizing the stewing effectiveness.

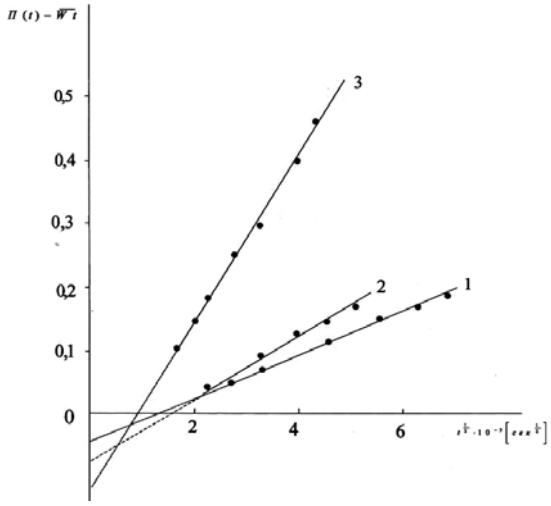

Fig.3. The kinetics type of static disorder decomposition of the level $^4F_{3/2}$ Nd^+ in glass $(La_{1-x}Nd_x)_2S_3{\cdot}2Ga_2O_3$. 1-x=0.03; 2-x=0.05; 3-x=0.1

The value R_{min} in glass $La_2S_3{\cdot}2Ga_2O_3$-Nd^{3+} was obtained by us by several methods. First was in the measurement of the velocities of static order stewing

$$W_H = \frac{4\pi}{3} n_A \frac{C_{DA}}{R_{\min}^3}\ . \qquad (30)$$

Substituting in this formula the value of microparameter C_{DA}, found before on the region of static disorder decomposition, we obtain $R_{min} \approx (3{,}8 \pm 0{,}3)$ Å.

The second method is the following one. It is known, the function expression of non-radiation losses at static dipole-dipole energy transfer taking under consideration of minimal distance of donor-acceptor, which isn't equal to zero, has the form [10]:

$$\Pi(t) = \frac{4\pi}{3} n_A R_{\min}^3 \left(e^{-y_1} - 1 + 2\sqrt{y_1}\int_0^{\sqrt{y_1}} e^{-x^2}\,dx\right), \qquad (31)$$

where $y_1 = \dfrac{tC_{DA}}{R_{\min}^6}$.

At big times $\left[t \rangle\rangle \tau_1 = \left(\dfrac{C_{DA}}{R_{\min}^6}\right)^{-1}\right]$ we obtain:

$$\Pi(t) = -\frac{4\pi}{3} n_A R_{\min}^3 + \frac{4\pi^{3/2}}{3} n_A C_{DA}^{1/2} t^{1/2}, \quad (32)$$

Thus, that extrapolating the experimental dependence $\Pi(\sqrt{t})$ till *t=0* we obtain the value on "a":

$$a = \frac{4\pi}{3} n_A R^3{}_{\min}, \quad (33)$$

where the value R_{min} is defined from. The value R_{min}, defined with the help of (33), was (3,8 ± 0,3) *Å*, i.e. coincided with the value $R_{min} \approx$ (3,8 ± 0,3) *Å* , defined by other method.

The critic neodymium concentration at the increase of which the concentration stewing of luminescence Nd^{3+} in glass carries out in the mode of kinetic limit, was $n^* \approx 3.5 \cdot 10^{21} cm^{-3}$. The time was equal to $\tau_1 = 3 mkc$.

At the definition of R_{min} by the two above mentioned methods the emphasizing of the region of static disorder decomposition and definition on it C_{DA} is the weak place. Indeed, after δ-excitement of the sample the single process of the establishment of stationary profile of density of donor excitement round acceptor (at this it is possible to say about non-stationary migration-raped stewing) takes place and say about the emphasizing of the static disorder stewing from this process only at $R_W >> R_{min}$, where in stewing sphere the big enough number of seats are present, causes the dispersal of the distances donor-acceptor in different spheres (in "joint sphere"). By other words, the ratio $\tau_0 \rangle\rangle \tau_1$ (34) $\left(\frac{R_W}{R_{\min}} \approx (\frac{\tau_0}{\tau_1})^{1/6} \right)$ should be carried out. This is expressed in strong modulation of decomposition curve, i.e. it will be quite different from the curve in semi-logarithmic scale. For the use of the usual analysis methods of the static disorder decomposition ($e^{-\gamma\sqrt{t}}$) should be the following: $\tau_1 \langle\langle t \langle\langle \tau_0$ (35) can be smoothed, if don't use $\Pi(t)$, but use the expression $\Pi(t) = \gamma\sqrt{t}$, defined by the formula (31). The condition (30) smoothes at this: $0 \le t \langle\langle \tau_0$ (36). In such cases, when nor (35), neither (36) aren't carried out, the describing of the decomposition curve in all investigated time interval and the definition of interaction microparameters (C_{DA} and C_{DD}) and minimal distance R_{min} from the condition of the experimental and calculated data, is the only right way.

In the limits of Zusman approach [6] taking under consideration of donor-acceptor distance (R_{min}) the analysis of the decomposition curves was carried out by us. From the coincidence of the calculated and experimental data the following values of the above mentioned parameters had been defined from the calculated and experimental data:

$$R_{\min} \approx (3{,}5 \pm 0{,}5)\, Å$$
$$C_{ДА} \approx (3{,}5 \pm 1{,}5) \cdot 10^{-40}\, cm^6\, s^{-1}$$
$$C_{ДД} \approx (2 \pm 1) \cdot 10^{-39}\, cm^6\, s^{-1}$$

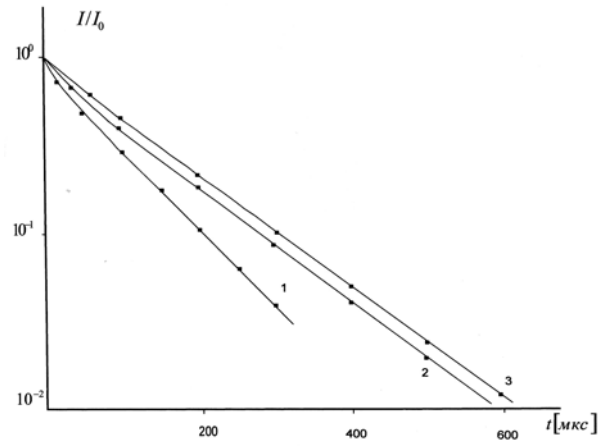

Fig.4. The experimental (continuous lines) and calculated (points) of decomposition curves of metastable state $^4F_{3/2}$ Nd^{+3} in glass $(La_{1-x}Nd_x)_2S_3 \cdot 2Ga_2O_3$. 1-x=0.05; 2-x=0.03; 3-x=0.01

The experimental decomposition curves are given by continuous lines, the calculative curves are given by points. The results, obtained with the help of the describing of experimental decomposition curve in all time scale are close to the results, obtained by the way of the emphasizing of the region of static disorder decomposition and on formula (18). The closeness of the results is explained by well carrying-out of the condition $\tau_0 \rangle\rangle \tau_1$ at the investigated neodymium concentrations.

The concentration dependence of the value of quantum output of the luminescence Nd^{3+} at the different lengths of excitement waves is shown in table 1.

Table 1

The concentration dependence of the value of the quantum output of the luminescence of Nd^{3+} ions in glass $La_2S_3 \cdot 2Ga_2O_3$ at different wave lengths of excited light.

Material	Concentrations Nd^{3+}(%)	λ_B (mcm)	η_{dir} (%)	η_{kin} (%)
$La_2S_3 \cdot 2Ga_2O_3$	1	0.596	90	88
	1	0.812	95	88
	5	0.812	61	57
	10	0.812	27	22

It is seen, that with the increase of Nd^{3+} concentration the quantum output $^4F_{3/2}$ of the level Nd^{3+} decreases because of the concentration stewing. The values η, measured with the use of balance and indirect methods are well coincide between each other in the relation to the squares under decomposition curves of excited state $^4F_{3/2}$ at the impulse excitement. At Stockes-law excitation the quantum output of the luminescence doesn't change in the limits of experiment mistake at the different lengths of excitement waves.

Thus, the carried out investigations evidence about the perceptivity of the use in the capacity of the laser material of semiconductor glass $La_2S_3 \cdot 2Ga_2O_3$ - Nd^{3+}, and also allow to describe the processes of concentration stewing of ion luminescence in the investigated materials in wide range of the concentrations of active impurity.

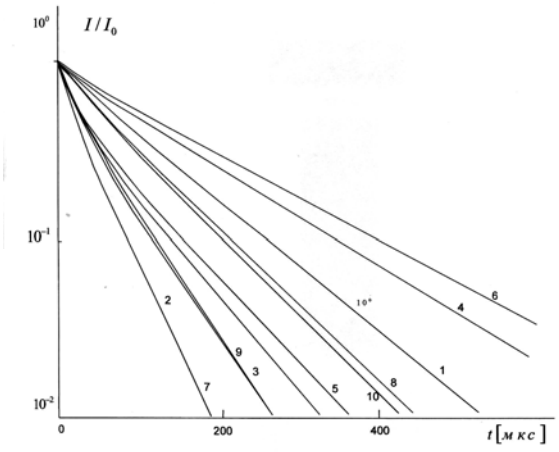

Fig.5. The damping kinetics of luminescence from $^4F_{3/2}$ Nd^{+3} level at the excitation of glass samples by the light with wave length
λ_b=0,6 mcm
1 - 0,004 Nd_2O_2S · 0,996 La_2O_2S · 3Ga_2S_3;
2 - 0,11 Nd_2O_2S · 0,89 La_2O_2S · 3Ga_2S_3;
3 - 0,085 Nd_2O_2S · 0,915 La_2O_2S · 3Ga_2S_3;
4 - 0,003 Nd_2O_2S · 0,997 La_2O_2S · 2,3Ga_2S_3;
5 - 0,097 Nd_2O_2S · 0,903 La_2O_2S · 3Ga_2S_3;
6 - 0,003 Nd_2O_2S · 0,997 La_2O_2S · 3Ga_2S_3;
7 - 0,112 Nd_2O_2S · 0,888 La_2O_2S · 3Ga_2S_3;
8 - 0,004 Nd_2O_2S · 0,996 La_2O_2S · 3Ga_2S_3;
9 - 0,095 Nd_2O_2S · 0,905 La_2O_2S · 2,3Ga_2S_3;
10- 0,003 Nd_2O_2S · 0,997 La_2O_2S · 2,3Ga_2S_3;

At the sample excitement by light of second laser harmony on crystal YAG - Nd^{3+}(λ=0,53 mcm), the evolution population of excitation state $^4F_{3/2}$ Nd^{3+} in glasses $La_2O_2S.3Ga_2S_3, La_2S_3.3Ga_2S_3, La_2S_3.2,3Ga_2S_3, La_2S_3.3Ga_2O_3, La_2S_3.2,3Ga_2O_3$ had pronounced maximums. This fact is connected with that given in glasses have less extensive oscillation spectrums, than the many known laser materials, that causes the low velocities of many-phonon of internal-centered energy relaxation in Nd^{3+} ions, also between the state $^2K_{13/2}+^2G_{9/2}+^4G_{7/2}$,, till which the Nd^{3+} ions are excited at given excitation method and close state to it below $^4G_{5/2}+^2G_{7/2}$ (energetic space between given states was ~1500 cm^{-1}). The luminescence flaming up from the level $^4F_{3/2}$ Nd^{3+} is practically absent (fig.5), i.e. the energetic gap between below lying (till to $^4F_{3/2}$) states Nd^{3+} are significantly less than above mentioned one at the sample excitation by the light, the wave length of which is λ~0,6 mcm directly into levels $^4G_{5/2}+^2G_{7/2}$. These decomposition curves of excited state $^4F_{3/2}$ Nd^{3+} had been used by us for the analysis of processes of inter-ion interaction in investigated glasses.

As it is known three time region can be emphasized on damping curve of donor luminescence after sample δ-excitement. First-exponential is realized on the initial beginning stage:

$$I(t) = I(0)\exp(-W_H t - \frac{t}{\tau}) \ , \qquad (37)$$

where τ is own life time of metastable state, W_H is maximally possible velocity of luminescence stewing in given particle collective (at Stockes their distribution). In the ref. [11] the expression of the type was supposed by the way of analysis of the expression for W_H at different packs of impurity complexes

$$W_H = 7\frac{C_{DA}}{R_{\min}3}n_A \ , \qquad (38)$$

where R_{min} is minimal distance between interactive particles, n_A is acceptor concentration.

The second non-exponential region is observed in damping kinetics of luminescence after order region:

$$I(t) = I(0)\exp(-\gamma\sqrt{t} - \frac{t}{\tau}) \qquad (39)$$

where $\gamma = \frac{4}{3}\pi^{3/2}n_A C_{DA}^{1/2}$.. Subtracting from total function of non-radiation losses of $\Pi(t)$ that part, which is connected with migration-limited relaxation, it is possible to obtain the $\Pi(t)$, defining the static disorder decomposition (39), from which it is possible to define γ parameter and C_{DA} constant. Knowing the value C_{DA} we can find the value R_{min}.

Table 2

The values of C_{DA}, C_{DD}, R_{min} microparameters in semiconductor glasses

Material	Microparameters
0,112 Nd_2S_3 · 0,888 La_2S_3 · 3Ga_2S_3	C_{DA}=5,8 · 10^{-40} cm^6 sec^{-1} C_{DD}=9,2 · 10^{-39} cm^6 sec^{-1} R_{min}=4Å
0,095 Nd_2S_3 · 0,905 La_2S_3 · 2,3Ga_2S_3	C_{DA}=2,4 · 10^{-40} cm^6 sec^{-1} C_{DD}=4,2 · 10^{-39} cm^6 sec^{-1} R_{min}=3,8Å
0,097 Nd_2S_3 · 0,903 La_2S_3 · 3Ga_2O_3	C_{DA}=5,3 · 10^{-40} cm^6 sec^{-1} C_{DD}=1,4 · 10^{-39} cm^6 sec^{-1} R_{min}=4,3Å
0,085 Nd_2S_3 · 0,915 La_2S_3 · 2,3Ga_2O_3	C_{DA}=4,5 · 10^{-40} cm^6 sec^{-1} C_{DD}=1,2 · 10^{-39} cm^6 sec^{-1} R_{min}=4Å
0,11 Nd_2O_2S · 0,89 La_2O_2S · 3Ga_2S_3	C_{DA}=4,7 · 10^{-40} cm^6 sec^{-1} C_{DD}=3,1 · 10^{-39} cm^6 sec^{-1} R_{min}=4,3Å

On the third exponential region the migration-limited luminescence stewing takes place, the velocity of which is defined by the expression (18).

Knowing $\overline{W}$ and C_{DA}, we can define the constant C_{DD}. The obtained values of corresponding parameters are given in the table 2.

[1] *Yu.K. Voronko, T.G. Mamedov, V.V. Osiko, A.M. Proxorov, V.P. Sakun, I.A. Sherbakov.* JETF, 1976, t.71, s. 478-501.

[2] *İ.A. Sherbakov*. Avtoreferat dokt. diss. Moskva, FIAN, 1978.

[3] *S.I. Golubov, Yu.V. Konobeev*. FTT 13. 3185 (1971).

[4] *I.A.Bondar, A.I.Burshteyn, A.V.Krutikov, L.P.Mezentseva, V.V.Osiko, V.P.Sakun, V.A.Smirnov, I.A.Sherbakov*. JETF, 81, 96 (1981).

[5] *M.V. Artamanova, Ch.M. Briskina, A.İ. Burshteyn, L.D.Zusman, A.Q.Skleznev*. JETF 62, v.3, (1972), 863-871.

[6] *L.D. Zusman*. JETF 73, v.2(8), 1977, s.662-669.

[7] *Yu.S. Privis, V.A. Smirnov, I.A. Sherbakov*. Vliyanie strukturi kristallicheskoy reshetki na kinetiku prijkovogo tusheniya lyuminessensii. Preprint FIAN №220, 1983.

[8] *A.I. Burshteyn*. JETF, t.84, v.6, 2001-2013, (1983).

[9] *A.I. Burshteyn*. JETF, t.62, v.5, 1972, 1965-1701.

[10] *V.M. Agranovich, M.D. Galanin*. «Perenos energii elektronnogo vozbujdeniya v kondensirovannikh sredakh». M., «Nauka», 1978.

[11] *A.G.Avanesov,T.T.Basiev,Yu.K.Voronko,B.İ.Denker, Q.V.Maksimova, V.A. Mızina, V.V. Osiko, V.S. Fedorov*. JGTF 84.1028 (1983).

H.İ. Abutalıbov, A.Ə. Məmmədov

YARIMKEÇİRİCİ ŞÜŞƏLƏRDƏ Nd^{3+} İONLARININ LYUMİNESSENSİYASININ SÖNMƏSİ

Şüşə materiallarda elektron həyəcanlanmasının ötürülməsi və deqredasiyası tədqiq olunub. Müxtəlif metodlarla qarşılıqlı təsir mikroparametrləri və Nd - Nd minimal məsafəsi təyin edilmişdir.

Г.И. Абуталыбов, А.А. Мамедов

ТУШЕНИЕ ЛЮМИНЕСЦЕНЦИИ ИОНОВ Nd^{3+} В ПОЛУПРОВОДНИКОВЫХ СТЕКЛАХ

Исследованы процессы передачи и деградации энергии электронного возбуждения в стеклообразной матрице. Различными методами определены микропараметры взаимодействия и минимальное расстояние Nd - Nd .

Received: 06.12.05

MİSİN XALKOQENİDLƏRİNİN FAZA KEÇİDLƏRİNİN TERMODİNAMİKİ TƏDQİQİ

F.M. MUSTAFAYEV
Mingəçevir Politexnik İnstitutu
Mingəçevir D. Əliyeva küçəsi 21

Elektrik hərəkət qüvvəsi (E.H.Q.) metodu ilə misin xalkoqenidlərinin (Cu_2S, Cu_2Se, Cu_2Te) faza keçidlərinin termodinamikası (temperatur, entropiya və entalpiya) öyrənilmişdir. Elementin E.H.Q.-nin temperatur asıllığında faza keçidləri uyğun olaraq 370 K (Cu_2S), 380 K (Cu_2Se) və 440 K (Cu_2Te) temperaturlarında müşahidə olunmuşdur.

Misin xalkoqenidləri (Cu_2S, Cu_2Se, Cu_2Te) perspektivli yarımkeçirici materiallar olmaqla elektron texnikasında termoelektrik generatorlarda enerji çevrilmələrində geniş tətbiq edilir [1]. Bu yarımkeçirici birləşmələrdə struktur faza çevrilmələrinin olması, onların fiziki və fiziki-kimyəvi xassələrinin sıçrayışla dəyişməsinə səbəb olmaqla, yarımkeçiricilərin elektronikasında istifadə etməyə imkan yaradır [1].

Misin xalkoqenidlərinin faza çevrilmə istiliyi az olduğundan bu materiallar üzərində kalorimetrik və buxar təzyiqi metodları ilə termodinamiki tədqiqat aparmaq çətinliklər törədir. Bu məqsədlə biz tədqiqat obyekti olaraq elektrik hərəkət qüvvəsi (E.H.Q.) metodunu seçdik.

Misin xalkoqenidlərində faza keçidlərinin termodinamiki xassələrini öyrənmək üçün bərk elektrolitli E.H.Q. metodundan istifadə edilmişdir.

Tədqiqatda bərk elektrolitli aşağıdakı növ qalvanik element tətbiq edilmişdir:

$$(-)\,pt\left|Cu\right|Cu^{Z+}\ \text{bərk elektrolitdə}\ \left|Cu_X B^{VI}_{1-X}\right|pt(+) \qquad \text{(I)}$$

burada Cu^{Z+}-misin ionunun yükü, B^{VI}-S, Se, Te; x-misin $Cu_X B^{VI}_{1-X}$ -xəlitəsində molyar payıdır.

Tədqiqatda bərk elektrolit olaraq $Cu_4RbCl_3J_2$ götürülmüşdür. Superionlu $Cu_4RbCl_3J_2$ bərk elektroliti otaq temperaturunda yüksək ion keçiriciliyinə malikdir [2].

Superionlu $Cu_4RbCl_3J_2$ bərk elektrolitinin alınma texnologiyası [3]-də göstərilmişdir.

Tədqiqat üçün Cu-S sistemində Cu_2S-CuS və CuS-S faza oblastları üçün uyğun olaraq 37,00; 41,00 və 45,00 at % S; 55,00, 65,00 və 70,00 at %S; Cu-Se sistemində Cu_2Se-Cu_3Se_2, Cu_3Se_2-CuSe, CuSe-$CuSe_2$ və $CuSe_2$-Se faza oblastları üçün uyğun olaraq 38,00, 46,00, 59,00 və 78,00 at % Se; Cu-Te sistemində Cu_2Te-Cu_4Te_3; Cu_4Te_3-CuTe və CuTe-Te faza oblastları üçün uyğun olaraq 39,00, 48,00 və 55,00 at % Te tərkiblərdə elektrod xəlitələr təcrübi olaraq vakuum şəraitində ampula metodu ilə sintez edilmişdir.

Bərk elektrolit və xəlitələr-200 saat müddətində homogen dəmə qoyulmuşdur.

Təcrübələrin temperatur intervalı 298-500 K olmuşdur. Tədqiqat üçün qurğu, ölçmə sxemi və metotdikası [4]-də verilmişdir.

(I) qalvanik elementinin E.H.Q.-ni ölçməklə və E.H.Q.-nin temperatur asıllığından misin xalkoqenidlərinin faza keçidlərinin termodinamik funksiyaları aşağıdakı termodinamiki münasibətlərlə təyin olunur:

$$\Delta S_{f.k.} = -\left(\frac{\partial \Delta G_{f.k.}}{\partial T}\right)_p = Z\cdot F\left(\frac{\partial \Delta E_{f.k.}}{\partial T}\right)_p \cdots\cdots\cdots \qquad (1)$$

$$\Delta H_{f.k.} = T_{f.k.}\cdot \Delta S_{f.k.} \cdots\cdots\cdots \qquad (2)$$

hardakı $T_{f.k.}$-faza keçidinin temperaturu, Z-ionun yükü, F-Faradey ədədidir, $\Delta E_{f.k.}$-elementin E.H.Q.-nin dəyişməsi, $\Delta G_{f.k}$, $\Delta S_{f.k}$ və $\Delta H_{f.k}$ isə faza keçidinin Gibbs enerjisi, entropiyası və entalpiyasıdır.

Şəkil 1-3-də elektrodları müxtəlif tərkibli xəlitələr olan qalvanik elementlərin E.H.Q.-nin temperatur asıllıqları verilmişdir.

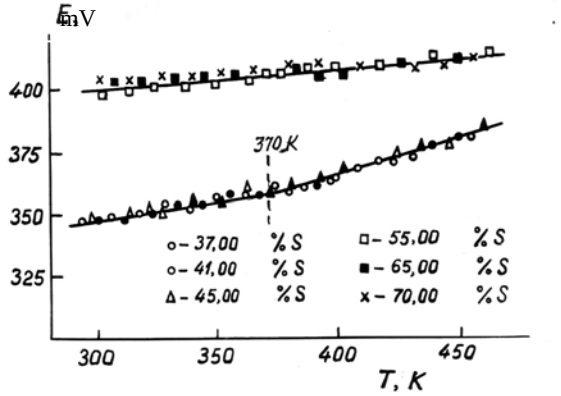

Şəkil 1. Cu-S sistemindəki xəlitələr üçün elementin E.H.Q.-nin temperatur asıllığı

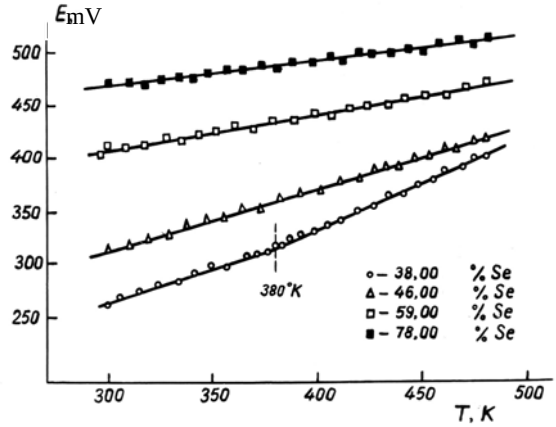

Şəkil 2. Cu-Se sistemindəki xəlitələr üçün elementin E.H.Q.-nin temperatur asıllığı

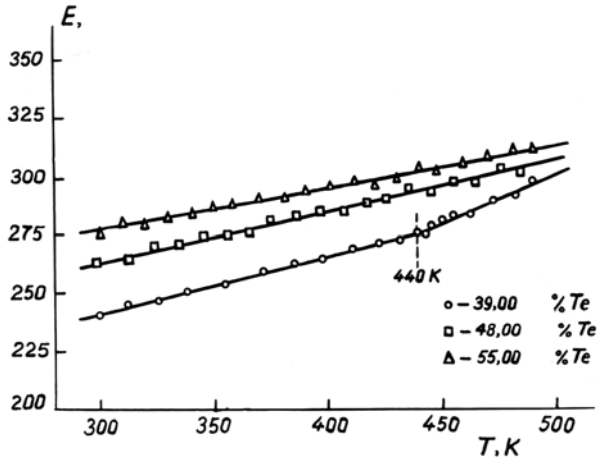

Şəkil 3. Cu-Te sistemindəki xəlitələr üçün elementin E.H.Q.-nin temperatur asıllığı.

Şəkil 1-3-dən görünür ki, Cu-S sistemi üçün Cu_2S-CuS faza oblastında elementin E.H.Q.-nin temperatur asıllığında elementin E.H.Q.-nin temperatur əmsalı olan $\left(\frac{\partial E}{\partial T}\right)_p$ 370 K, Cu-Se sistemi üçün Cu_2Se-Cu_3Se_2 faza oblastında 380 K və Cu-Te sistemi üçün Cu_2Te-Cu_4Te_3 faza oblastında isə 440 K temperaturlarda dəyişilir. (1) ifadəsinə görə elementin E.H.Q.-sinin temperatur əmsalının dəyişməsi faza keçidinin entropiyası ilə bağlı olduğuna görə belə nəticəyə gəlirik ki, faza keçidi temperaturlarında entropiya sıçrayışla dəyişilir və Cu_2S, Cu_2Se və Cu_2Te uyğun olaraq 370, 380 və 440 K temperaturlarda faza oblastları sərhədlərində *I* növ faza keçidlərinə məruz qalırlar.

Ölçmələr *B*·7-30 tipli voltmetrlə aparılmışdır. Bütün xəlitələr üçün alınmış təcrübi nəticələr aşağı temperatur (α) və yuxarı temperatur (β) fazaları üçün ən kiçik kvadratlar metodu ilə işlənilmişdir [5]. Hesablamalar Pentiyum-4 tipli hesablama maşınında aparılmışdır. Aşağı və yuxarı temperatur fazaları üçün $E=(A+BT)\pm 2\ D(E)$ şəklində reqressiya tənlikləri alınmışdır, hardakı *A* və *B* –reqressiya əmsalları, *D(E)*- ölçülmüş hər bir elementin E.H.Q.-nin seçilmiş dispersiyasıdır. α və β fazaları üçün reqressiya tənliklərindən istifadə etməklə faza keçidi temperaturasında elementin E.H.Q.-nin dəyişilməsinin temperatur asıllığı tapılmışdır.

(1) və (2) ifadələrindən istifadə etməklə faza keçidi temperaturunda misin xalkoqenidlərinin (Cu_2S, Cu_2Se, Cu_2Te) entropiyası və entalpiyası təyin edilmişdir.

Tədqiqat işlərinin nəticələri cədvəldə verilmiş və ədəbiyyatda olan məlumatlarla tutuşdurulmuşdur.

Cədvəl

Misin xalkoqenidlərinin faza keçidinin termodinamiki xarakteristikaları

Maddə	Keçid növü	$T_{f.k}$, K	$\Delta E=f(T)$, *V*	$\Delta H_{f.k}$, kC/mol	$\Delta S_{f.k}$, C/mol·K	Ədəbiyyat
Cu_2S	$\alpha\rightarrow\beta$	370	$-0{,}0551+0{,}1486\cdot10^{-3}\cdot T\pm2\cdot10^{-3}$	5,4±0,9 5,6 [6]	14,3±1,1 14,8 [6]	Bizim tədqiqat
Cu_2Se	$\alpha\rightarrow\beta$	380	$-0{,}0560+0{,}1750\cdot10^{-3}\cdot T\pm2\cdot10^{-3}$	6,4±0,9 6,8 [6]	16,8±1,1 17,2 [6]	Bizim tədqiqat
Cu_2Te	$\alpha\rightarrow\beta$	440	$-0{,}0190+0{,}0430\cdot10^{-3}\cdot T\pm2\cdot10^{-3}$	1,8±0,9 1,50 [7]	4,1±1,1 3,1 [7]	Bizim tədqiqat

[1]. *V.V. Qorbaçev*. Poluprovodnikovıye soyedineniya $A^{I}_{2}B^{VI}$, M., İzd.«Metallurqiya», 1980, s. 4-10. (Rusca).

[2]. *Yu.Ya. Qureviç*. Tverdıye elektrolitı M., 1986, s. 46-52. (Rusca).

[3]. *S.A.Geller, T.K.Axridge, S.A.Wilber*. Crystal structure and conductivity of the solid electrolyte α-$RbCu_4Cl_3J_2$. Phys. Rev., B.1979, v.19, №10, p. 5396-5402.

[4]. *F.M. Mustafaev*. Termodinamiçeskiye, qalvanoelektriçeskiye, elektronnıye, ionnıe svoystva i vıraşşivaniye monokristallov xalkoqenidov medi i serebra. Monoqrafiya, İzd. "Elm", Baku 1998, s. 25-29. (Rusca).

[5]. *V.V. Nalimov*. Primeneniye matematiçeskoy statistiki pri analize veşşestva. M., 1960, s. 263. (Rusca).

[6]. Termiçeskiye konstantı veşşestv (pod red. *V.P. Qluşko*), M. İzd. VNİİTİ, 1973, vıp. VI, ç. 1, s. 486. (Rusca).

[7]. *K.C. Mills, M.J. Richardson*. The heat capacity of Cu_2Te, Ag_2Te and $Ag_{1.84}Te$, Thermochim. acta, 1973, v.6, №5, p. 427-438.

F.M. Mustafayev

INVESTIGATION OF THE THERMODYNAMICS OF PHASE TRANSITION OF COPPER HALCOGENYDES

The thermodynamics of phase transition of copper halcogenydes (Cu_2S, Cu_2Se and Cu_2Te) has been investigated by the electromotive forces methods with solid electrolyte.

Temperature, entropy and enthalpy of phase transition of Cu_2S, Cu_2Se and Cu_2Te have been obtained from temperature dependence of electromotive forces of galvanic element. Phase transitions of I kind are discovered in temperatures 370 (Cu_2S), 380 K (Cu_2Se) and 440 K (Cu_2Te).

Ф.М. Мустафаев

ИССЛЕДОВАНИЕ ТЕРМОДИНАМИКИ ФАЗОВЫХ ПЕРЕХОДОВ ХАЛЬКОГЕНИДОВ МЕДИ

Термодинамика фазовых переходов халькогенидов меди (Cu_2S, Cu_2Se, Cu_2Te) изучена методом э.д.с. с твердым электролитом. Из температурных зависимостей э.д.с. гальванических элементов определены температуры, энтропии и энтальпии фазовых переходов Cu_2S, Cu_2Se и Cu_2Te.

Фазовые переходы I рода были обнаружены при температурах 370 K (Cu_2S), 380 K (Cu_2Se) и 440 K (Cu_2Te).

Received: 17.11.05

NANOSTRUCTURAL CENTERS IN THE CRYSTALLINE LAYER OF THE BISMUTH TELLURIDE AND THEIR INFLUENCE ON THE KINETIC PROPERTIES

S.Sh. GAKHRAMANOV
SMU "Selenium" of NAS of Azerbaijan,
F.Agayev str.14, Baku

The level-to-level and island growth of nano-layers: cuprum, nickel and boron realizes spontaneously between the layers Te^1-Te^1 in the process of the directed crystallization of bismuth telluride (doped by easily diffusing impurities). This was proved by the electron-microscopic photos of the chipped surface (0001) Bi_2Te_3<B>, Bi_2Te_3<Cu> and Bi_2Te_3<Ni>. The wide set of island sizes 50-200nm was revealed.

The appearance nature of nano-layers, islands and their enlargement in the interlaminar space of the layered crystal of bismuth telluride is the same as on the open surfaces of the systems semiconductor-metal. The two-dimensional islands, which combining form the wetting layer of nano-thickness appear on the initial steps of the growth.

It is established, that the cuprum layers, nano-sized by the height, are charged with extremal behavior of Hall thermoelectromotive force and other kinetic parameters Bi_2Te_3<Cu>. The temperature dependencies of coefficients of Hall, electroconductivity, mobility and other kinetic parameters revealed the oscillation character. These extremums can be connected with the consecution of the phase transfers, known as order-disorder transfers, connected with positional order. The anomal increase of the mobility of the charge carriers (more, than in 5 times) in the direction along axes of the (0001) Bi_2Te_3<Cu> layers at the temperature 105K is observed.

1. Introduction

Above all, we note, that properties of the island films significantly differ from properties of massive crystals and total metallic films. The mechanisms of the electroconductivity and nature of anomalous optical properties of the island films are widely studying. The impurity layers are created in many layered crystal of the types $A^{III}B^{V}$ and $A_2^{III}B_3^{VI}$. The structure and properties of the island films of the metals on the semiconductor surfaces can be analogical in some degree (or repeated) on the external form in the comparison with film interlaminar impurity structures of layered crystals. Thus impurity films of cuprum in the crystals of bismuth telluride totally increase the mechanical properties and reveal the anomalous kinetic effects [1-2].

Let's consider the set of properties and mechanism of growth of thin island films for the comparative description. Usually the films, the sheet resistance of which changes from 10^6 till 10^{13} Om and which consist on the islands with average diameter 5-100 nm, separated by the spaces 1-3 nm correspondingly, are related to the island ones [3].

Knowing the form of the islands, it's possible to connect the atom number in the island with its size and obtain the dependence of the covering degree of the substrate on the time. The knowing of the form of the islands is significantly for all growth theories of island films [3-4].

The investigations of the last years of recombination centers, connected with nano-sized clusters As-Sb in the low-temperature As, have revealed the islands-islands, the sizes of which are less, than 8 nm [5-6]. The doping of GaAs, grown by the method of low-temperature molecular-beamed epitaxy can be used for the managing of the space distribution of clusters-islands in this material [7]. The "two-dimensional" cluster layers, obtained at this, have the significant quantity of atoms of doping element besides the atoms of exceed arsenic. This circumstance influences on the properties of the layers and traps for the electrons, having in them [6].

Now let's consider the growth mechanisms of the films and information, needed for us for the comparison with mechanisms of film growth – layers in layered crystals of the type Bi_2Te_3. If the chemical reactions between evaporated substance and substrate are absent (for the given temperature interval), then in the dependence from the chemical nature of the substrate and adsorbate, it's possible to emphasize the following growth mechanisms of metallic films [3-4; 8]: two-dimensional (2D), or layer-to-layer growth (fig1.a), typical, for example, the metallic film on the metallic substrate for the system; three-dimensional (3D) or island growth (fig 1.b), which is characteristic for the metallic film on the dielectric substrate and intermediate (2D→3D) growth (fig 1.c), i.e. the island layer on the preliminary formed mono-layer of adsorbed atoms (adatoms). This mechanism is considered as characteristic one for the system metallic film on the covalent semiconductor. The consideration of the layer $Te^{(1)}$-$Te^{(1)}$ in Bi_2Te_3 is interesting, as this space will be considered as the substrate (quintets) $Te^{(1)}$-$Te^{(1)}$ on the basal plane (0001), on which the inputted impurities will be settled in the process of the natural growth.

Fig.1. The scheme image of possible mechanisms of thin films [4].

Moreover, the biggest attempts will be directed on the investigation 2D and 3D mechanisms at the studying of the process of the film growth. It is known, that the growth (2D→3D) realizes on the covalent semiconductor for the metallic film system [4]. The results, proving about the importance of the diffusion process of adatoms in the substrate (3D* mechanism) on the earliest steps of the growth, i.e. about the existence one more growth mechanism – (3D*→3D) have been obtained for the metallic film system on the amorphic dielectric (fig.1.d) [8]. Nowadays as (2D→3D), so (3D*→3D) mechanisms in the metals and semiconductors, are widely used.

The monolayered evaporation of the metal on the atom pure surface (APS) of the semiconductor (at T=300K) leads to the quazihomogineous film growth without island creation. For example, the islands on the APS Si are created only in the case, if the substrate temperature during the aurum evaporation is higher, than 100°C [8]. The APS evaporation of the metal semiconductor, having thickness about in monolayer, at the high temperatures leads to the formation of two-dimensional ordered surface phases (2D), which are character for the given metal and crystal-graphical orientation of the substrate [8]. The further enlargement of the surface degree gives the three-dimensional growth of the metallic islands, i.e. the mechanism 2D→3D of metal film growth realizes in summary. The investigation of the nanoparticle semiconductors, created on the surface, is at the high point of the question now.

The chemical methods of film evaporation. The electron-microscopic (EM) photos (x 60000) of G surfaces, doped by the metals (Au, Ag) from the water solution, revealed their island character. The island coverings, obtained on the silicon at the adsorption from the solution in the water in *Hf* differ as qualitative, so quantitative. The islands of the size, more than 2 nm were fixed [8]. The silver islands are bigger by the sizes, among them the large enough ones (25-80 nm) had met (especially on Si). They are created because of the coagulation of the more small islands, which are closely situated.

The creation of the island structures at the adsorption of electropositive metals (Ag, Au, Cu, Pt and others) was observed on the binary semiconductors also. For example, (EM) investigations, carried out at Au adsorption on GaAs showed, that the same regularities of metal adsorptions and creations of island structures, as on the Si and Ge, were observed. The quality of the islands on GaAs was changed in the limits $4\cdot10^{10}$-$9\cdot10^{11}$ cm^{-2}, and their sizes were changed in the limits 3-50 nm.

The consideration of such island structures for us is very important from the point of view of the comparison of such ones with the structures in the closed volume of interlaminars Bi_2Te_3<metal>. From the other hand, they themselves have the set of the interesting properties, connected with the electroconductivity, phenomena of electron emission, luminescention and thermoelectricity. The island metal evaporation structure on the semiconductor reveals also catalytic properties and successfully is used in heterogeneous catalyst [8]. That's why the investigation of the surface morphology with island structures and electron processes on them presents the significant interest for the different regions of physico-chemistry and semiconductor techniques independently from the methods of creation.

The aim of the given paper was the revealing of monolayers and island centers between the layers $Te^{(1)}$-$Te^{(1)}$ in Bi_2Te_3<Cu, Ni, B>, the studying of the surface morphology (0001) and their influence on the extremums in the temperatures dependencies of kinetic effects in Bi_2Te_3<Cu>.

2. The samples and method

The samples were obtained by the method of vertically directed crystallization at the band traverse speed 5mm/h. The materials: Bi, Te, Cu, B and Ni by the frequency, not less than 99.999% were used. The synthesis was carried out at T=700°C during the hour, the temperature in crystallization band was regulated and was not less, than 660°C.

The electron=microscopic photos were carried out on the microscope by type JEOL-JSM 5410LV. The monocrystal roentgenograms Bi_2Te_3 and Bi_2Te_3<Cu> were investigated on the installation Philips Panalytical XRD (X-ray difractometer). The green planes (0001) Bi_2Te_3<Cu>, Bi_2Te_3<B> and Bi_2Te_3<Ni> – ething wasn't carried out. With the help of the roentgeno-difractometer peaks of the surfaces of basis plane (0001) of stoichiometric Bi_2Te_3 and Bi_2Te_3<Cu>, the information about situation of cuprum layers on the скол surface (0001) had been obtained. The impurities Cu, Ni and B were inputted into Bi_2Te_3 during the synthesis. In the process of the crystal growth they had all intermediate levels, but mainly they were combining in more wide Van-der-Waalse intervals $Te^{(1)}$-$Te^{(1)}$. The studying of surface morphology (0001) and surface roentgenogram Bi_2Te_3<Cu, Ni, B> proved the above mentioned.

On the base of the measurements of Hall coefficients R_x and electroconductivity coefficient σ the temperature dependencies of the mobility (u) were calculated, the concentrations of current carriers (N) in $H\perp C\perp I$ and $H \,||\, C\perp I$ directions of magnetic field (H) and current (I) were measured magnetoresistance $\Delta\rho/\rho$.

3. The results and their discussion

Firstly let's consider the electron-microscopic surfaces (0001) of bismuth telluride, doped by the cuprum, Ni and B. The photos of surface chip Bi_2Te_3<Cu> are presented on the fig2 (a,b,c,d). The photos Bi_2Te_3<Ni> are given on the fig.3 (a,b), and photos Bi_2Te_3<Bi> are presented on the fig.4 (a,b). From roentgeno-difractometer peaks the only pure Bi_2Te_3 and surface (0001) of Bi_2Te_3<Cu> monocrystal have been considered (see fig.5 (a,b)). The kinetic effects (temperature dependencies R_x and $\Delta\rho/\rho$ are given for Bi_2Te_3<Cu> fig.6 (a,b). The temperature dependencies of Hall concentration of the charge carriers - (N) and mobility (u) of Bi_2Te_3<Cu> crystal are presented on the fig.7 (a,b).

The surface morphology (0001) of Bi_2Te_3<Cu>, Bi_2Te_3<Ni> and Bi_2Te_3<Bi> crystals has the set of peculiarities:

- all they have island character of the different form and sizes,
- the unity tendency of small particles into big ones is seen;
- the creations of the round islands of bigger sizes are character for all impurity layers (see fig.2,3,4).

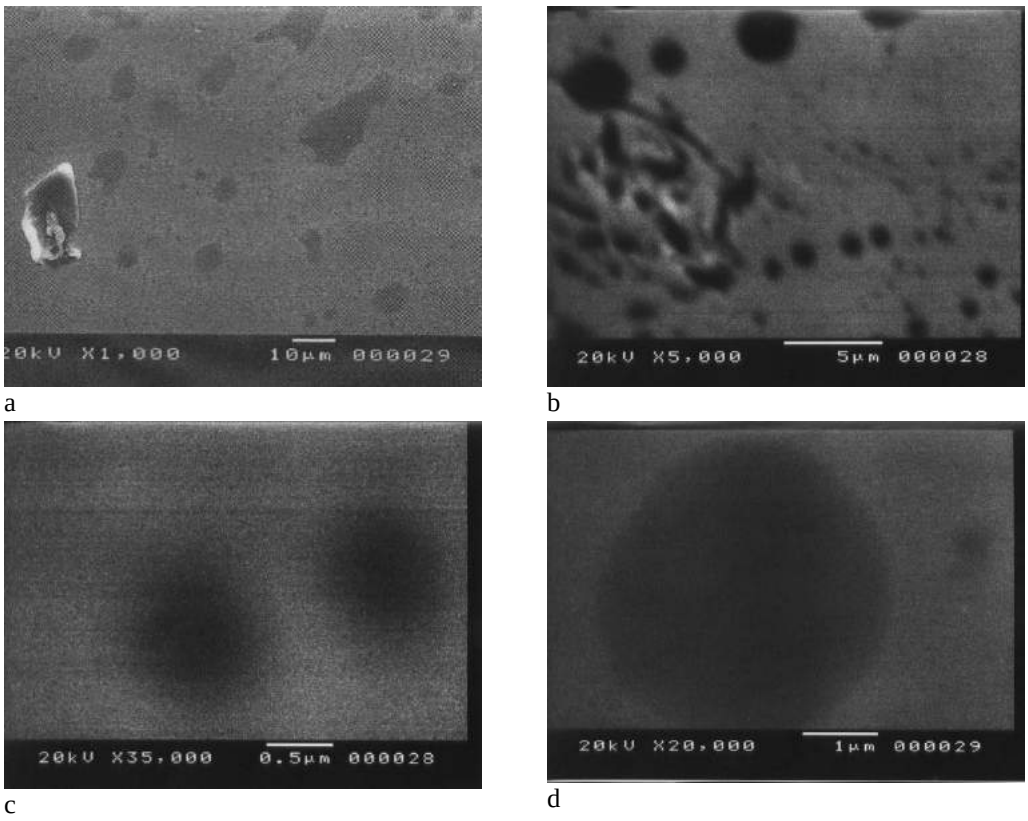

a b c d

Fig.2. (a,b.c.d) Electron-microscopic photos Bi_2Te_3<Cu>.

Unfortunately, we can't to make conclusions in the relation to the nanoparticles by the size less, than 50 nm on the base of the data of electron-microscopic photos, though they are present on the fig.2 ©. The more large islands are significant for Bi_2Te_3<Cu>, (see fig.2 d), for Bi_2Te_3<Ni> (see fig.3 b), for Bi_2Te_3 crystals, doped by B, the biggest sizes of the particles (see fig.4 (b,c)) are observed. Besides big round islands, the other forms – departures also are present, so for Bi_2Te_3<Cu> (fig.2 (a) left below), and for Bi_2Te_3<B> (fig.4 (a), left up) the polyhedron is seen, created in the process of the space island distribution. It is possible to say, that initial evaporation connects with very small cluster systems (by the size less, than 10-20 nm). This moment is the most interest in "earlier history" of particle migration on the internal basis plane of bismuth telluride. The studying of the island distribution gives the significant information about regularities of the obtaining of their interaction with the substrate and between themselves [3-4]. The island, the size of which is already bigger, than other have, becomes the effect center of the adatom drain, in the result of which the concentration of other islands in the neighborhood of the given islands decreases. The analogical situation appears not only in the island films, obtained by the different methods, mentioned in [3,4,8], but in the layers-films in closed system $Te^{(I)}$-Cu-$Te^{(I)}$, $Te^{(I)}$-Ni-$Te^{(I)}$ and $Te^{(I)}$-B-$Te^{(I)}$ of bismuth telluride. This is seen from the fig.2 (a), where the white spots around the biggest particle are seen, from these places the particles have been migrated in more big creations. Besides it, the big Cu island, situated on the Cu monolayer on the basis plane Bi_2Te_3, is seen on the fig.2 (c). The one from these monolayers, consisting from the Cu film, by the size less, than 100 nm, is illustrated on the fig.2.(c). The two islands, less by the size, "eaten" round each other very small islands (approximately ≈50 nm) are clearly seen on the fig.2 (c). The distance between the islands ≈200 nm. The big island Ni (see fig.3 (b)) is seen on the surface (0001) also on the layer of the same Ni for the system $Te^{(I)}$-Ni-$Te^{(I)}$.

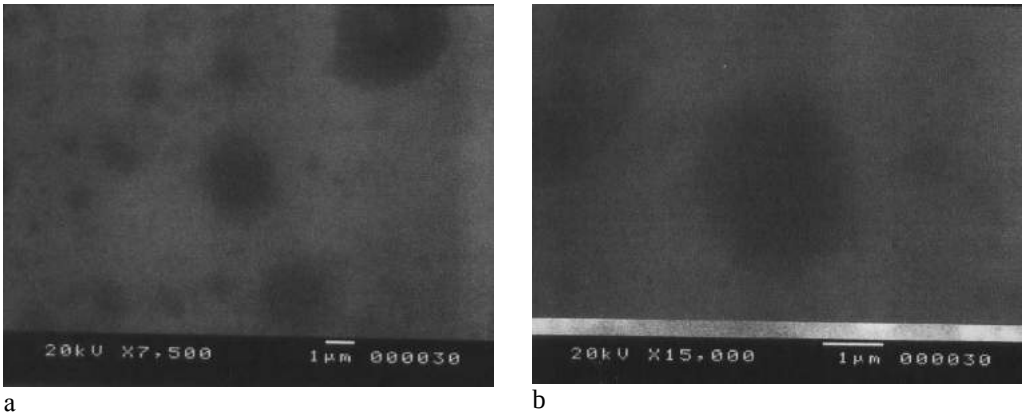

a b

Fig.3. Electron-microscopic photos Bi_2Te_3<Ni>.

The B creations close the set of the big islands (fig.4). Here even the island on the island is seen with edge spaces, from which B atoms have migrated into bigger islands (fig.4 a,b). Moreover, in all investigated systems the common quantities of the islands increases in the result of the light shifting of easily diffusing islands, that naturally leads to the coalescence. Here the temperature mode plays the important role in migration process.

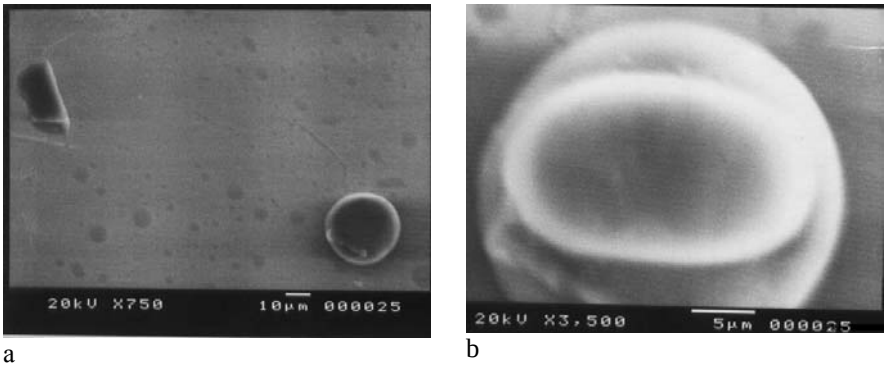

a b

Fig.4. (a,b) Electron-microscopic photos Bi_2Te_3<B>.

Even small temperatures increase the mobility not only very small nano-clusters, but also the islands of bigger sizes, that leads to the earlier coalescence. The accumulations of Cu islands are seen upper on the fig.2 (b), the process of island combining is seen in left (below), bridge-linear ("bridges"), on which the accretion and their joining in more big islands is carried out, is seen on the fig.2 (d). The temperature annealing (T=400°K, t=1hour) accelerates the particle combining (on the fig.2. (b)) into big round islands (fig.2. (c)). Moreover, the island unity takes place as in the result of the mobility of many particles by the creation of the unit island in the intermediate state, so in the result of the migration of the one of the coalescent islands to the other one. At the low-temperature annealing (till 500°K) the island number decreases. The degree of infill of the surface (0001) Bi_2Te_3 practically shouldn't change. The analogical one is also observed in the Ag-C, that is the result of the coagulation, i.e. the joining of the migrating islands without change of the initial form [4]. As we see, the migrational mobility of the islands is non-regular. And its direction, as it was mentioned in [4], doesn't depend on the crystallographical orientation of the substrate. The morphology studying of impurity layers showed, that for Cu, Ni and B the substrate orientation isn't so significant at the growth of the metallic films between telluride quintets. Here very small ion radiuses of inputted impurities play the significant role, their high diffusion coefficient along surface (0001) Bi_2Te_3 and distance between the layers $Te^{(I)}$- $Te^{(I)}$- 2,61Å.

It is need to also note the peculiarity of the deformation of island films – so-called stimulated coalescence, which was earlier mentioned in [9]. The island is shifted by the jump on the surface and joins to the other islands, even situated from it on the significant distance in the initial moment. The coalescence on the limited squares of the substrate can have the avalanche character.

The nonhomogeneity of island films. At the condensation on the "fresh" surfaces of crystal скол, the morphology and orientation of island films are nonhomogeneous. This can be connected with the fact, that the real surface of crystal скол is nonhomogeneous. It has the set of active places of different nature: steps of growth and скол, point defects of vacancy or impurity origin, outputs of dislocation and grain boundaries, including of secondary phases and pores. That's why the kinetics of creation and growth, the orientation of the films should be defined by the nature and activity of crystallization centers on the real surface. The confirmation of the above mentioned is the study of the kinetics on segregation nonhomogeneity of the impurities on intercrystal and interphase boundaries [10]. In the case of the gravity between the impurities, they reveal the tendency to the formation in adsorption layer of island structure. The main characteristics of this structure evolve during the time by the nonmonotonic way. The preposition has been said, that similar nonhomogeneous segregation of impurities on the interfaces can lead to the acceleration of the process of metal enlargement with impurities (Sn, S, As). The kinetics of island growth of new phase is considered in the preposition, that two-dimensional germs have already formed, i.e. on the binodal stadium or coalescence stadium [10].

The above mentioned confirmations increase the interest to the investigation of the behavior of two-dimensional island system in different atom layers of thin film, evaporated on singular crystal surface on the growth kinetics of the islands on crystal surfaces. Such analysis will help to us to reveal the one of the possible transfer mechanisms from 2D to 3D with the increase of evaporated band without growth parameters.

The morphology of the processes of island enlargement at the formation of several constituent growing atom layer we had considered on the fig.2, 3 and 4. Additionally, we present the roenthgen-difractograms of bismuth telluride (fig.5 (a)) and doped by Cu Bi_2Te_3 (fig.5 (b)). As it is seen in nondoped bismuth telluride, the observable peaks are sharp, high and thin ones; beginning from 53°C the doublet splitting is seen. The cuprum layers, evaporated on the сколах of basis plane, significantly change the heights and widths of roenthgen-difractogram peaks. In these changes the appeared resistances in lattice in layers $Te^{(I)}$ - Cu - $Te^{(I)}$ reflected. These resistances are explained by the structure peculiarities of island and total, but comparatively thin films, consisting probably from joined islands, connected by the parts of the film of nano-sized width. The cuprum impurity is situated in the interlayer space $Te^{(I)}$ - $Te^{(I)}$ Bi_2Te_3, having the width 0,26 nm.

However, let's back to the discussion of structure formation on the surface of the formed layer and islands on them. As it was seen from the fig. 2, 3 and 4 the many small

nanoparticles are created on the initial steps of the growth on the polish surface. Further, these particles combining practically form the total layer (fig 2 (c,d)). The beginning of the second layer takes place earlier than the total combining of the first one. The islands of the second layer, forming outside the poor bands, themselves become the strong drains for adatoms (see fig.2. (a), fig.4. (a)). The poor bands are also created around them, that limits the creation of new islands. The islands in the second layer are bigger, than in the first one at the one and the same covering in the layer (fig.2(c), fig.3. (b), fig.4. (b). All given data are related to the creations of the layers in the crack $Te^{(I)}$ - $Te^{(I)}$ of bismuth telluride by B, Cu and Ni atoms with very small atom (ion) radiuses. Such character of redistribution of two-dimensional islands on the sizes in constituent growing atom layers on the surface of the different crystals has been considered in the authors' investigations [11].

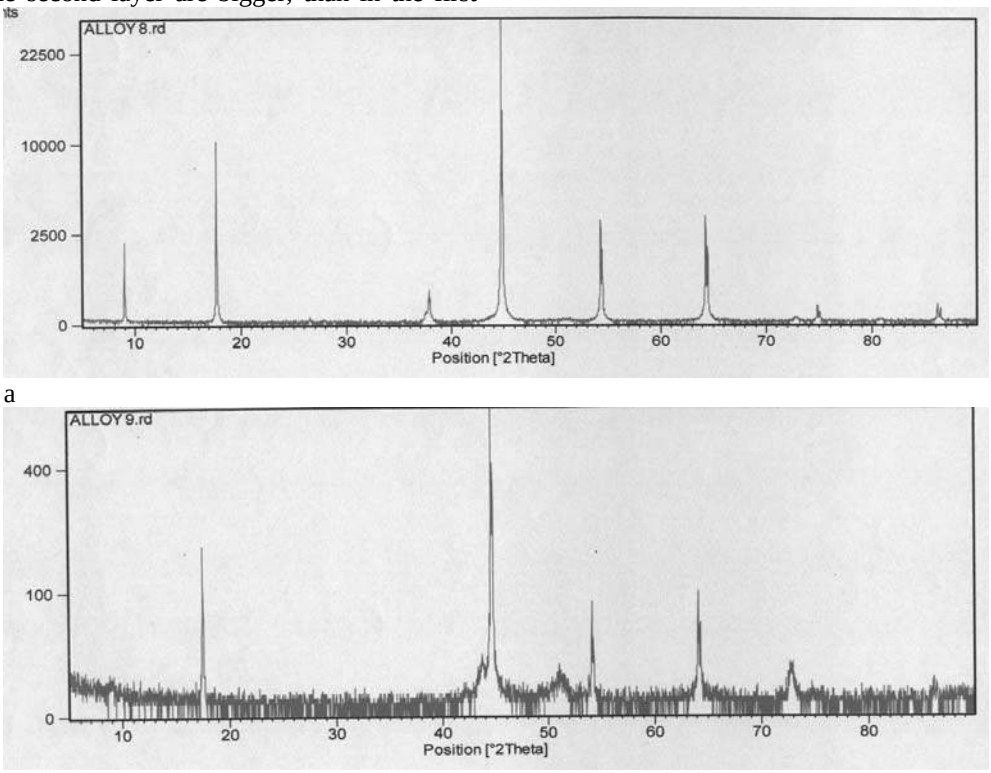

Fig.5. (a,b) Roentgen-difractograms of stoichiometric Bi_2Te_3 -(a) and Bi_2Te_3<Cu> (b).

It is shown, that the enlargement of the island sizes with the increase of layer number takes place, moreover, this effect is more clearly expressed in heterosystems. The mechanism of the transfer from the two-dimensional-layered growth to the three-dimensional one, observing in the one growth process (growth on Stransky-Krastanov mechanism) has been suggested [11].

All self-organizing created islands (fig.2, 3 and 4) of the different sizes and effect of their enlargement in each nanolayer with simultaneous increase of atom flux of the constituent nanolayer allow to us to accept for the base the given growth mechanism.

The influence of Cu creations on kinetic effects in bismuth telluride

The measurements had been carried out on the samples Bi_2Te_3<Cu> with resisted stable parameters. The surface morphology (0001) was given on the fig.2 (c,d), roenthgenograms were given on the fig.5 (a,b). Earlier, the angle position of 12 order of diffraction picture was measured by us [2] for the increase of the accuracy of the measurements of lattice parameter. The main parameter of structure-period of the repetition of fife-layered packs (quintets) is equal: in nondoped *n*- Bi_2Te_3 *d=10,1619*Å, in doped by Cu is equal to Bi_2Te_3<Cu>Å. Thus, the increase of the *d* structure period of Bi_2Te_3<Cu> d=10.1650Å sample becomes equal to $\Delta d \approx 3 \cdot 10^{-3}$Å. If this result connects with the order of neutral atoms of Cu in Van-der-Waals spaces, so it should be accompanied by the decrease of the concentration of charge carriers. The measurements confirm the changes: the decrease of the concentration from $N=2{,}1 \cdot 10^{19} см^{-3}$ till $N=9{,}7 \cdot 10^{18} см^{-3}$ is revealed. Naturally, that this is connected with the created nanolayers on Cu width on basis surface (0001) of bismuth telluride. The distance change between quintets should led to the forecasted change of energy spectrum Bi_2Te_3. According to the model of chemical connection in the bismuth telluride [12] the electron valence densities of $Te^{(1)}$ atoms, being on the edges of quintets are almost totally inputted inside the layers, thus, that the weak gravity takes place between them. The potential barrier between the quintets is symmetrical. The Cu neutral atoms, separating the quintets, increase the potential barrier. This should lead the energy spectrum of the crystal to more two-dimensional form. From the other side, as the structure of five-layered pack doesn't change, so its potential relief stays the same. Thus, the energy bands, connected with atom states, situated in the plane of quintet should stay unstable. The temperature dependencies (in region 77-300°K Bi_2Te_3<Cu>) $R_x(T)$ is Hall coefficient, $\Delta\rho/\rho$ is magnetoresistance *N* is concentration of charge carriers and

U is sample Bi_2Te_3<Cu> mobility, hade been investigated on such systems. The investigation results are given on the fig.6 and 7.

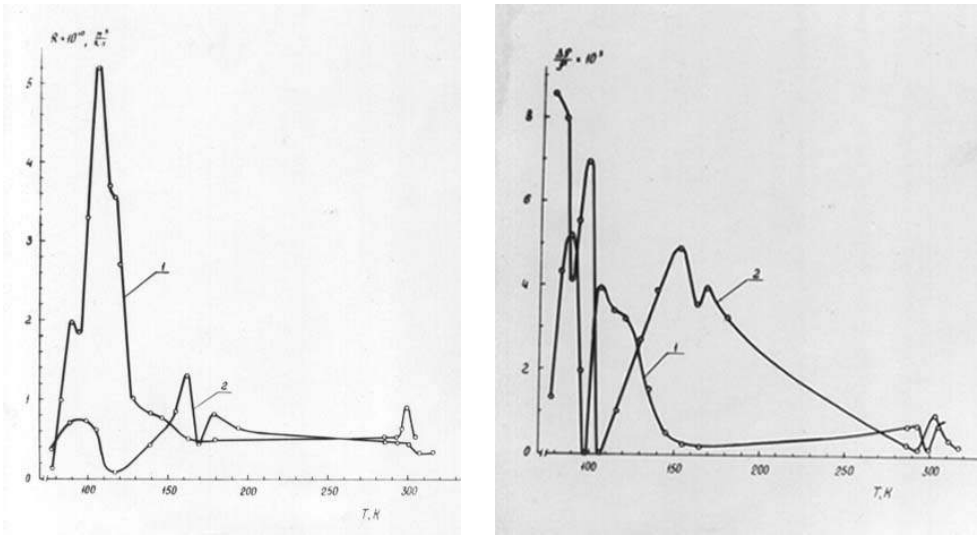

1 2

Fig.6. Temperature dependencies of Hall-R_x coefficient and $\Delta\rho/\rho$a-magnetoresistance of the sample Bi_2Te_3<Cu>) at the experiment directions 1- H⏐⏐C ⊥I, 2- H⊥C⊥I .

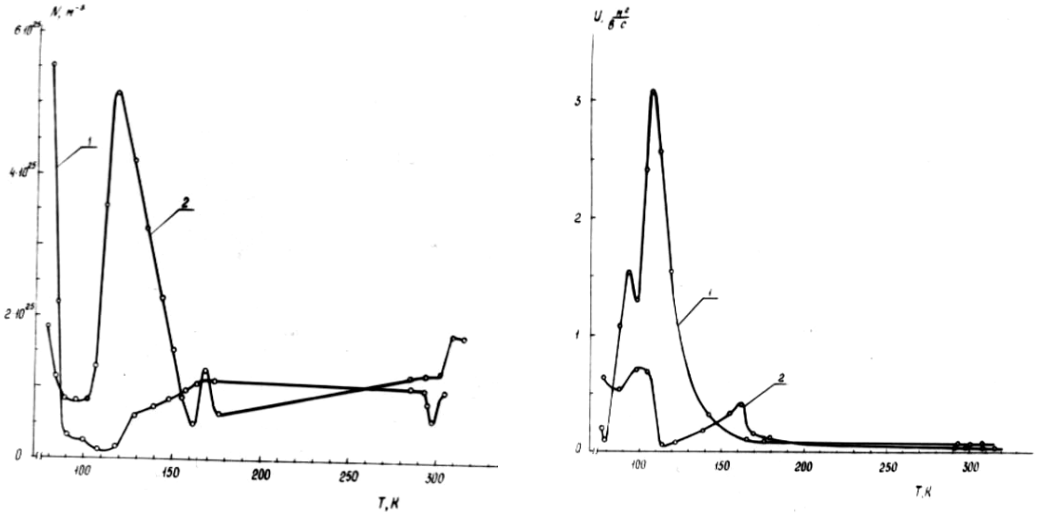

1 2

Fig.7. Temperature dependences of Hall concentration of charge carriers – *N* and mobility of the sample Bi_2Te_3<Cu> at 1- H⏐⏐C ⊥I, 2- H⊥C⊥I.

The comparison of the presented results with measurement data on pure crystals of bismuth telluride [13] show, that changes of kinetic parameters took place not only quantitatively, but also qualitatively. The dependences *R(T), Δρ/ρ, n(T)* и *U(T)* obtain the oscillation character in their considered temperature interval. The extremum demonstrations at temperatures near (290-310K), (155-180K), (105-120K), (980-90K) are clearly seen on the temperature dependencies of Hall coefficient, magnetoresistance, concentration and mobility of current carriers as for the directions parallel, so perpendicular to axes *C*. In the region of the above mentioned temperatures the increase of Hall concentration of carriers perpendicular to layers and decrease along the layers takes place. Moreover, the temperature dependency of mobility has the oscillating character; moreover, in region of 105K temperature the mobility along the layers has the anomalous big value *(3,1·10⁴cm²/Vs).* The above mentioned processes are accompanied by the redistribution of electron density in crystal lattice that probably is connected with phase transfers in the state with disproportionate waves of charge density into state of chaos structure. The ordered state of Cu atoms between the layers probably changes on the state with the creation of island accumulation (macroclusters) of Cu with small probability of the covering of wave functions of electrons between macroclusters. The localization of the definite part of the electrons on the boundary quintet-cluster, connected with transfer of charge carriers from the layers through the quintet boundary into below-situated impurity cluster states of Cu, leads to the redistribution of electron density. This is the reason of so-called shunting of the layers through clusters, that the increase of Hall concentration at the direction H⊥C⊥I (*C* is axes of third order, *H* is direction of magnetic field, I is current direction) is explained. The decrease of Hall concentration at the directions H⏐⏐C ⊥I can be connected with localization of the definite part of the

electrons by clusters and by very small probability of covering them by the wave functions between each other. Probably, the big mobility of current carriers is the result of space separation of the electrons and ions at the transfer of the part of the carriers from the layers into following (in energetic meaning) impurity cluster states, and part of the carriers to the quintet boundary. Thus, the quazi two-dimensional electron system, spatially separated by its ions, is created. The reason of high mobility, caused on the boundaries of the layers is also the decrease of carrier concentration in the layers at the given temperature. The anomaly in the mobility value can be combined with Konov's anomaly [14], when the value of the definite phonon mode decreases till the zero, i.e. the structure transfer takes place the, when the frequency of any phonon mode becomes very small. The layers-films of Cu on the surface (0001) (i.e. along axes *C*) Bi_2Te_3 shift the interlayer modes to the side of the less frequencies as the temperature decrease does. This phenomenon can lead to the state of the Konov's anomaly. The introduction of Cu islands in Van-der-Waalse cracks leads to the increase of potential barriers $Te^{(I)}$-$Te^{(I)}$ and Bi_2Te_3-$Te^{(I)}$, that leads to the shifting of electron density in the connection Bi-$Te^{(I)}$, to the side $Te^{(I)}$.

The extremums in temperature dependencies of Hall effect and effect of magnetoresistance probably are connected with consistency of phase transfers, known as transfers of type order-disorder, connected with positional disorder.

The extremums in temperature dependencies of Hall effects in Bi_2Te_3<Cu> can be combined with such ones in layered crystal InSe<Li, Pb> [15]. For the explanation of obtained experimental results, the several homogeneous layers with different σ and N were given by author and the potential topology was calculated in layered transfers and on the base of found expressions the (R_x) of such system was defined. Not taking under the consideration the details of the calculation, let's consider the analysis results: the obtained expression has three substance and positive roots, corresponding to the three extremums for Hall effects. At the solving of this problem the model, consisting from three layers, had been considerated: semiconductor, dielectric and metal.

It was shown, that layers of inputted Li were in nonconducting "dielectric" state [15]. At the lead concentration less, than n_{cur} ($n_{cur} \approx 10^{24}$ at/m^3) the extremums on the curve $R_x(T)$ weren't observed. This proved about the fact that lead layers were into nonconducting state, the inputted atoms situated far from each other, their wave functions don't change.

The appearance of extremums was mentioned in the crystals with concentration of inputted lead $n > n_{cur}$. As the expression for R_x [15], obtained by the author takes under consideration the existence of the one from the layers in conducting "metallic" state and moreover the analysis results correspond to the experimental data, then we can conclude about the realization of transfer of type dielectric-metal in inputted lead layer in semiconductor matrix of InSe. At $n > n_{cur}$ the covering of wave functions inputted atoms takes place. It accompanies by the growth σ of Pb layer, which begins to play the significant role in σ crystal that is caused the extremum appearance on curve $R_x(T)$ [15].

Thus, the existence of extremums in $R_x(T)$ of layered crystal InSe<Li, Pb> and $R_x(T)$ other layered narrow-band sample Bi_2Te_3<Cu> evidences about significant influence of monolayers and islands in layered crystals on their electron properties.

Conclusions

The common nature of self-regulation of impurity of nanolayers in layered crystal Bi_2Te_3 is analogical on the morphology (islands on monolayers) of semiconductor surfaces, with evaporated metals on them, is reflected in many electron processes, in particular on the extremal behavior of temperature dependency of Hall coefficient.

[1] *S.Ş. Kakhramanov, E.M. Maqerramov*. Termoelektricheskiy i mexanicheskiye svoystva leqirovannoqo i interkalirovannoqo *Bi_2Te_3<Cu>*. J. «Khovledqe Education» Society of Azerbaijan Republik, 2004, №2 r.29-32. (in Russian).

[2] *A.Q. Abdullaev, E.İ. Veliulin, S.Sh. Kaxramanov*. "Vliyaniye leqirovaniya i interkalirovaniya na svoystva xalkoqenidov vismuta, Preprint №420, İnstituta Fiziki NAN AR, Baku, 1991, s.3-54. (in Russian).

[3] *P.Q. Borzyak, Yu.A. Kulyupin*. Monoqrafiya "Elektronniye processi v ostrovkovix metallicheskix plenkax. Osnovniye svedeniya o mexanizme rosta plenok, 1980, 240 s. (in Russian).

[4] *V.M. Ievlev, L.I. Trusov, V.A. Xolmənskiy*. "strukturnıe prevraheniə v tonkix plenkax, Qlava 1. Prevrashsheniya na odnorodnoy poverxnosti , 1988. s.9-29. (in Russian).

[5] *P.N.Brunkov, A.A.Qutkin. Yu.G.Musixin, V.V.Chaldışev, N.N. Berq, S.Q. Konnikov, V.V. Preobrajenskiy, M.A. Putyato, B.R. Seməqin*. "İssledovaniye centrov rekombinacii, svyazannıx s nanorazmernimi klasterami As-Sb nizkotemperaturnom arsenide qalliya. J.Fizika i texnika poluprovodnikov, 2005, t.39, v.1., s.41-44. (in Russian).

[6] *P.N. Brunkov, A.A.Qutkin, V.V.Çaldışev, N.N. Berq, S.Q. Konnikov, V.V. Preobrajenskiy, M.A. Putyato. B.R. Seməqin.* "Lovushki dlya elektronov v tonkix sloyax nizkotemperaturnoqo arsenida qalliya s nanorazmernimi klasterami.. J. Fizika i texnika poluprovodnikov, 2005, t.39, v.9., s.1049-1052. (in Russian).

[7] V.V. Chaldyshev. Mater. Sci. Eng. B.88, 195 (2002)

[8] *V.E. Primaçenko, O.V. Snitko*. monoqr. "Fizika leqirovannoy metallami poverxnosti poluprovodnikov". Q. l.2. Fizicheskiye svoystva poverxnostey poluprovodnikov, 1988, s.230. (in Russian).

[9] *G.S. Jdanov.* "Nablyudeniye massoperenosa v ostrovkovix plenkax, J. İzv. An SSSR. Ser. Fiz. 1974. t.38, s.1472. (in Russian).

[10] *L.I. Stefanovich, E.P. Feldman, V.M. Yurchenko.* Kinetika neodnorodnostey seqreqacii primesey na mejkristallitnix i mejfaznix qranicax, J. Metallofizika. Noveyshie texnoloqii 2002, t.24. № 8, 1103-1123. (in Russian).

[11] *D.V.Brunev, A.N. Karpov, I.G. Neizvestniy, N.L.Shvarc, Z.Sh. Yanovickaya*. Pereraspredeleniye dvumernix ostrovkov po razmeram v posledovatelno rastushix atomnix sloyax na poverxnosti kristallov, J.Poverxnost. Rentqenovskie, sinxronniye i

neytronniye issledovaniya, 2003, V 10, c 15-19. (in Russian).

[12] *V.Q. Kuznecov.* O ximicheskoy svyazi v telluride vismuta- v knige: Ximicheskaya svyaz v poluprovodnikax i tverdix telax- Minsk: Nauka i texnika, 1965. s.311.

[13] *B.M. Golcman, V.A. Kudinov, İ.A. Smironov.* Poluprovodnikovie termoelektricheskie materiali na osnove Bi_2Te_3. M.: Nauka, 1972. 320 s.

[14] *L.N. Bulaevskiy*. J. Uspekhi fizicheskikh nauk, 1976, t.120, v.2. s.259-271.

[15] *K.D. Tovstyuk*. Poluprovodnikovoe materialovedenie, Kiev. Naukova Dumka. 1984, s. 218-223.

S.Ş. Qəhrəmanov

TELLURİD VİSMUTUN KRİSTALLİK LAYDA NANOSTRUKTUR MƏRKƏZLƏRİ VƏ ONLARIN KİNETİK XASSƏLƏRİNƏ TƏSİRİ

Tellurid vismutun istiqamətlənmiş kristallaşma prosesində (yüngül diffuzion aşqarlarla leqirə olunmuş) Te^I-Te^I laylar arasında öz-özünə laylı və adalı nanolay artma olur. (0001) Bi_2Te_3<B>, Bi_2Te_3<Cu> və Bi_2Te_3<Ni> elektron-mikroskopik şəkilləri bunu təsdiq edir. “Adaların müxtəlif ölçüləri-50-200nm-dir. Tellurid vismutun nanolayların və “adaların yaranma təbiəti yarımkeçirici-metal sistemlərin təbiəti ilə eynidir. Başlanğıc artma mərhələsində ikiölçülü “adalar əmələ gəlir və birləşərək nano-qalınlıqlı lay yaradır.

Göstərilir ki, xoll əmsalının və Bi_2Te_3<Cu> digər kinetik parametrlərinin ekstremal dəyişməsinin səbəbi misin layının hündürlük nanoölçüsüdür. Xoll əmsalının elektrik keçirməsi, yürüklüyü və digər kinetik parametrlərinin temperatur asılılığı ossilə xarakterlidir. Bu ekstremumları faza keçidləri ardıcıllıqlarla uzlaşdırmaq olar.Yürüklüyün anomal artması (5 dəfədən çox) Bi_2Te_3<Cu> (105º K-tempraturda) eksperimental müəyyən olub.

С.Ш. Кахраманов

НАНОСТРУКТУРНЫЕ ЦЕНТРЫ В КРИСТАЛЛИЧЕСКОМ СЛОЕ ТЕЛЛУРИДА ВИСМУТА И ИХ ВЛИЯНИЕ НА КИНЕТИЧЕСКИЕ СВОЙСТВА

В процессе направленной кристаллизации теллурида висмута (легированных легкодиффундируемыми примесями) самопроизвольно между слоями Te^I-Te^I реализуется послойный и островковый рост нанослоев: меди, никеля и бора. Это подтвердили электронно-микроскопические снимки сколотой поверхности (0001) Bi_2Te_3<B>, Bi_2Te_3<Cu> и Bi_2Te_3<Ni>. Был выявлен широкий набор размеров островков 50-200 нм.

Природа возникновения нанослоев, островков и их укрупнение в межслоевом пространстве слоистого кристалла теллурида висмута такая же, как и на открытых поверхностях систем полупроводник-металл. На начальных этапах роста образуются двумерные островки, которые, сливаясь, формируют смачивающий слой нано-толщины.

Установлено, что за экстремальное поведение эдс Холла и другие кинетические параметры Bi_2Te_3<Cu> ответственны наноразмерные по высоте слои меди. Температурные зависимости коэффициента Холла, электропроводности, подвижности и другие кинетические параметры обнаружили осцилляционный характер. Эти экстремумы можно увязать с последовательностью фазовых переходов, известных как переходы порядок-беспорядок, связанных с позиционным разопрочнением. Обнаружено аномальное увеличение подвижности носителей заряда (более чем в 5 раз) в направлении вдоль оси слоев (0001) Bi_2Te_3<Cu> при температуре 105^0K.

Received: 15.11.05